5. SITE 759[1]

Shipboard Scientific Party[2]

HOLE 759A

Date occupied: 7 July 1988

Date departed: 8 July 1988

Time on hole: 12.5 hr

Position: 16°57.25'S, 115°33.61'E

Bottom felt (rig floor; m, drill pipe measurement): 2103.0

Distance between rig floor and sea level (m): 11.4

Water depth (drill pipe measurement from sea level; m): 2091.6

Total depth (rig floor; m): 2131.0

Penetration (m): 28.00

Number of cores (including cores with no recovery): 1

Total length of cored section (m): 0.00

Total core recovered (m): 0.00

Core recovery (%): 0.00

HOLE 759B

Date occupied: 8 July 1988

Date departed: 11 July 1988

Time on hole: 3.6 days

Position: 16°57.24'S, 115°33.63'E

Bottom felt (rig floor; m, drill pipe measurement): 2103.0

Distance between rig floor and sea level (m): 11.4

Water depth (drill pipe measurement from sea level; m): 2091.6

Total depth (rig floor; m): 2411.00

Penetration (m): 308.00

Number of cores (including cores with no recovery): 39

Total length of cored section (m): 129.60

Core recovery (%): 42

Oldest sediment cored:
Depth (mbsf): 308.00
Nature: siltstone and claystone
Age: Carnian
Measured velocity (km/s): 2.21

Principal results: Site 759 (proposed Site EP10A') is located on the southeastern flank of Wombat Plateau, a small subplateau in the northeastern part of the Exmouth Plateau. A half graben separates Wombat Plateau from Exmouth Plateau proper. The site was chosen to sample the older Mesozoic record in order to unravel the early rift, drift, and subsidence history of this sediment-starved passive margin, and to provide a record of sea-level fluctuations for testing the eustatic cycle chart of Haq et al. (1987).

The 308.0-m-long cored section consists of an upper 26.7 m of Quaternary foraminiferal-nannofossil ooze unconformably overlying 4.7 m of early Miocene nannofossil ooze with foraminifers. This unit is unconformably underlain by a 9.5-m-thick foraminifer-quartz sand containing mixed Quaternary to early Miocene assemblages (downhole contamination). The sand forms a mixed terrigenous/pelagic lag deposit overlying a major late Triassic unconformity. The sediments below this unconformity can be subdivided into three discrete units representing several large, upward-shallowing (regressive) cycles. The upper 95.5-m-thick unit consists of alternating neritic (intertidal to shallow subtidal) carbonates and paralic claystones of Norian age. These may represent sea-level fluctuations or delta-lobe migrations. Above 136 meters below seafloor (mbsf), a major transgression indicated by oyster- and wood-fragment-bearing calcareous quartz sandstone and rudstone (and by high gamma-ray and thorium peaks on the logs) separates two regressive sequences. A middle unit (135.9–205.0 mbsf) consists of interbedded neritic carbonates and dark gray silty claystones.

The lower unit (205.0–308.0 mbsf) is largely devoid of carbonates and consists of a 172-m-thick sequence of laminated silty claystones, bioturbated mudstones with mollusks, siltstones, sandstones, and coal seams. This unit is of Carnian age and represents an upward-shallowing cycle. The cycle starts with laminated marginal-marine mudstones having sideritic interbeds that were deposited rapidly in an oxygen-poor environment. These grade upward into a series of mudstones with sandstones (turbidites or tempestites) and finally into a paralic (lagoonal, fluviodeltaic, and coal swamp) coal measure sequence.

Spores and pollen proved to be the best source of age information for the Triassic. However, coccoliths were encountered in two intervals within the lowermost unit, and occurred sporadically throughout the Triassic section. This is the oldest record of nannofossil occurrence in the world and detailed study may be significant for biostratigraphic subdivision of the interval. The recovery of Carnian to Norian sediments at this site represents the oldest marine sediments recovered by deep-sea drilling.

High-quality logging results (gamma ray, resistivity, and acoustic velocity) helped delineate sandstone, mudstone, and limestone successions in intervals with poor recovery. Logs also helped define upward-coarsening or upward-fining sequences caused by fluctuations of relative sea level within the highstand system tracts.

BACKGROUND AND OBJECTIVES

Background

Geophysical and geological studies of the northern margin of Exmouth Plateau have previously been conducted by the Australian Bureau of Mineral Resources (BMR) and the Bundesanstalt für Geowissenschaften und Rohstoffe (BGR) (Exon and Willcox, 1978; von Stackelberg et al., 1980; von Rad and Exon, 1983; Exon and Williamson, 1988). These show that faulting occurs in two directions: northeasterly trends believed to be Triassic to middle Jurassic in age, and easterly trends of late Jurassic to early Cretaceous age. The older faulting could be related to the Callovian breakup of the northern margin, whereas the younger faulting is probably related to the Neocomian breakup of the western and southern Exmouth Plateau margins. The northern Exmouth Plateau margin is a mixed transform/rifted margin with long east-

[1] Haq, B. U., von Rad, U., et al., 1990. *Proc. ODP, Init. Repts.*, 122: College Station, TX (Ocean Drilling Program).

[2] Shipboard Scientific Party is as given in the list of Participants preceding the contents.

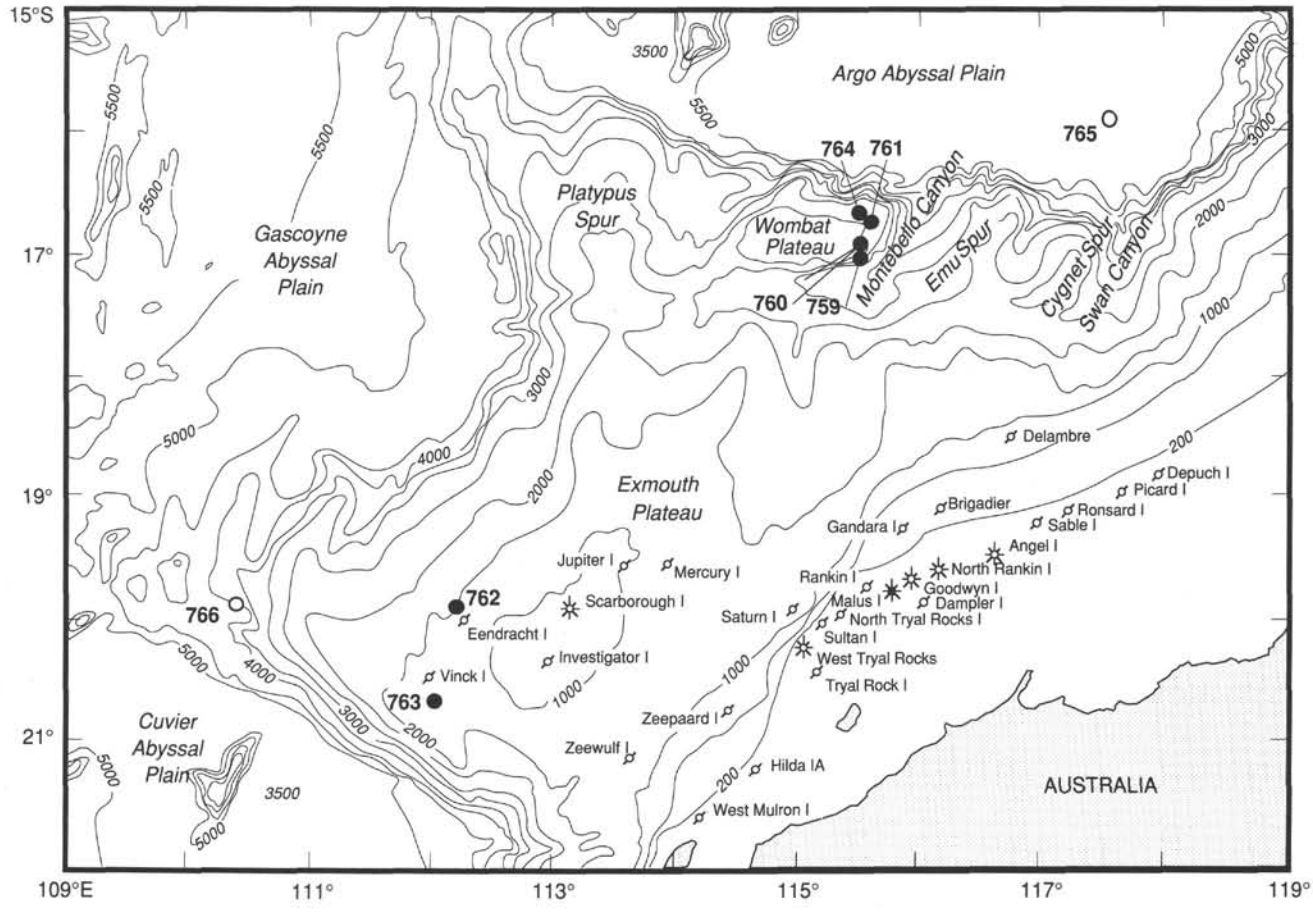

Figure 1. Bathymetric map of Exmouth Plateau region showing locations of ODP sites (closed circles = Leg 122 sites; open circles = Leg 123 sites) and commercial wells. Leg 122 Sites 759 and 760 are at the position of proposed Site EP10A. Site 761 corresponds to Site EP9E. Bathymetry is shown in meters (Exon, unpubl. data).

trending transform and shorter northeast-trending rift segments (Exon et al., 1982).

The northeast-trending faults have cut the margin into a series of high blocks or horsts from the Platypus Spur in the west, across the Wombat Plateau and the Emu Spur to the Cygnet Spur near Swan Canyon in the east (Fig. 1). The horsts are separated from each other by northeast-trending faults, such as the northern Montebello Canyon, and the deeply incised Swan Canyon (Fig. 1). Displacement on the faults separating the horsts from the half-grabens is approximately 2000 m. West-trending faulting occurred along and north of the east-trending "North Exmouth hingeline," which underlies the 2000-m isobath along the northern edge of the central Exmouth Plateau (see "Introduction," Fig. 4, this volume). Seismic profiles show that north of the hingeline all the sequences above the top Triassic Reflector F thicken greatly (see "Introduction," Fig. 4, this volume).

The stratigraphic sequences seen in the half-grabens (e.g., Wombat half-graben) and the high blocks or horsts (e.g., Wombat Plateau) appear to be similar, at least below the Upper Cretaceous. They have similarities to (and differences from) the central Exmouth Plateau sequences (Figs. 2 and 3). On the high blocks there is a marked, almost flat Oligocene unconformity that is underlain by rocks that may be as old as early Jurassic to middle Triassic. This unconformity is locally superimposed on the regional B, C, and D unconformities (Figs. 2 and 3).

The Wombat Plateau is a 5800-km^2 subplateau located at 2000 m water depth on the northern margin of Exmouth Plateau (Fig. 4). Its upper surface slopes gently northward, but its fault-bounded margins to the south, east, and west form steep, 1000–2000-m-high escarpments. The northern margin of Wombat Plateau (facing the Argo Abyssal Plain) is a 3500-m-high scarp. According to Exon et al. (1982), the southern boundary faults of the Wombat Plateau did not develop into a major feature until after the deposition of the E-D seismic sequence (i.e., post-Neocomian). During late Cretaceous times, an older fault was rejuvenated, downfaulting the Wombat half-graben and separating Wombat Plateau from the rest of Exmouth Plateau (see "Introduction," Fig. 4, this volume). After that time the Wombat Plateau was tilted northward, possibly a result of either isostatic rebound after the downfaulting of the half-graben or of asymmetric uplift during a later rifting event (detachment faulting?).

Today, the Wombat Plateau is a planed block of Triassic sediments with generally only a thin cover of Cretaceous to Neogene sediments. The Cretaceous E-(D-C) seismic sequence reaches a maximum thickness of about 100 m below the central Wombat Plateau where proposed Site EP9E (Site 761) is located. The presence of numerous diffractions on the northern margin suggests the occurrence of large volcanic bodies. The F (top Triassic) seismic unconformity is the oldest reflector identified on the seismic records. The E (Callovian) unconformity is characterized by reflections atop tilted and

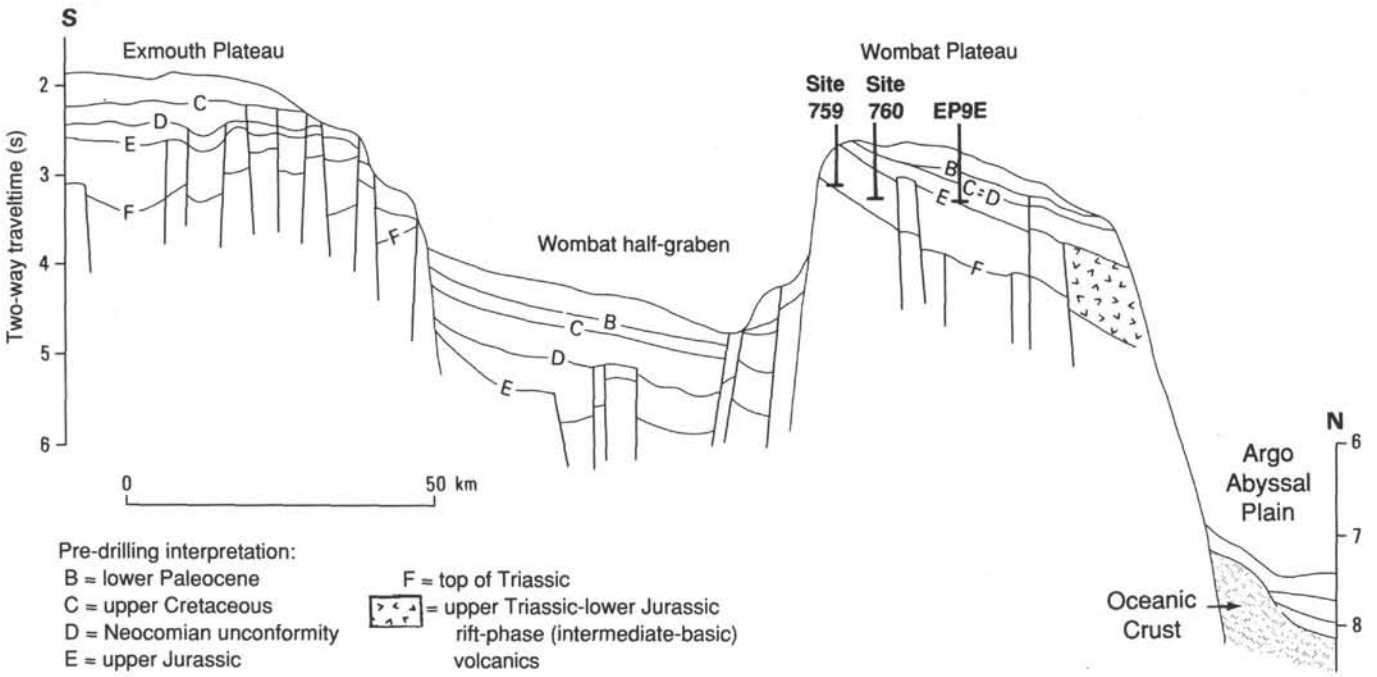

Figure 2. Geological-structural interpretation of BMR *Rig Seismic* Line 56-13 prior to drilling Sites 759, 760, 761, and 764 (modified from Exon and Williamson, 1988). Letters correspond to regional unconformities (see text). Note that the interpretation of the E and F reflectors below Site 759 proved to be erroneous, as Sites 759, 760, and 761 encountered upper Triassic (not Jurassic) rocks below the main unconformity.

eroded fault blocks. Some of these faults extend up to the D (Neocomian) unconformity. The upper Cretaceous/Oligocene (C and B) unconformities mark the top of the horst blocks. Sedimentation rates in the region declined, as pelagic sedimentation became dominant in the late Cretaceous. During most of the Tertiary, pelagic deposition on the top of the plateau was interrupted by extended periods of nondeposition, (due to winnowing by strong bottom currents) and/or erosion.

Dredge sampling of the steep northern and southern escarpments of Wombat Plateau during the *Sonne* 8 and *Rig Seismic* 56 cruises yielded a great variety of marine limestone and clastic rock types of Late Triassic (Carnian/Rhaetian), Liassic, Dogger(?), early Cretaceous, and Tertiary age (von Stackelberg et al., 1980; von Rad and Exon, 1983; von Rad et al., in press). This information provided tentative dates for the seismic interpretation from which the region's paleogeographic evolution and the Wombat Plateau drilling plan were developed. Volcanic material dredged from the northern margin of Wombat Plateau suggests the presence of volcanic sequences of late Triassic to lowermost Liassic age (213–193 Ma; von Rad and Exon, 1983; von Rad et al., in press).

In April/May 1986 BMR carried out a detailed site survey to meet JOIDES Pollution Prevention and Safety Panel (PPSP) requirements for proposed Leg 122 Site EP-10 (Exon and Williamson, 1988). The site survey area lies in the southeastern corner of the Wombat Plateau, northwest of a steep scarp running down to the northeast-trending Montebello Canyon (Fig. 4). *Rig Seismic* Line 56-13 (Fig. 2) is a regional north-south seismic cross line extending from the north Exmouth hingeline across Wombat Plateau to the Argo Abyssal Plain (Exon and Williamson, 1988). Structure contour maps of the C and E seismic horizons indicate that there is a regional dip to the northeast, suggesting that any hydrocarbons migrating through the location of Site EP-10A would be safely vented at the scarp. Cross-sections through the site (Fig. 2) emphasize that there is some small-scale north-south faulting near the site. Site EP-10A was originally located at the intersection of BMR Line 56-13/56-20A at 16°56.6′S, 115°33.1′E, in a water depth of 2050 m (von Rad et al., 1986). However, the PPSP requested a relocation of the site to an updip position about 1.5 km downslope of the proposed Site EP-10A, on *Rig Seismic* Line 56-20B (shotpoint 114:1037). Site 759 was drilled at this location at a water depth of 2091.6 m at 16°57.24′S, 115°33.63′E.

Objectives

Site 759, on the uplifted southeastern flank of the Wombat Plateau, has a very thin cover of post-breakup sediments, and thus was expected to be an optimal site for sampling the upper Triassic through lower Jurassic sequences. The recovery of this early Mesozoic record is crucial to the study of the evolution of Exmouth Plateau, especially as this part of the stratigraphic record was not intended to be recovered on any of the other sites proposed for Legs 122 and 123. The specific objectives of all sites from the Wombat Plateau transect (Sites 759, 760, and 761) were as follows.

1. Retrieve the older Mesozoic record on the northern Exmouth Plateau in order to unravel the pre-, syn-, and post-rift history and the associated sedimentary changes that typify this starved passive continental margin.

2. Provide the "ground truth" concerning the seismic section and prominent reflections along the slope of the

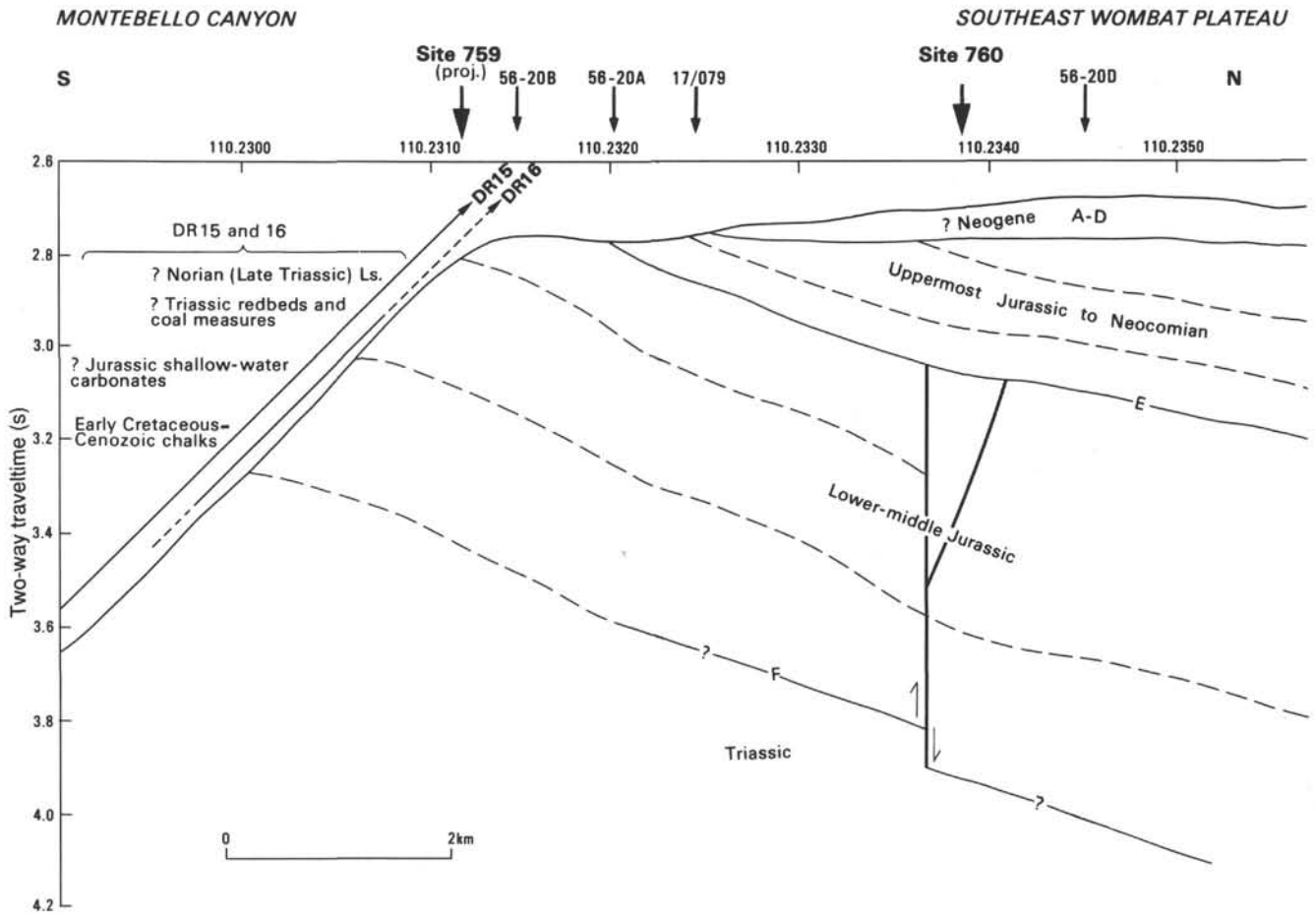

Figure 3. Pre-drilling geological interpretation of BMR and *Rig Seismic* line 56-13 (ages determined from dredge samples). See Figure 31, Site 764 chapter (this volume) for a post-drilling interpretation. Letters refer to regional unconformities (see text).

Wombat Plateau and the northern Exmouth Plateau in general. Prior to drilling, the only available data concerning the age and environment of deposition of the strata were from samples dredged from the slopes of the plateau.

3. Study the depositional sequences of the lower Mesozoic. Sequence stratigraphic analysis and geohistory interpretation of the section were planned to separate the effects of regional tectonics, subsidence, and varying sediment input from the eustatic signal. Testing the new eustatic cycle chart (Haq et al., 1987) was an important objective of all the sites drilled during Leg 122.

4. Establish and/or refine early Mesozoic chronostratigraphy. Microfossil assemblages of the older Mesozoic are poorly known. Site 759 represents a good opportunity to establish a practical biostratigraphic subdivision for the interval.

On the basis of regional seismic stratigraphic data, Sites 759, 760, and 761 (Fig. 2) were designed to recover a fairly complete record of the Triassic to lower Cretaceous in the region. The record at Site 759 would not only compliment the younger section at EP9E (Site 761), but would also ascertain the presence or absence of hydrocarbon source intervals in the strata underlying the section at EP9E.

OPERATIONS

Singapore Port Call

Leg 122 officially commenced in Singapore, Republic of Singapore, at 0230 hr (local time, or LT), 29 June 1988, when *JOIDES Resolution* dropped anchor in Johor Anchorage to await the pilot. At daylight the ship proceeded through Serangoon Harbor to the Loyang Offshore Supply Base, and the first line was on the dock at 0905 hr (LT). Airfreight and Leg 121 cores were offloaded. The incoming freight and 2017 sacks of barite were taken aboard, and drill pipe was unloaded from the riser hold. Inspection of the drill pipe and cleaning of two fuel tanks began. The fuel tanks were cleaned in order to allow installation of a new geophysical dome. A new Schlumberger logging cable was installed on the winch and the old one was offloaded. A total of 407,447 gallons of fuel was taken aboard. Inspection of the drill pipe continued, but intermittent rain hampered the inspection operation. By the afternoon of 2 July 1988, all of the 5-in. (444 joints) and 54 joints of the 5-1/2-in. drill pipe had been inspected; sufficient time was not available to finish the inspection. *JOIDES Resolution* departed Singapore at 1645 hr (LT) on 2 July 1988.

The course was southeast across the Java Sea to the island of Bali, through the Strait of Lombok to the Indian Ocean, and then nearly due south to the first site. During the second day at sea the Cyberex system, which supplies regulated power to the lab stack, suffered a catastrophic failure. Many surge protectors and equipment in the labs, including the VAX computer, were damaged. A temporary partial fix was to equip critical equipment with a limited number of small surge protectors while parts were being obtained for the Cyberex from the USA. No attempt was made to power up the VAX computer. Subsequently, a medical emergency necessitated a helicopter evacuation as the ship neared the island of Bali.

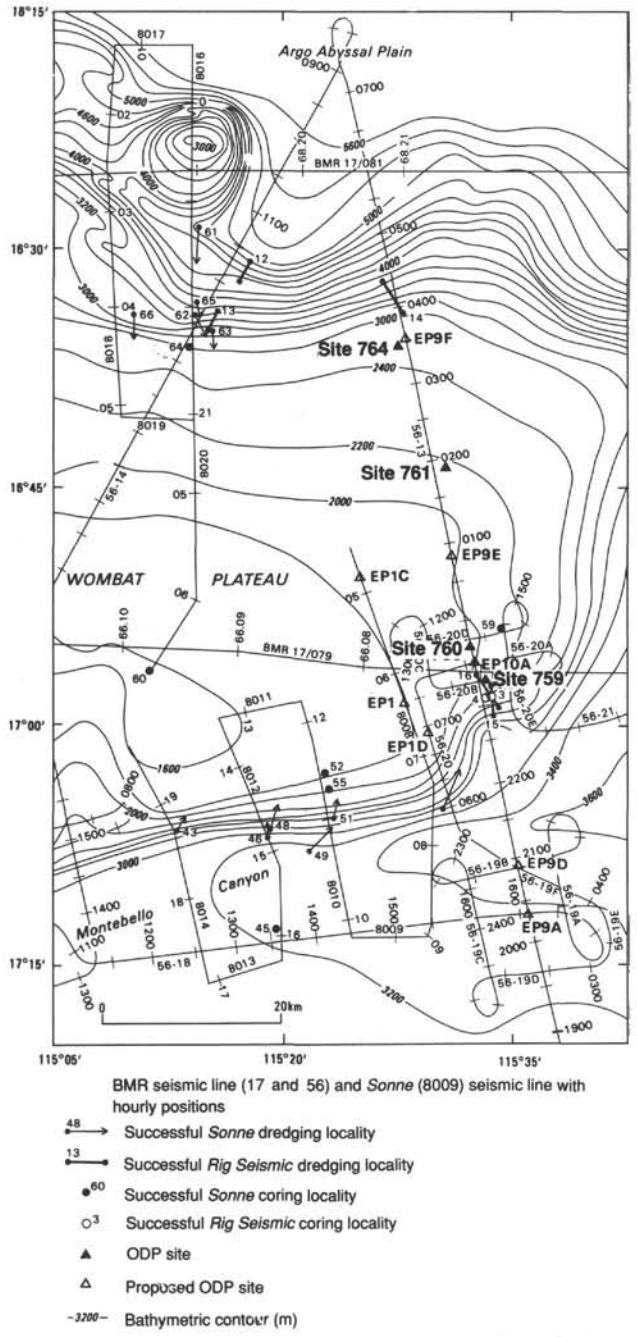

BMR seismic line (17 and 56) and *Sonne* (8009) seismic line with hourly positions

48 → Successful *Sonne* dredging locality

13 → Successful *Rig Seismic* dredging locality

•60 Successful *Sonne* coring locality

○3 Successful *Rig Seismic* coring locality

▲ ODP site

△ Proposed ODP site

-3200- Bathymetric contour (m)

Figure 4. Bathymetry of Wombat Plateau showing locations of seismic lines and dredge stations from BGR (*Sonne*-8) and BMR (*Rig Seismic*-56) surveys. Open triangles = proposed ODP sites; closed triangles = drilled ODP sites; arrows = SO-8 and RS-56 dredge samples.

The weather during the voyage to the site was excellent, with calm seas and little or no wind. At 1830 hr (LT), 7 July 1988, beacon SN396 was dropped at 16°57.25'S, 115°33.61'E. The voyage of 1483 nmi had been made in 123.25 hr at 12 kt.

Site 759

The predicted penetration of the first hole was 1300 m. It was anticipated that more than one bit would be required to drill the hole and that a reentry cone would be needed. The primary scientific interest was not in the near-surface sediments but in the deeper materials. Hard material was expected near the sea floor, so we decided to spud-in with the rotary core system (RCB) and accept limited recovery in the soft material.

Hole 759A

The bit selected was an Rock Bit International (RBI) C4. The bottom-hole assembly (BHA) consisted of the 9-7/8-in. bit, mechanical bit release, head sub, control length drill collar, long top sub, head sub, seven 8-1/4-in. drill collars, cross-over (XO), one 7-1/4-in. drill collar, and two stands of 5-1/2-in. drill pipe. Beacon SN396 began to broadcast intermittently, and 7.5 hr after it had been dropped it was necessary to launch the standby SN397.

The precision depth recorder (PDR) indicated a water depth of 2107.3 m. At 2103 m the bit appeared to take weight in a very soft sea bottom, and the bit easily penetrated 9.5 m. The core barrel was pulled but there was no recovery. The bit was raised above the sea bottom, and a jet-in test was performed to determine the feasibility of washing in 16-in. casing. The bit was jetted in 28 mbsf with 2000–10,000 lb of weight and 250 gpm (gallons per minute). At that depth, hard, firm formation was encountered and deeper penetration was not possible.

Hole 759B

The ship was moved 20 m north. The first 12.5 m were cored with no bit rotation through very soft material and there was no recovery (Table 1). Cores 122-759B-3R and 122-759B-4R recovered a total of 12.7 m of sediment, but the next 199.5 m of advancement (Cores 122-759B-5R to 122-759B-26R) produced only 50.3 m of core (Fig. 5). The sediment alternated from hard to extremely soft, and apparently the soft material was not being captured. At 230 mbsf, the formation began to become firmer, and recovery gradually increased to 3–4 m per core. The material being cored was packing tightly into the core catcher after coring the 3–4 m, and was preventing additional core from entering the barrel. A half core was cut in an effort to increase the recovery. Although the overall penetration rate decreased, percent recovery improved dramatically (Fig. 6), meters of penetration per hour of rotation levelled off (Fig. 7A), and the increase in total rotating hours per core increased more linearly (Fig. 7B). During the last 77.5 m cored, the recovery was 87%.

In summary, the first 175 m at Hole 759B may represent the type of formation best recovered with the APC/XCB coring system. In material that cannot be optimally cored with either the APC/XCB or the RCB systems, recovery may be enhanced by taking half cores with the RCB. The last core, taken between 298.5 and 308.0 mbsf and advanced 9.5 m, had 78% recovery, which suggests that a formation suitable for RCB coring had been reached. The scientific party determined that the upper section of the desired stratigraphic sequence was missing, and the proposed 1300 m hole was terminated at 308 mbsf.

Two logging runs were planned. The hole was conditioned for logging by pumping mud from the bit to the seafloor five times, a bit wiper trip to two stands below the mud line was made, and mud was again pumped from the bit to the seafloor, six times. The mechanical bit release was activated, and the bit was released into the hole. Fifty barrels of mud were circulated and the hole was filled with logging mud. The logging mud was made up of 30 PPB (pounds per barrel) bentonite that had been prehydrated in fresh water, and pre-treated with 0.25 PPB soda ash and 0.25 PPB caustic. An equal amount of seawater, 9 PPB KCl, and 1 PPB Drispac was added to this mix. The bottom of the drill string was pulled to 40 mbsf; after a tool failure, the phasor inductor (DIT-E), digital array sonic (SDT), and spectral gamma ray (NGT) tools were run from 308 through 69 mbsf. Hole conditions were excellent for logging. The second log was not run because the time taken by the tool failure had used the allotted logging time.

Table 1. Coring summary for Site 759.

Core no.	Date (July 1988)	Time (local)	Depth (mbsf)	Cored (m)	Recovered (m)	Recovery (%)
122-759A-						
1W	8	0705	0.0–28.0	0.0	0.00	0.0
Coring totals				0.0	0.00	0.0
122-759B-						
1R	8	0835	0.0–3.0	3.0	0.00	0.0
2R	8	0910	3.0–12.5	9.5	0.00	0.0
3R	8	0940	12.5–22.0	9.5	7.51	79.1
4R	8	1055	22.0–31.0	9.0	5.20	57.8
5R	8	1300	31.0–40.5	9.5	1.52	16.0
6R	8	1400	40.5–50.0	9.5	1.58	16.6
7R	8	1600	50.0–59.5	9.5	2.91	30.6
8R	8	1850	59.5–69.0	9.5	1.02	10.7
9R	8	2010	69.0–78.5	9.5	0.21	2.2
10R	8	2120	78.5–88.0	9.5	0.18	1.9
11R	8	2250	88.0–97.5	9.5	2.44	25.7
12R	9	0100	97.5–107.0	9.5	2.30	24.2
13R	9	0350	107.5–116.5	9.5	4.22	44.4
14R	9	0645	116.5–126.0	9.5	3.46	36.4
15R	9	0800	126.0–135.5	9.5	0.00	0.0
16R	9	1000	135.5–145.0	9.5	1.17	12.3
17R	9	1130	145.0–154.5	9.5	1.96	20.6
18R	9	1315	154.5–164.0	9.5	2.37	24.9
19R	9	1450	164.0–173.5	9.5	5.23	55.1
20R	9	1555	173.5–183.0	9.5	5.14	54.1
21R	9	1715	183.0–192.5	9.5	3.88	40.8
22R	9	1910	192.5–202.0	9.5	4.03	42.4
23R	9	2115	202.0–211.5	9.5	3.30	34.7
24R	9	2225	211.5–221.0	9.5	3.41	35.9
25R	10	0010	221.0–230.5	9.5	3.79	39.9
26R	10	0130	230.5–235.5	5.0	3.35	67.0
27R	10	0235	235.5–240.5	5.0	4.13	82.6
28R	10	0330	240.5–245.5	5.0	4.58	91.6
29R	10	0425	245.5–250.5	5.0	4.63	92.6
30R	10	0520	250.5–255.0	4.5	3.67	81.6
31R	10	0615	255.0–260.0	5.0	4.86	97.2
32R	10	0700	260.0–265.0	5.0	3.99	79.8
33R	10	0815	265.0–270.0	5.0	3.73	74.6
34R	10	0945	270.0–274.5	4.5	4.01	89.1
35R	10	1120	274.5–279.5	5.0	4.44	88.8
36R	10	1245	279.5–284.0	4.5	4.50	100.0
37R	10	1415	284.0–289.0	5.0	4.19	83.8
38R	10	1615	289.0–298.5	9.5	5.32	56.0
39R	10	1850	298.5–308.0	9.5	7.37	77.6
Coring totals				308.0	129.60	42.1

As the hole was located on a continental margin, safety requirements dictated that it be cemented. A 150-sack cement plug was emplaced with the end of the drill pipe at 120 mbsf. The ship was underway to the next site at 2115 hr (LT), 11 July 1988.

LITHOSTRATIGRAPHY

The 308-m-thick section recovered at Site 759 is divided into five lithologic units on the basis of visual core, smear slide, and thin-section descriptions (Table 2, Fig. 8). Throughout the hole, coring disturbance was minor.

Unit I (0–31.0 mbsf)

Interval 122-759B-1R-1, 0 cm, to -4R-CC, 13 cm.

Unit I consists of Quaternary through early Miocene foraminifer nannofossil ooze, and nannofossil ooze with foraminifers. This unit is divided into two subunits on the basis of microfossil composition and color, with the contact at 26.7 mbsf (122-759B-4R-4, 25 cm).

Subunit IA (0–26.7 mbsf)

This subunit is composed of pink (5YR 7/4), pink gray (7.5YR 7/2), light gray (5YR 7/1), and light red-brown (5YR 6/3) foraminifer nannofossil ooze. Both sharp and gradational color variations occur on the order of 2 to 130 cm, and there are minor variations in nannofossil and foraminifer abundance. Accessory minerals include glass shards (rhyolitic?) and pyrite (which commonly fills foraminifer tests). Bioturbation structures are rare, and when present include *Planolites*. A 2-mm-thick, dark green gray (10Y 5/2) lamina of nannofossil ooze with clay, foraminifers, and rare rhyolitic glass shards occurs at 14.5 mbsf (122-759B-3R-2, 25 cm).

Subunit IB (26.7–31.0 mbsf)

Subunit IB consists of light blue gray (5G 7/1) to green gray (5G 7/1) nannofossil ooze with foraminifers. Several color gradations were observed. At 26.9 mbsf (122-759B-4R-4, 36 cm) a rounded 1.4-cm-wide fragment of rhyolitic pumice was recovered. The Quaternary/lower Miocene contact occurs in

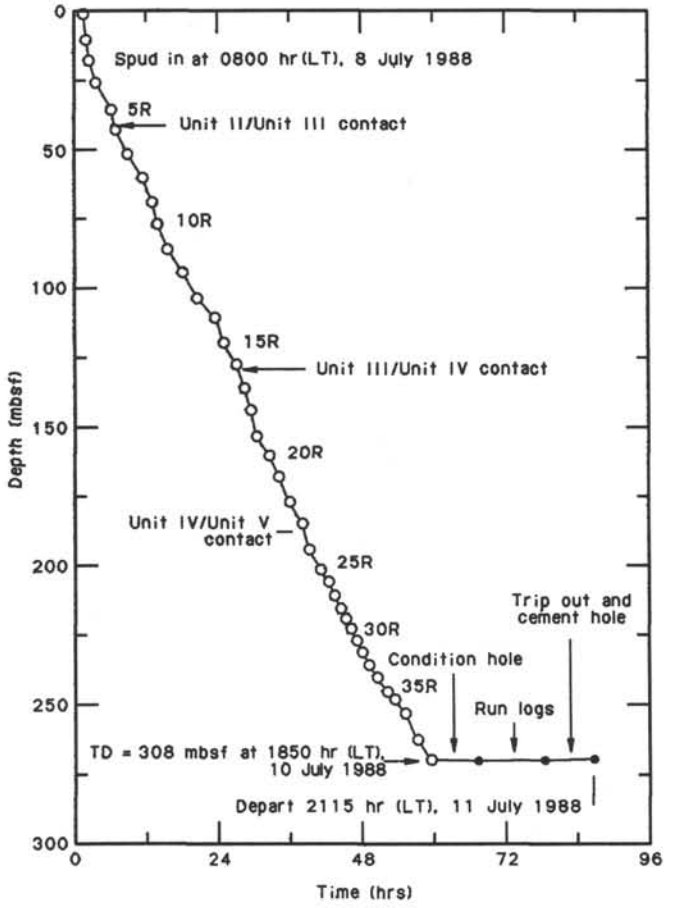

Figure 5. Total time (in hr) versus penetration depth (in mbsf) at Hole 759B. Core numbers are indicated.

the upper 7 cm of this subunit (see "Biostratigraphy," this chapter).

Unit II (31.0–40.5 mbsf)

Interval 122-759B-5R-1, 0 cm, to -5R-CC, 12 cm.

Unit II is composed of unconsolidated, structureless, yellow-brown (10YR 5/6) foraminifer quartz sand. The quartz grains are subangular and medium- to coarse-grained; some are stained yellow. Feldspar, mica (muscovite), and rock fragments are also present. The foraminifers are predominantly unbroken, and include both planktonic and some benthic forms. The contact between Units I and II occurs between cores (and thus was not observed).

Unit III (40.5–135.9 mbsf)

Interval 122-759B-6R-1, 0 cm, to -16R-1, 40 cm.

Unit III is 95.4 m thick and consists of fossiliferous limestone, dolomite, and interbedded silty claystone of late Triassic (Norian) age. Minor lithologies associated with claystone are siltstone and fine-grained sandstone. Figure 9 shows the lithologies recovered, which amount to only a small part of the succession (30% recovery) and Figure 10 is a summary of the components identified in Units III–V.

Carbonate rocks are dominant in Cores 122-759B-7R through -10R. Claystone is present in Core 122-759B-6R and in the lower half of the unit, in Cores 122-759B-11R through -15R. However, poor recovery does not permit the determination of relative proportions of carbonate and noncarbonate components, except through the interpretation of wireline logs (see "Downhole Measurements," this chapter).

The dominant types of limestone are calcareous mudstone to wackestone and subordinate packstone. These contain, in order of decreasing abundance, peloids, calcareous lithoclasts, skeletal debris, oncoids, and mudstone intraclasts. Peloid-sized grains bearing a single-layer oolitic cortex (superficial ooids) are locally present. Mollusk shells, echinoderm ossicles (echinoids), and green algae are the most common skeletal components. Calcite-replaced solitary corals characterize the wackestone recovered in Core 122-759B-13R (Fig. 11). Grains coated by coralline red algae and phylloid algae were seldom noted. Benthic foraminifers are present and most are micritized. The siliciclastic component in mudstone and wackestone does not exceed a few percent.

A few layers of well-sorted, quartz-rich, fine- to medium-grained, dolomitic calcarenite (grainstone and/or packstone) are present in Intervals 122-759B-11R-1, 0–27 cm (Fig. 12A), -11R-2, 0–35 cm, -12R-2, 0–65 cm, -13R-3, 62–70 cm (Fig. 12B), and -14R, 80–100 cm. The dolomitized carbonate fraction in these calcarenites contains skeletal debris, ooids, peloids, coated grains, echinoid fragments, and algae. The siliciclastic component, variably from 1% to 20% of the calcarenite, consists of quartz and feldspar along with minor pyrite and coal fragments. A 1-mm-thick coal seam is present in Interval 122-759B-7R-1, 17–18 cm (59.7 mbsf).

Fine to very fine oolitic and oncolitic grainstones, 5–20 cm thick, are also present (e.g., Interval 122-759B-13R-2, 30–37 cm), but are a very minor component. One piece of algal laminated wackestone with a cone-in-cone structure is present at 122-759B-11R-2, 75 cm. A 13-cm-thick shell bed is present in Interval 122-759B-16R-1R, 28–40 cm, at the base of Unit III. This bed consists of a coarse-grained mollusk coquina in which pelecypods and a few gastropods are tightly packed in a fine-grained skeletal, peloidal, wood-fragment-rich calcarenite matrix (packstone or grainstone). The shell layer fines upward and grades into virtually shell-free, laminated, calcarenite matrix, with scattered bioclasts. Thick-shelled *Gervillia*-type pelecypods, with wall structure reminiscent of present-day oyster shells, occur at the base of the coquina (Fig. 13).

Mudstone and wackestone facies are strongly burrowed. Intense reworking by large burrowers is common, and is responsible for color mottling (Fig. 14). *Chondrites*-type burrows are also present. Fenestral voids and birdseye structures are noticeable in mudstone and wackestone facies. Calcarenite layers are not burrowed, and display normal grading and parallel current laminae.

Pervasive, patchy dolomitizaton affects the carbonates of Unit III to a varying extent, but does not obliterate pristine sedimentary features in most of the unit.

The dominant limestone colors include gray (5Y 5/1), gray-brown (2.5Y 5/2), green-gray (10Y 5/2), and gray-brown (2.5Y 4/2). Less common colors are olive gray (5Y 4/2), black (7.5Y 2/0), and lighter tints of gray (e.g., light gray-brown, 2.5Y 6/2, and light gray, 10YR 7/1, 10YR 7/2, and 2.5Y 7/2). The lighter grays (e.g., 5Y 7/2) and light olive gray (5Y 6/2) tend to characterize some of the dolomites.

Claystone is interbedded with limestone in the lower half of Unit III. The claystone is black (2.5Y 2/0, N3, and 7.5Y 2/0) to very dark green-gray (10Y 3/1), or dark gray (N4, 5Y 3/1, 5Y 4/1, and 7.5Y 4/0), and has a silt fraction that averages 15%–20%, but is as high as 40%. Siltstone and fine-grained sandstone beds, 10–30 cm thick, are present within claystone units (e.g., Intervals 122-759B-7R-1, 0–30 cm, and -14R-1, 0–15 cm). The siltstone and fine-grained sandstone are com-

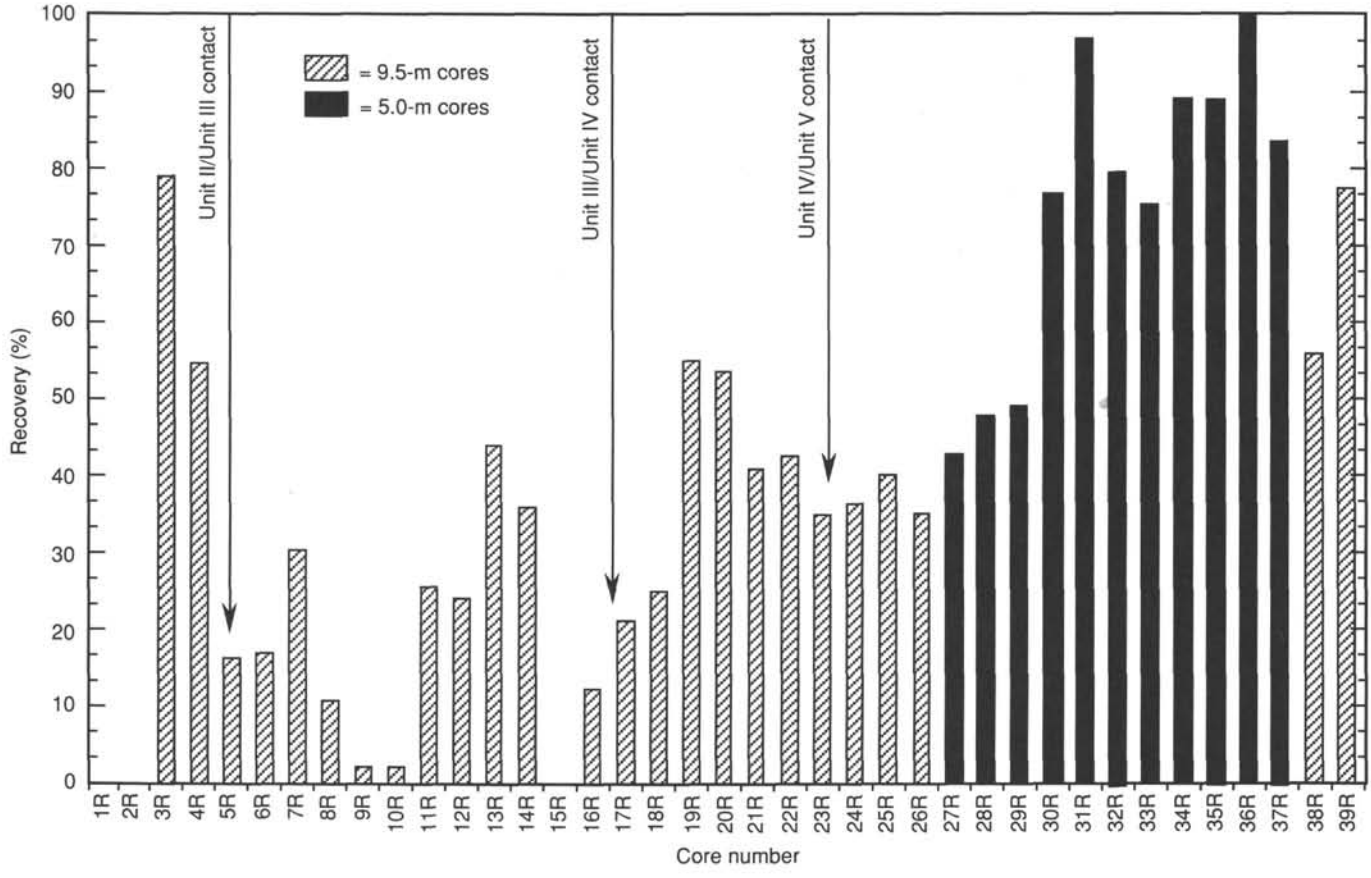

Figure 6. Core number versus recovery (%) for Site 759, showing lithologic units and enhanced recovery achieved by advancing half a core length (5.0 m) instead of a full core length (9.5 m). Arrows indicate position of lithological contacts.

posed of quartz and feldspar and contain up to a few percent of coalified plant debris. Coal layers were noted in Interval 122-759B-11R-2, 70–73 cm (Fig. 15). Sedimentary structures are common in the terrigenous lithologies. Claystone is often laminated or faintly banded and is seldom disturbed by burrowing. Coalified rootlets ("underclay" in coal cyclothems) penetrate into clayey siltstone in Section 122-759B-12R-1. Siltstone and clayey sandstone layers display parallel and convolute laminae, partially disturbed by bioturbation, and soft-sediment deformation (Fig. 16). Scattered pyrite nodules and pyritized grains and burrow-fillings are also associated with terrigenous lithologic types.

The upper boundary of Unit III was not sampled, but the sharp lithologic change and the extensive age gap between Cores 122-759B-5R and -6R suggest an unconformable contact. The lower boundary of Unit III is transitional and is marked by the relatively abrupt compositional change from carbonate (above) to terrigenous clastic (below). Below 122-759B-16R, 40 cm, claystone, siltstone and sandstone predominate, but limestone rocks similar to those observed in Unit III are found in deeper cores (e.g., Interval 122-759B-19R-3, 50 cm, through -19R-4, 60 cm, Interval 122-759B-22R-3, 10 cm, through 22R-CC, and Interval 122-759B-23R-1, 115 cm, through -23R-2, 140 cm).

Unit IV (135.9–205.0 mbsf)

Interval 122-759B-16R-1, 40 cm, to -23R-3, 0 cm.

Unit IV, 69 m thick and of late Triassic (Carnian–early Norian) age, is transitional between the overlying neritic carbonates that comprise Unit III and the underlying siliciclastic sediments that form Unit V. Most of the carbonate sediments are described in detail in the discussion of Unit III, whereas siliciclastic sediments are described in the discussion of Unit IV. The base of Unit IV is chosen at 205 mbsf, where the lowest appreciable limestone sequence occurs.

General Description

Unit IV is dominated by parallel-laminated, variably massive or bioturbated, black silty claystone and clayey siltstone with disseminated pyrite nodules. Siltier intervals are generally parallel-laminated; normally graded sequences have sharp bases and are less common. Bioturbation, including *Chondrites*- and halo-type burrows, occurs preferentially within these silty layers. Accumulations of carbonaceous matter along silty horizons enhance their recognition. Thin coal seams are associated with the silty horizons in Cores 122-759B-20R and -21R. Disseminated pyrite and pyrite nodules are found in Cores 122-759B-18R to -22R.

Coarser-grained layers of mixed siliciclastics and carbonates, interbedded with silty claystones and clayey siltstones, are present throughout Unit IV. Coarse- to fine-grained quartz sandstones were recovered in Cores 122-759B-17R and -18R (Fig. 17). These sandstone fragments are generally graded and carbonate-cemented. Sandstone fragments were preferentially recovered at the tops of cores and in the core catcher. Although recovery was poor in Cores 122-759B-17R and -18R (23% recovery), the interval represented by these cores (135.5–154.5 mbsf) corresponds with an interval of low gam-

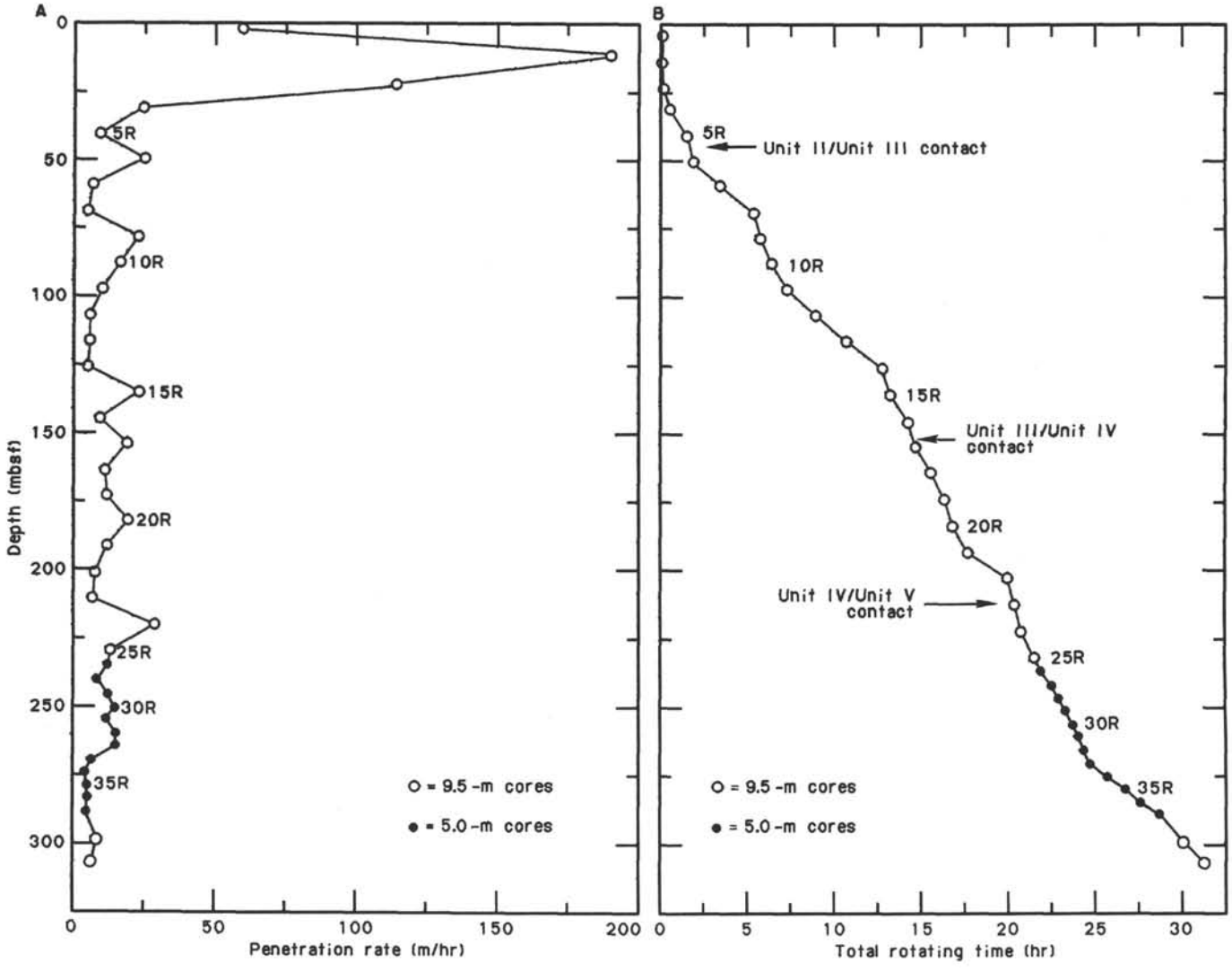

Figure 7. **A.** Penetration rate (m/hr) versus depth, Hole 759B. **B.** Total rotating time (hr) versus depth, Hole 759B.

ma-ray counts on the wireline log (140–150 mbsf; see "Downhole Measurements," this chapter).

Coarser-grained intervals also include carbonate wackestones, packstones and grainstones with shelly fragments and solitary corals (Fig. 18), and laminated siltstones. Bioclasts (mollusks and foraminifers), oncolites, and minor ooids compose the sand-sized fraction in the carbonates, with upward-fining sequences 1 to 1.5 m thick recovered in Cores 122-759B-19R and -23R, including intraformational breccias encased in carbonate mudstone in Core 122-759B-23R.

Detailed Description

Detailed descriptions of the carbonate and siliciclastic sediments are provided in discussions of Units III and V, respectively. Two minor lithologies from Unit IV are described here.

The upper portion of Unit IV contains a dark gray (5Y 4/1) sandy siltstone. Angular to sub-angular quartz is the dominant mineral observed in microscope study; rock fragments, feldspar, and accessory minerals compose most of the remainder of the components. This sandy siltstone is interbedded with the major lithologies, is generally parallel laminated and/or ripple cross-laminated, and is in some instances graded; a current regime is the depositional setting suggested for this lithology.

Core 122-759B-17R-1, 0–28 cm, contains two coarse- to medium-grained normally graded quartz sandstone beds. The sandstone is calcite cemented and the quartz grains are angular to sub-angular. Granule- to pebble-size fragments occur in the basal part of the lower sandstone bed.

Unit V (205.0–308.0 mbsf)

Interval 122-759B-23R-3, 0 cm, through -39R-CC, 17 cm.

Unit V is 103 meters thick and of late Triassic (Carnian) age. The major lithologies are silty claystone and clayey siltstone, with the silty claystone becoming more dominant in the lower part of the unit. Minor lithologies include: claystone (sideritic in part), sandy siltstone, coarse-grained quartz sandstone, and pyrite nodules. A brief description of each major and minor lithology follows.

Dominant Lithologies

Very dark gray (5Y 3/1) to black (5Y 5/2) silty claystone is the major rock type in Unit V. This silty claystone is variably massively bedded to laminated (Fig. 19). Biogenic sedimen-

Table 2. Lithostratigraphy of Site 759.

Unit	Lithology	Cores (122-759B-)	Depth (mbsf)	Thickness (m)	Environment	Age
IA	Light red-brown to pink foraminifer nannofossil ooze.	1R-1, 0 cm, to -4R-4, 25 cm	0.0–26.7	26.7	Pelagic, current winnowed(?).	Quaternary
IB	Light blue-gray to green-gray nannofossil ooze.	4R-4, 25 cm, to -CC, 13 cm	26.7–31.0	4.2	Pelagic.	Early Miocene
II	Yellow-brown foraminifer quartz sand with Mn grains.	5R-1, 0 cm to 5R-CC, 12 cm	31.0–40.5	9.5	Mixed terrigenous/ pelagic lag deposit on (?) unconformity above Triassic.	Early Miocene
III	Mainly gray carbonate grainstone, wackestone, packstone, and mudstone, interbedded with dark gray silty claystone.	6R-1, 0 cm, to 16R-1, 40 cm	40.5–135.9	95.4	Alternation of neritic limestones and paralic claystones suggests variations in sea level and/or locus of deltaic lobe deposition.	Late Triassic (Norian)
IV	Silty claystones with some coal, sandstones and interbedded carbonates as in Unit III.	16R-1, 40 cm, to 23R-3, 0 cm	135.9–205.0	69.1	Alternation of paralic claystones and neritic limestones suggests more deltaic version of Unit III environment.	Late Triassic (Norian to Carnian)
V	Dark gray, well-bedded silty claystones with coccoliths below Core 25R. Rare sandstones and limestones.	23R-3, 0 cm, to 39R-CC, 17 cm	205.0–308.0	103.0	Prodelta oxygen-poor muds with coccoliths and radiolarians; predominantly turbidites.	Late Triassic (Carnian)

tary structures are common to abundant, with *Chondrites*- and halo-type burrows most easily recognized. The burrows appear to be confined to distinct bedding horizons. The abundance of silty claystone decreases upward in the unit. Pyrite nodules are present within this lithology, and but preliminary inspection indicates that the abundance of pyrite increases towards the top of the hole.

Microscope study shows that the silty claystone contains clay minerals, quartz, minor feldspar, and rock fragments. Scattered carbonaceous opaque minerals were also observed and are partially responsible for the black color of the silty claystone; minor coal partings are preserved in Cores 122-759B-30R to -32R. The opaque minerals appear to decrease in abundance downhole, as does pyrite.

The second major lithology in Unit V is a dark gray (5Y 4/1) clayey siltstone. This clayey siltstone is laminated, with ripple cross-laminations becoming more evident as grain size decreases. Clayey siltstone decreases in abundance downhole. Biogenic sedimentary structures are rare to absent within the clayey siltstone. Microscopic features of these sediments are very similar to those of the silty claystones.

The silty claystone and clayey siltstone are interbedded throughout the unit, indicating that the depositional environments fluctuated. Siltier sediments are more abundant at the top of the unit and clay-sized sediments are more prevalent towards the base of the unit. Soft-sediment deformation (e.g., convolute bedding and syn-sedimentary minor faults) was observed in both lithologies and indicates instability in the sediment pile.

Minor Lithologies

A common lithology observed primarily in the deeper cores (Cores 122-759B-28R to -39R) is relatively hard, pale yellow (5Y7/3) authigenic carbonate identified as siderite that contains some quartz. The siderite is commonly laminated and interlayered with silty claystone (Fig. 20). The abundance of these layers and laminations increases downhole. The siderite is considered to be diagenetic (see "Summary and Conclusions," this chapter). Similar siderite is also observed infilling and/or surrounding burrows (Fig. 21); this supports the concept of a diagenetic origin. A siderite nodule approximately 5 cm in diameter was found in Core 122-759B-30R. Microscopic examination shows that the siderite consists of very small rhombohedra. In Core 122-759B-31R some radiolarian fragments were found in a siderite nodule.

Thin sandstone beds (Fig. 22) are graded and might be of turbidite origin (e.g., Core 122-759B-32R). One recrystallized algal limestone bed (Core 122-759B-33R, 5–40 cm) is also assumed to be a turbidite.

Discussion and Interpretation of the Depositional Environment

Depositional History of the Succession

The late Triassic stratigraphic succession at Site 759 consists of three units. The oldest, Unit V, is mainly a distal deltaic claystone sequence. The black color, pyritic/sideritic composition, lack of shelly fauna, presence of coccoliths, and

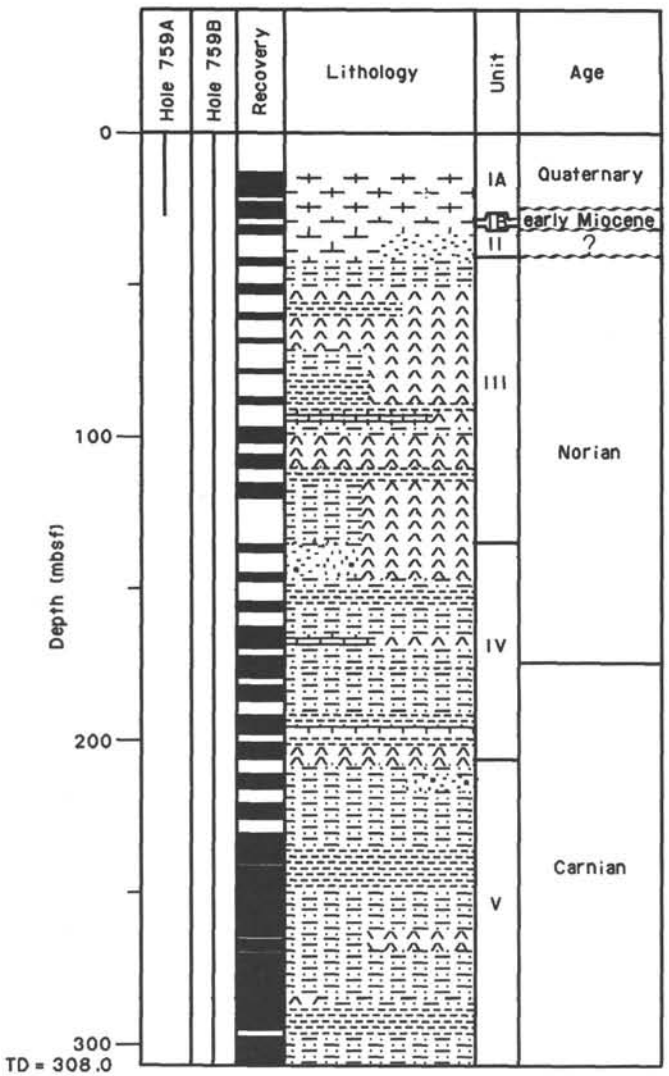

Figure 8. Lithologic column for Site 759, showing recovery, age, generalized lithologies, and lithologic units (see "Explanatory Notes," this volume, for key to symbols).

excellent preservation of laminations indicate restricted marine depositional conditions. This sequence shallows upward to Unit IV, which consists of interbedded limestone, sandstone, and claystone; rare coal seams also occur.

Units IV and V show a general upward-coarsening trend that is best interpreted as representing a general regression and progradation of a delta system. The association of scattered pyrite, abundant carbonaceous matter in siltier horizons, and lack of a diverse faunal component suggests that reducing, oxygen-depleted conditions prevailed at and below the sediment-water interface. Mass-transport processes deposited intervals of disturbed silty claystone and upward-fining sequences of carbonate grainstone to mudstone. Quartz sandstones occur at the top of Unit IV, and may mark the period of maximum regression.

The prevalence in Unit III of lithologies dominated by sediments rich in carbonate mud (carbonate mudstone, wackestone, packstone, and ostracode-bearing boundstone) suggest that deposition was in a marginal-marine, moderately low-energy environment. The presence of interbedded claystone and siltstone units indicates that localized carbonate banks formed in coastal areas dominated by river discharge. The paucity of non-skeletal grains, such as ooids (typical of high-energy marginal environments), and the lack of reef-derived debris excludes the development of organic buildups in the immediate vicinity of the depositional site.

The few packstone, grainstone, and coquina layers in Unit III (such as the one in Interval 122-759B-16R-1, 26–40 cm; Fig. 13) can be interpreted as storm deposits (tempestites) and they presumably were derived from nearshore shelly beach ridges ("cheniers").

Terrigenous sediment input probably controlled Unit III deposition at the site. Shifts in terrigenous clastic depocenters in deltaic areas, for example, occur as a result of switches of the distributary channel system. Similarly, shifts in the distribution of terrigenous sediments might have driven the onset and demise of carbonate deposition at Site 759, developing the acyclic repetition of carbonate and claystone. The wireline logs indicate that there are several upward-shallowing sequences (claystone, sandstone, and carbonate) that may be related to movement of distributary channels (see "Downhole Measurements," this chapter). Minor coal clasts in the limestones suggest that nearby coal swamps were eroded on occasion.

The shallow-water carbonates of Unit III are dolomitized in part, and contain fossils such as solitary corals, coralline red algae, green algae, small benthic foraminifers (miliolids), mollusks, and echinoderms. Peloids are common. Unit III is capped by a siltstone/claystone sequence at least 4 m thick. The sequence is truncated by a major unconformity beneath Tertiary pelagic sediments (Fig. 8). Reflection seismograms show this contact to be an angular unconformity (see "Seismic Stratigraphy," Site 761 chapter).

During late Middle to late Triassic times, deposition was largely fluviatile beneath the present-day Northwest Shelf, fluviodeltaic further to the north, and restricted distal deltaic to the south of Site 759 (Cook et al., 1985). Near Site 759, shallow-water carbonate banks provided a source for the carbonate detritus interbedded with siliciclastic sediments. Further south, during the late Triassic (Cook et al., 1985), carbonate sediments similar to those of Unit III transgressed southeastward across the older claystone, which had been deposited in a restricted marine basin. A similar situation may have developed near Site 759.

Although there was almost certainly some Jurassic and Cretaceous deposition at Site 759, uplift and erosion removed any such deposits, and eroded the top of the Triassic sequence. The erosional surface is overlain by a reworked sand (Unit II) consisting of quartz, manganese fragments, and early Miocene foraminifers (although the latter, as well as younger material, probably represent downhole contamination). This reworked sand might be of (early?) Cretaceous age and documents the onset of renewed deposition; it contains elements from both the Triassic sequence and a manganese pavement that once overlaid it (see "Lithostratigraphy," Site 760 chapter).

The reworked sand is overlain by pelagic carbonate (Unit I) consisting of nannofossil ooze with pelagic foraminifers. Subunit IB is early Miocene, and Subunit IA is Quaternary. The pelagic carbonates document the late(?) Cretaceous to Cenozoic sinking of the Wombat Plateau to lower bathyal depths. The disconformity between Subunits IA and IB was probably caused by erosive deep-water currents. Rhyolitic pumice in Subunit IB and glass shards in Subunit IA were probably derived from Quaternary eruptions in the Sunda volcanic arc (in which case the pumice was carried southward by flotation and the shards by wind transport).

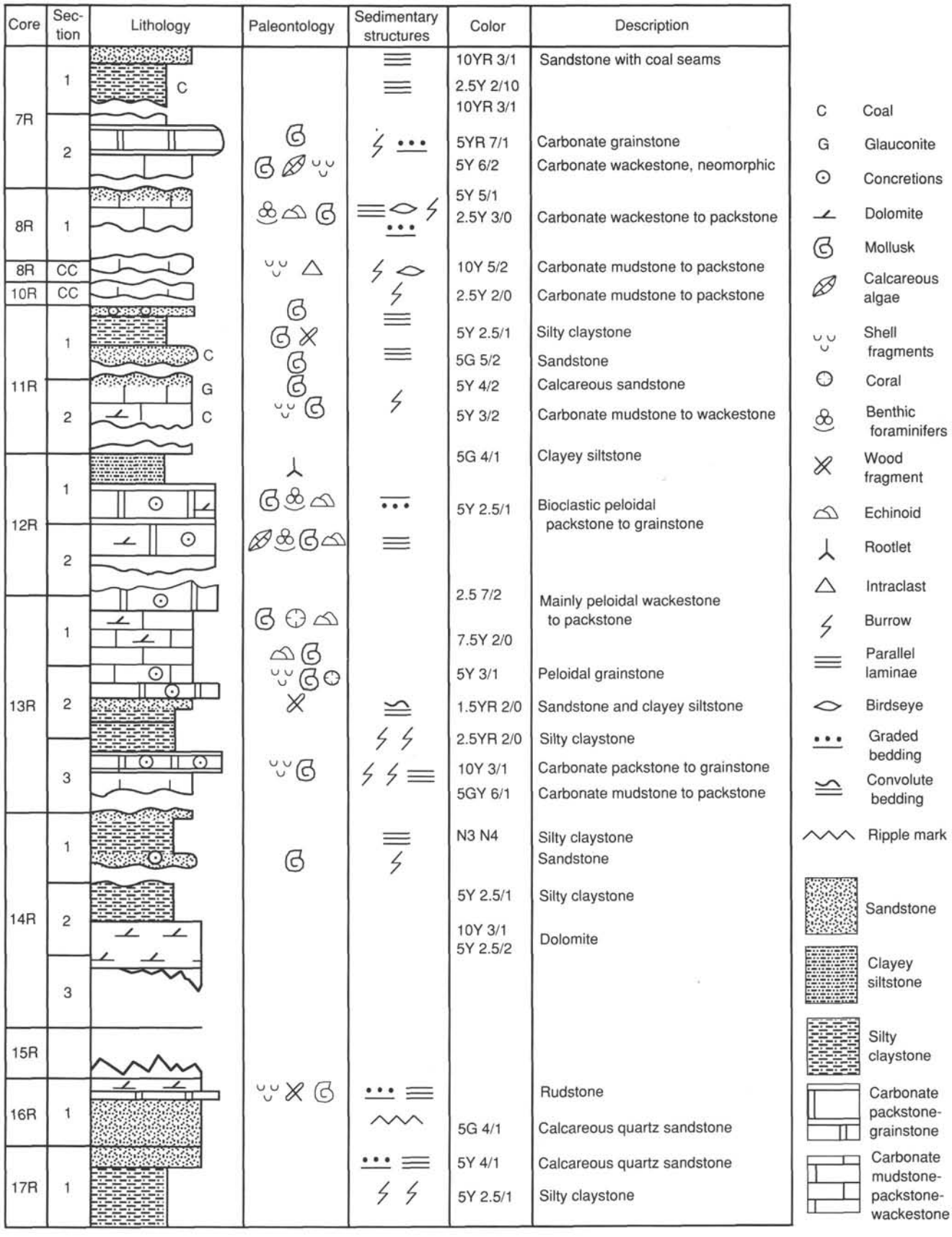

Figure 9. Succession of lithologic components recovered in Unit III (40.5–135.9 mbsf) at Site 759. Note that unrecovered intervals are not shown (overall recovery = 30%). Note key to lithological and paleontological symbols.

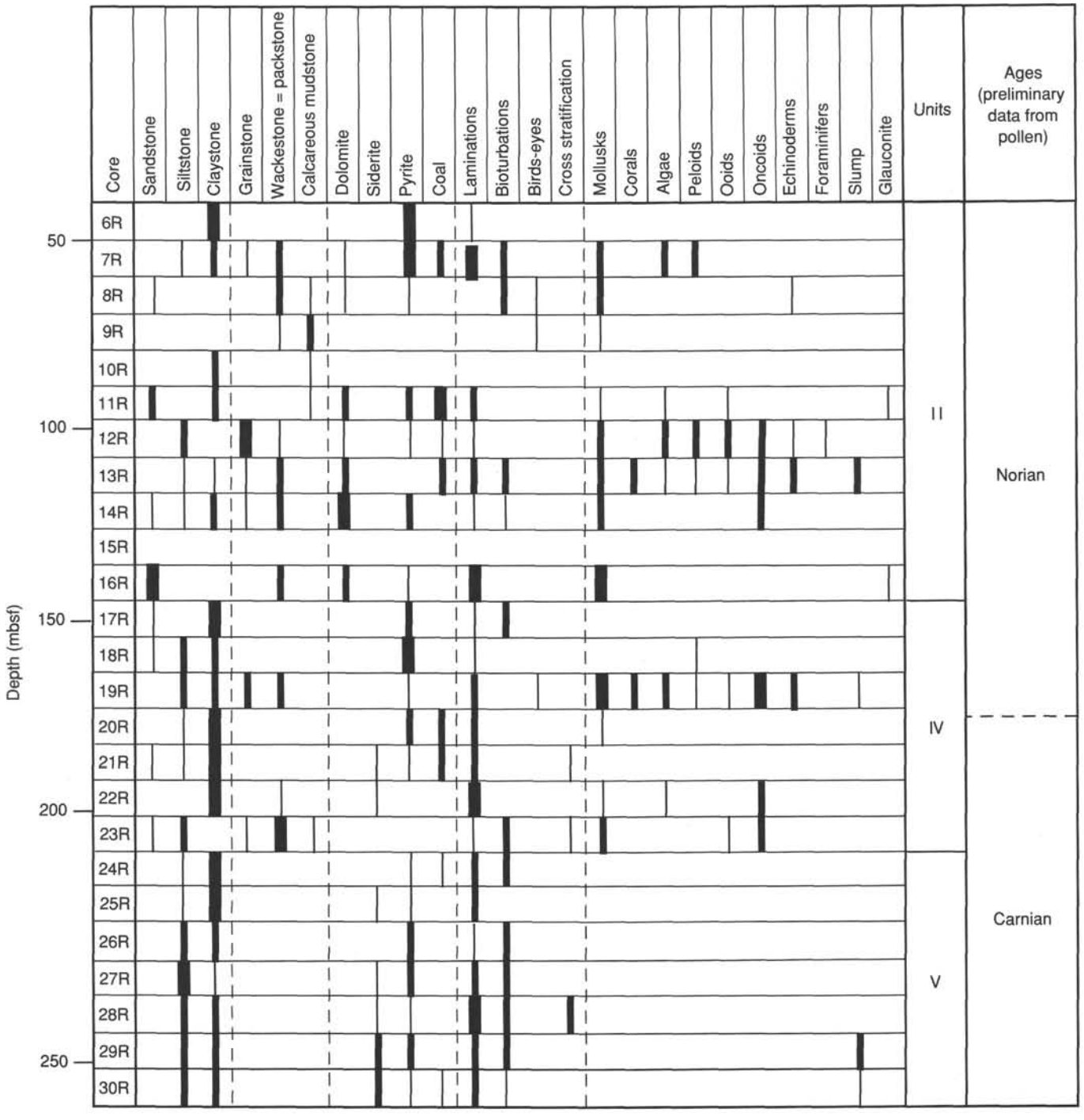

Figure 10. Summary of components of Units III–V, Site 759; data are shown individually for each core from Core 122-759B-6R through -30R. Depth intervals are uneven because penetration rates varied (see Table 1). Width of bar indicates relative abundance: thin bar = trace; thicker bar = common; thickest bar = abundant.

BIOSTRATIGRAPHY

Introduction

Hole 759B is situated on the northern edge of the Exmouth Plateau at 2092 meters water depth. The hole was drilled to 308 mbsf with a total recovery of 129.6 m of sediment. No sediment was recovered from the first two cores. With the exception of Cores 122-759B-3R to -5R, biostratigraphic investigations were carried out only on core-catcher samples. A summary of preliminary biostratigraphic results at Hole 759B is given in Table 3.

Hole 759B can be divided into two distinct parts: (1) the upper section (Units I and II) is composed largely of calcareous ooze and is dated using both calcareous nannoplankton and foraminifers, and (2) the lower section (Units III–V) consists of mudstone, limestone, siltstone, and sandstone and is dated most accurately using palynology, although nannoplankton also occur in this interval. The upper section is early Miocene to Quaternary in age, and contains a major hiatus, while the lower section is late Triassic (Carnian-Norian) in age, and represents the oldest marine material recovered by deep-sea drilling.

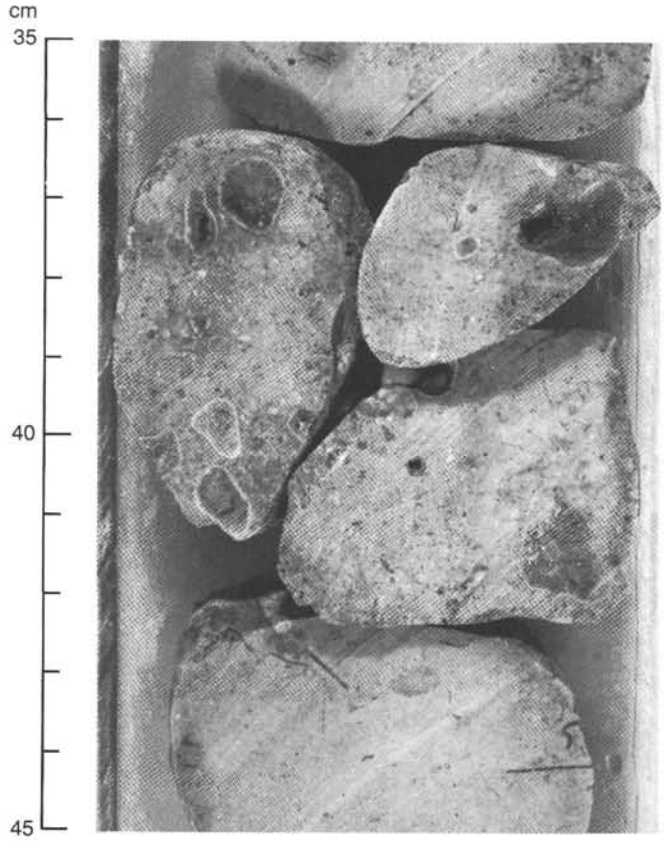

Figure 11. Interval 122-759B-13R-1, 35–45 cm. Calcite-replaced solitary corals characterize the skeletal peloidal wackestone, burrowed and faintly laminated, with solitary, ahermatypic coral.

All depths referred to are sub-bottom depths (mbsf), and samples are from the core catcher (CC) unless otherwise specified.

Calcareous Nannofossils

The top three cores recovered at this site are composed of calcareous ooze and microfossiliferous quartz sand, contain well-preserved nannoplankton, and can be accurately dated using calcareous nannofossil stratigraphy. The interval from the top of Core 122-759B-3R to Core -4R-4, 25 cm, is Quaternary in age and lies between the *Pseudoemiliania lacunosa* Zone (NN19), and the *Emiliania huxleyi* Zone (NN21) of Martini (1971). Nannofossil assemblages are dominated by *Emiliania huxleyi*, *Pseudoemiliania lacunosa*, *Rhabdosphaera claviger*, and *Helicosphaera kamptneri*. The interval from Core 122-759B-4R-4, 25 cm, through Core -5R is early or early middle Miocene in age, within the *Helicosphaera ampliaperta* (NN4) or *Sphenolithus heteromorphus* (NN5) Zone of Martini (1971). This is indicated by the combination of the presence of *Sphenolithus heteromorphus* with the absence of *Sphenolithus belemnos*. The presence of *Discoaster formosus* would favor the age being NN5, as the range of this secondary marker is believed to be limited to this zone (e.g., Martini, 1971). These assemblages are dominated by *Cyclococcolithus floridanus*, *Discoaster deflandrei*, *Sphenolithus moriformis*, and *S. heteromorphus*. Detailed stratigraphy was carried out on either side of the lithologic break in Core 122-759B-4R-4, 25 cm; samples above this level contain the Quaternary assemblage, whereas assemblages below it are early Miocene. There is, therefore, an unconformity at Core

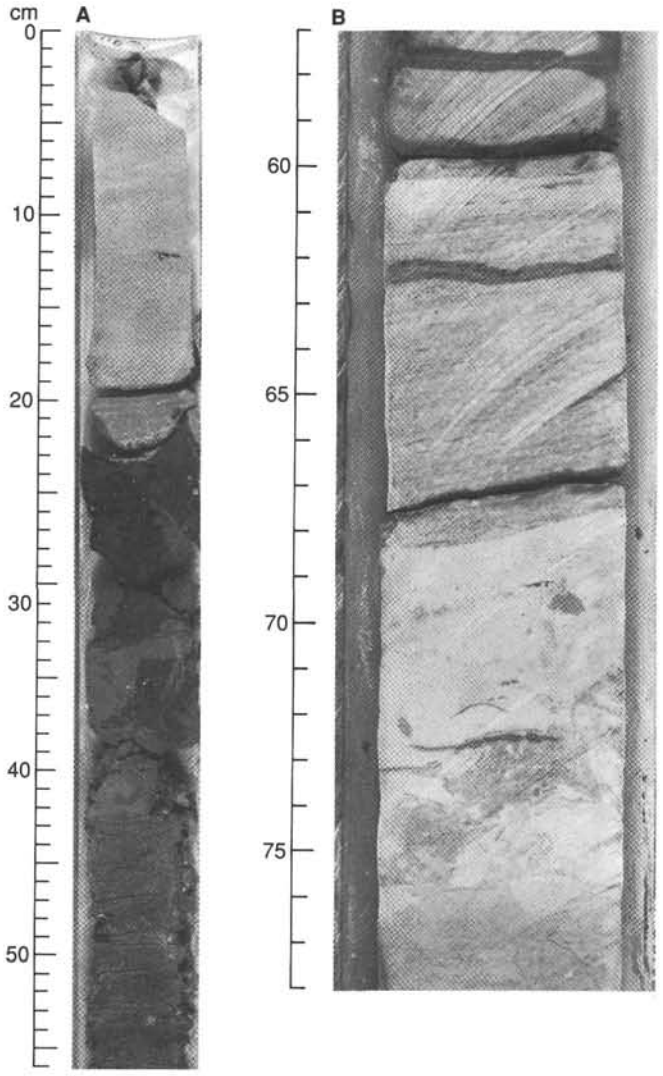

Figure 12. **A.** Interval 122-759B-11R-1, 0–56 cm. Parallel-laminated and graded bed of calcarenite (grainstone), with scattered mollusks and coalified wood fragments. Claystone, silty claystone, and fine clayey sandstone below 22 cm are intensely disturbed by drilling. **B.** Interval 122-759B-13R-3, 57–78 cm. Bioturbated, fossiliferous wackestone and mudstone (below) overlain by parallel-laminated grainy sediment, partly dolomitized (probably grainstone).

122-759B-4R-4, 25 cm, that represents approximately 15 m.y. and corresponds to the boundary between Subunits IA and IB.

Cores 122-759B-7R through -24R are barren of calcareous and siliceous microfossil groups and of dinoflagellates, indicating that these sediments are largely nonmarine or paralic in origin. The sediments from Core 122-759B-25R through -39R possess numerous nannofossiliferous intervals. They contain an assemblage of at least seven different forms, three of which have been previously described by Jafar (1983) from upper Triassic (Rhaetian and Norian) sediments from Germany and Austria. These are *"Tetralithus" cassianus*, *Prinsiosphaera triassica*, and *Hayococcus floralis*, the latter taxon being by far the most abundant. At least four other undescribed forms have been observed and warrant future detailed taxonomic investigation. From our brief light-microscope study, all of these taxa have a very simple construction and appear to have been replaced with a highly birefringent mineral, possibly siderite.

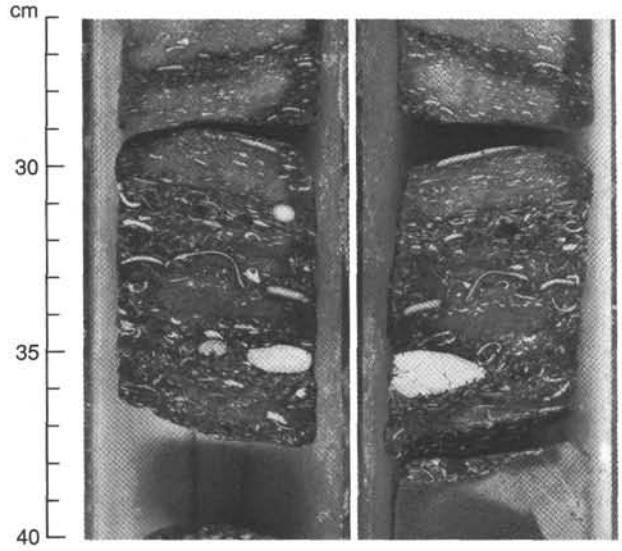

Figure 13. Interval 122-759B-16R-1, 26–40 cm (both the working and archive halves of the core are shown). A coarse-grained shell layer, 13 cm thick, with mollusk shells packed in a fine-grained, skeletal, peloidal, wood-fragment-rich matrix (packstone) occurs at the base. Note the normal grading of mollusk shell size, the convex-upward orientation of shells (indicative of current transport), and the few thick-shelled pelecypods .

The presence of these various taxa, which have not been observed above the Triassic, and the absence of the numerous marker species that characterize lower Jurassic sediments, including *Annulithus arkelii*, *Crucirhabdus primulus*, *Schizosphaerella punctata*, and *Parhabdolithus liasicus*, suggests that the interval is Triassic in age. This is supported by the palynology, which indicates a middle Triassic age.

There appear to be two dominantly fossiliferous intervals, from Core 122-759B-25R to Core -27R, and from Core 122-759B-36R to Core -39R. Samples within these intervals contain common and abundant nannofossils. Between these two intervals nannofossils are rare and only occur in isolated samples. This indicates that there were two periods of marine deposition separated by an episode of largely paralic or nonmarine deposition, although the rarity of nannofossils in the intermediate interval may be the result of poor preservation.

The discovery of nannofossils in sediments of late Triassic age in Hole 759B, despite their uncertain taxonomic affinities, is significant because these are the oldest known taxa that can be directly related to later Mesozoic and Cenozoic nannofossil evolutionary lineages.

Planktonic Foraminifers

Well-preserved assemblages of Quaternary and Neogene planktonic foraminifers were recovered from Cores 122-759B-3R to -5R. In contrast, planktonic foraminifers were not found from Cores 122-759B-6R to -39R. This is because the sediments in those cores were deposited in nonmarine to shallow-marine environments and/or prior to the first appearance of planktonic foraminifers. As typical low-latitude faunas dominate the Neogene and Quaternary assemblages, the zonal scheme of Blow (1969) was applied.

A Pleistocene fauna was recovered from Section 122-759B-3R-CC through Section -4R-3. The planktonic foraminiferal assemblage is dominated by *Globorotalia menardii*, *Globorotalia tumida*, *Globigerinoides sacculifer*, *Pulleniatina*

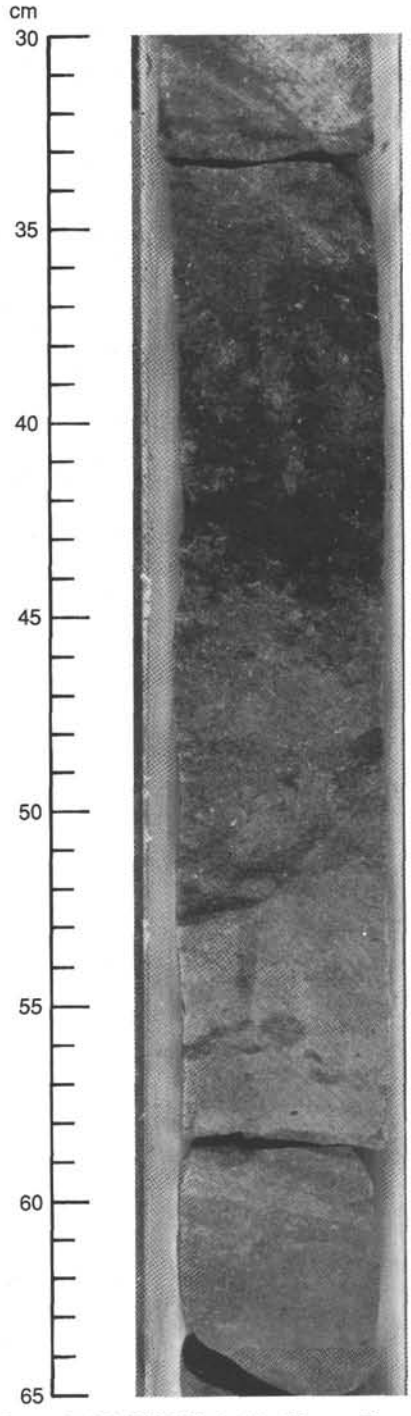

Figure 14. Interval 122-759B-7R-2, 30–65 cm. Burrowed peloidal skeletal wackestone and packstone, partly dolomitized (light). A well-sorted grainstone layer occurs at 59–65 cm.

obliquiloculata, and *Spharoidinella dehiscens*, which are typical of other low-latitude sites in the Indian Ocean (Vincent, 1977). The presence of *Globorotalia truncatulinoides* and a form close to *Globorotalia tosaensis* assigns this sample to the Pleistocene, Zone N22.

Sections 122-759B-4R-4 to 4R-CC are characterized by a dominance of the genus *Globigerinoides* (i.e., *G. triloba*, *G. sacculifer*, *G. altiapertura* and *G. diminutus*). The occurrence of these *Globigerinoides* species and the lack of the *Praeor-*

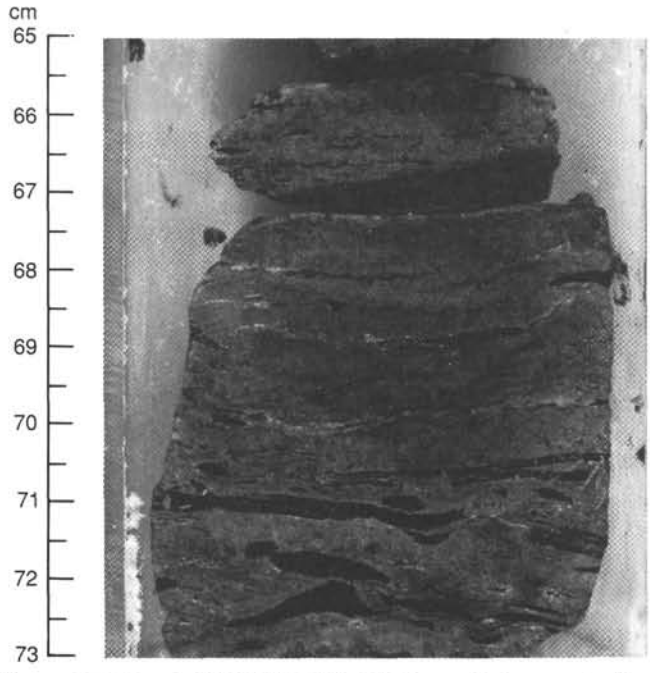

Figure 15. Interval 122-759B-11R-2, 65–73 cm. Coal layers in fine-grained clayey sandstone.

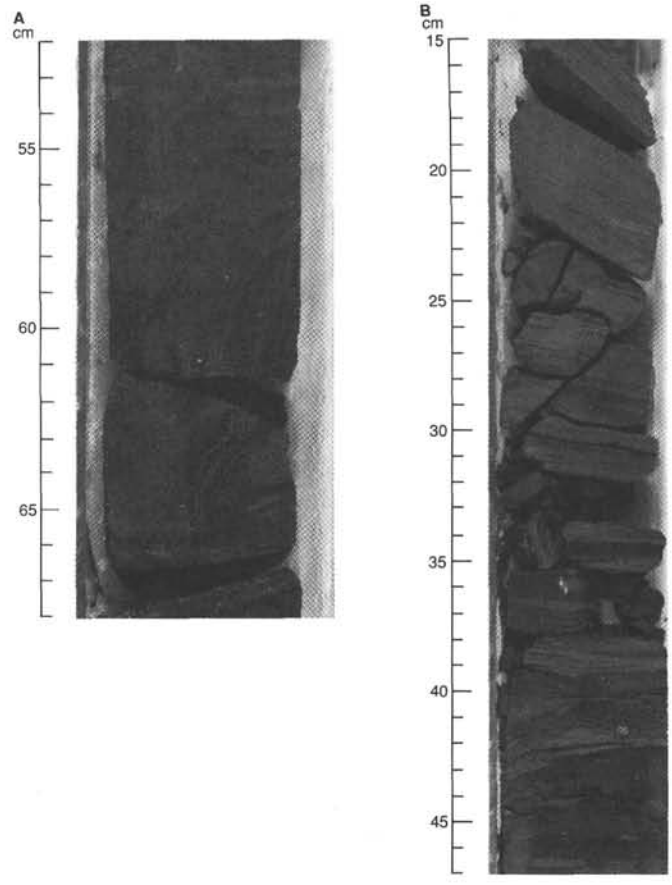

Figure 16. **A.** Interval 122-759B-13R-2, 52–68 cm. Convoluted (slumped) fine-grained clayey sandstone. **B.** Interval 122-759B-7R-1, 15–47 cm. Parallel-laminated, wood-fragment-rich, fine-grained sandstone layer (15–31 cm) and alternating claystone and fine-grained clayey sandstone, partially disturbed by bioturbation and soft-sediment deformation (loading) (31–49 cm).

bulina-Orbulina group and of *Catapsydrax dissimilis* indicate an early Miocene age (Zone N7). Pliocene and upper to middle Miocene sediments appear to be missing in this hole.

Sample 122-759B-5R-CC yielded mixed Pleistocene and Miocene assemblages as described above, with predominantly sand-size planktonic foraminifers present. This sample is thought to be the result of downhole contamination and washing-out of the larger forms, with possibly some of the lower Miocene being *in situ*. The remainder of the section does not contain planktonic foraminifers.

Thin sections were made of 32 samples in Units III, IV, and V. Several carbonate samples yielded miliolid, involutid, and ammodiscid foraminifers of late Triassic affinities. These samples include: 122-759B-8R-1, 34–37 cm, -10R-CC, -12R-2, 24–26 cm, and -19R-CC. Further detailed shore-based investigations are planned for these taxa.

Radiolarians

The sediments drilled at Site 759B contain very few radiolarians. Sample 122-759B-3R-2, 119–121 cm, contains an undifferentiated Quaternary radiolarian fauna, including *Anthocyrtidium angulare*, *Didymocyrtis tetrathalamus*, *Stylacontarium aquilonium*, and *Theocorythium trachelium*. Section 122-759B-3R-CC contains only rare and broken forms cited above. Section 122-759B-4R-CC is barren of radiolarians. A poorly sorted sandstone in Section 122-759B-5R-CC contains reworked Quaternary radiolarians assignable to *Stylacontarium acquilonium* and broken, poorly preserved collosphaerids. Radiolarians do not occur in Cores 122-759B-6R through -29R. Section 122-759B-30R-CC contains poorly preserved radiolarians assigned to *Capnodoce*? sp. This genus makes its first occurrence in the upper Triassic (lower Carnian). A fragment of *Acanthocircus* sp. was also observed in a strewn slide in Section 122-759B-30R-3. *Acanthocircus* first occurs in the Middle Triassic (Ladinian). Sections 122-759B-31R-CC to -39R-CC are completely barren of radiolarians.

A dark brown, reworked, chert fragment in Sample 122-759B-30R-1, 3–4 cm, contains a single radiolarian, assignable to *Thanarla* sp., and a Cretaceous foraminifer. The genus *Thanarla* is restricted to the Cretaceous.

Ostracode fragments occur in the residues of material from Cores 122-759B-9R, -11R, and -13R sieved for radiolarians. Plant cuticle, carbonized wood fragments, and non-age-diagnostic megaspores were found in Cores 122-759B-20R, -21R, -24R, -27R, -29R, -32R, -37R, and -39R.

Palynology

The upper five cores recovered at this site are barren of palynomorphs. The interval from Sample 122-759B-6R-CC through Sample -20R-1, 60–64 cm, contains variably abundant but predominantly poorly to moderately preserved palynomorphs. Samples 122-759B-9R-CC, -12R-CC, -16R-CC and -19R-CC are barren. This interval is Norian in age and belongs to the *Minutosaccus crenulatus* Zone (Dolby and Balme, 1976; Helby et al., 1987), indicated by the dominance of *Falcisporites australis* and the rare occurrence of *Samaropollenites speciosus*. *Minutosaccus crenulatus*, *Enzonalasporites vigens*, *Semiretisporis denmeadi*, and *Playfordiaspora velata* occur in variable abundance. The environment of this interval evidently fluctuated several times between open marine and coal swamp conditions. Marine conditions are indicated by the presence of dinoflagellates (undescribed species of *Rhae-*

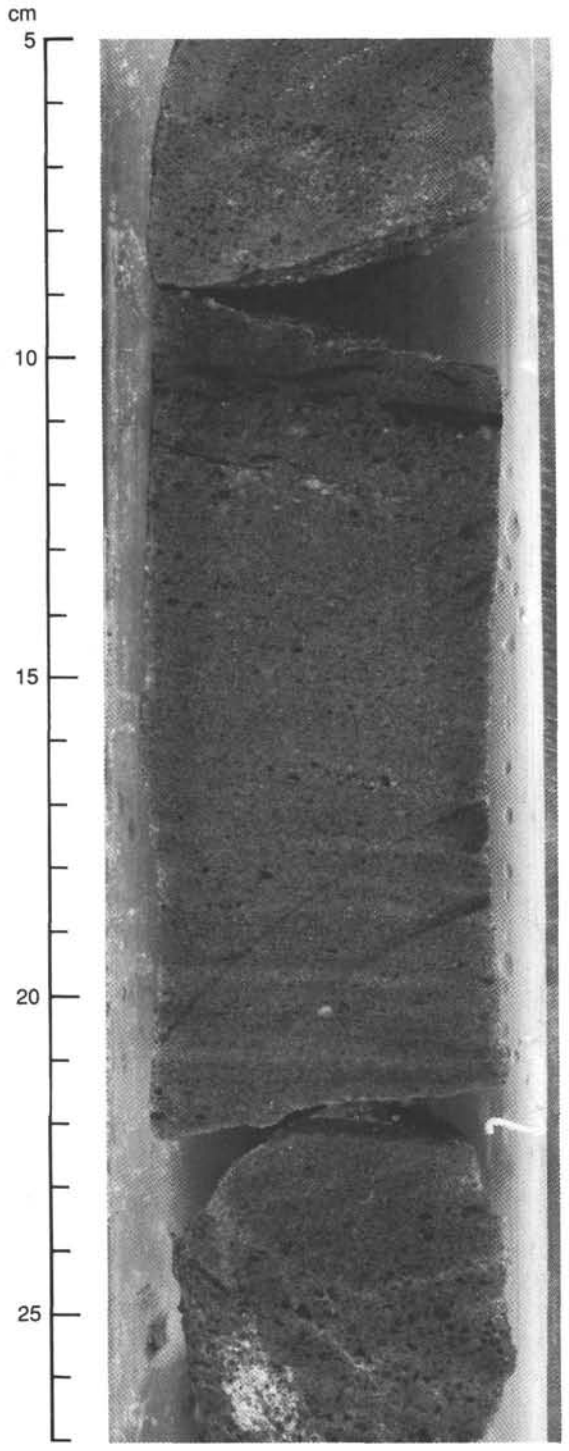

Figure 17. Interval 122-759B-17R-1, 5–27 cm. Coarse- to fine-grained carbonate-cemented sandstone containing coal flakes and layers, as well as quartz, feldspar, and rock fragments.

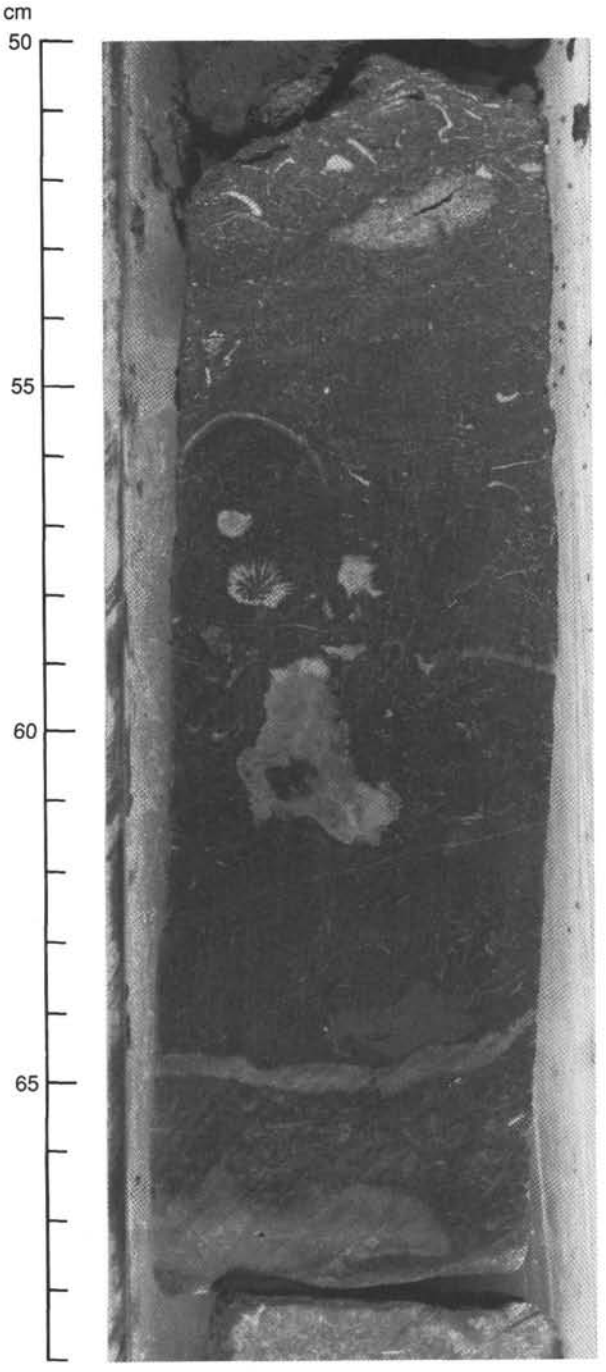

Figure 18. Interval 122-759B-19R-3, 50–69 cm. Carbonate wackestone containing shelly fragments, including solitary corals.

togonyaulax and *Dapcodinium*) and acritarchs from Sample 122-759B-7R-CC through Sample -10R-CC. However, the presence of the freshwater alga *Plaesiodictyon* and the absence of marine palynomorphs in Samples 122-759B-11R-CC and -18R-CC indicate a nonmarine environment (e.g., a flood plain or swamp); this interpretation is supported by high proportions of cuticles and wood fragments in these samples.

Samples 122-759B-13R-CC, -14R-CC and -17R-CC contain the acritarchs *Plaesiodictyon* and *Botryococcus*, but no dinoflagellates. This assemblage indicates restricted marine conditions. Sample 122-759B-16R-1, 18–20 cm, and Sample -19R-1, 72–76 cm, contain several species of the dinoflagellate genus *Shublikodinium* and undescribed species of the dinoflagellate genus *Hebecysta*, which indicate open-marine conditions.

The interval from Sample 122-759B-20R-2, 60–64 cm, through Sample -21R-CC contains an assemblage of nonmarine palynomorphs, dominated by spores and cuticles. Megaspores and the freshwater alga *Plaesiodyction* are common. The abundance of *Samaropollenites speciosus* and *Enzonalasporites vi-*

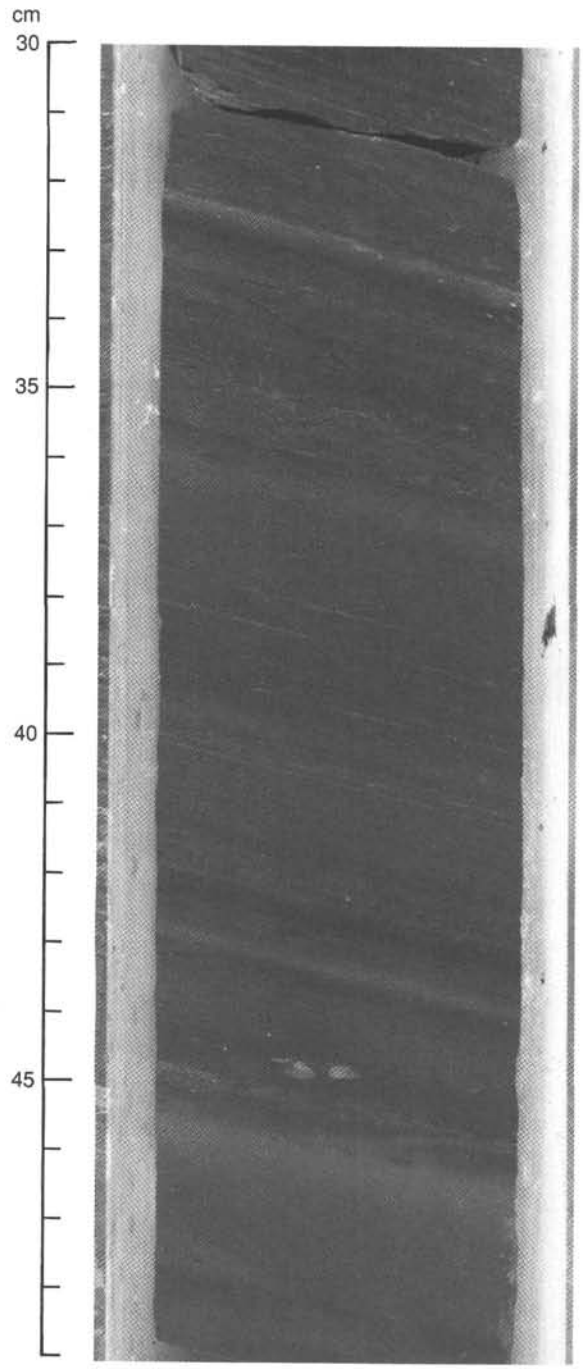

Figure 19. Interval 122-759B-39R-4, 30–49 cm. Upward-fining sequences consisting of pale olive sideritic clayey siltstone and very dark gray silty claystone, typical of Unit V. The tilt of the laminae is caused in part by hole deviation. *Chondrites*-type burrows are visible, among others. This interval probably represents a prodelta turbidite sequence.

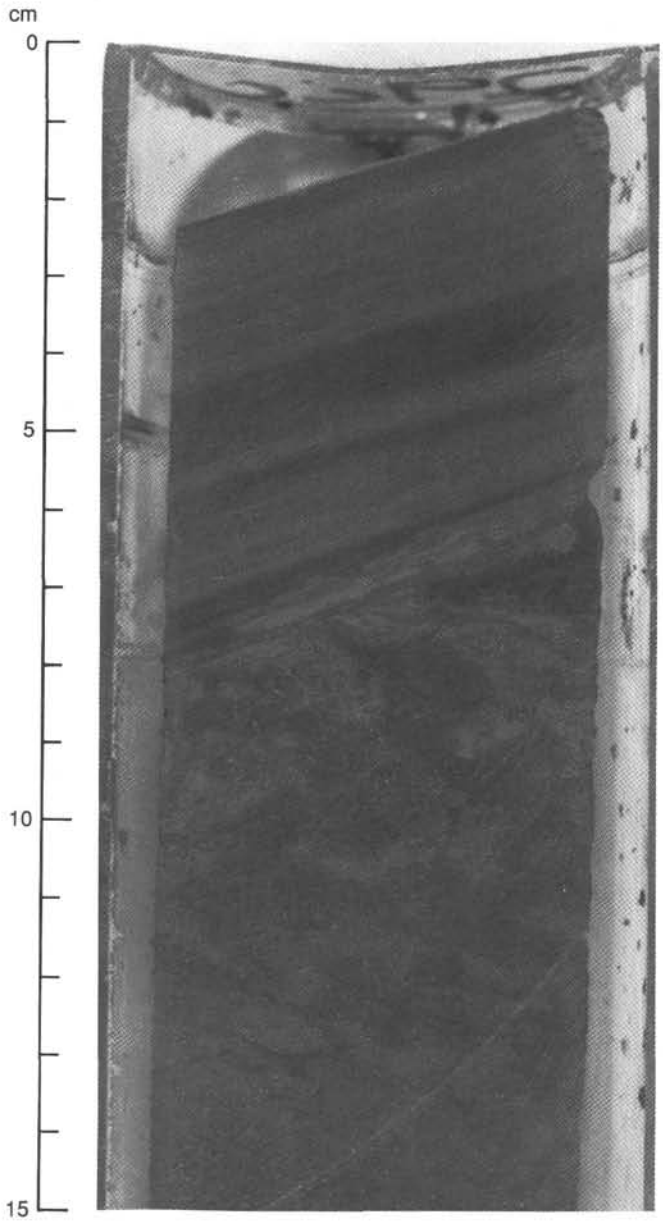

Figure 20. Interval 122-759B-29R-CC, 0–15 cm. Laminated silty claystone, with lighter sideritic layers, overlying clay- to sand-sized slumped material. Slumping probably occurred down an oversteepened prodelta face.

gens and the increase in abundance of *Falcisporites australis* indicate a late Carnian age (i.e., *Samaropollenites speciosus* Zone Subunit B; see Dolby and Balme, 1976 Helby et al., 1987). Samples 122-759B-23R-CC and -24R-CC are barren.

The interval from Sample 122-759B-25-CC through Sample -39-CC contains a pollen-dominated spore-pollen assemblage. Cuticles are common, whereas acritarchs and *Plaesiodictyon* are rare. The palynomorph assemblage indicates a restricted marine environment. However the occurrence of coccoliths in this interval is indicative of open-marine conditions. This could be interpreted as resulting from either a high influx of terrigenous material or high sedimentation rates during marine conditions (e.g., a delta-front environment). The presence of *Samaropollenites speciosus*, *Enzonalasporites vigens*, *Falcisporites australis*, *Staurosaccites quadrifidus*, and *Camerosporites pseudoverrucatus* in this interval indicates a late Carnian age (i.e., *Samaropollenites speciosus* Zone, Subunit B; see Dolby and Balme, 1976; Helby et al., 1987).

Discussion

The ages obtained using different microfossil groups at Hole 759B agree well, with one minor exception (Table 3). The foraminiferal age of Cores 122-759B-4R-4, 25 cm,

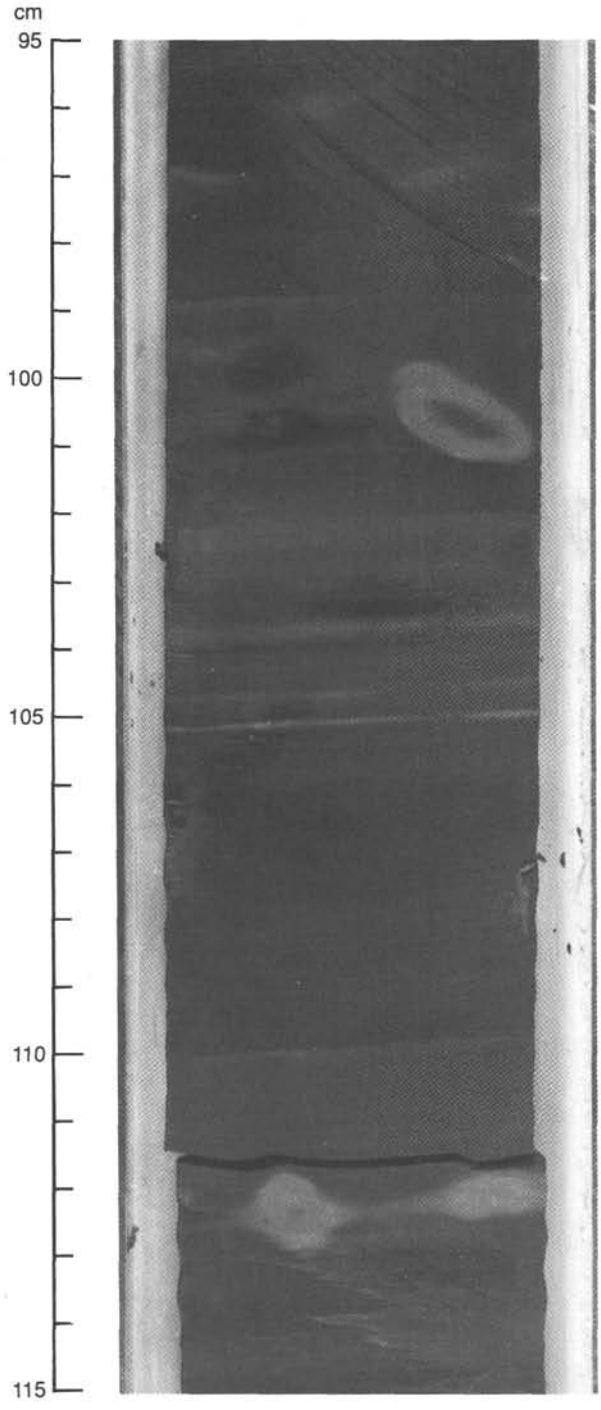

Figure 21. Interval 122-759B-36R-1, 95–115 cm. Dark gray silty claystone, with lighter sideritic layers and siderite infilling and surrounding burrows, including one halo-type burrow.

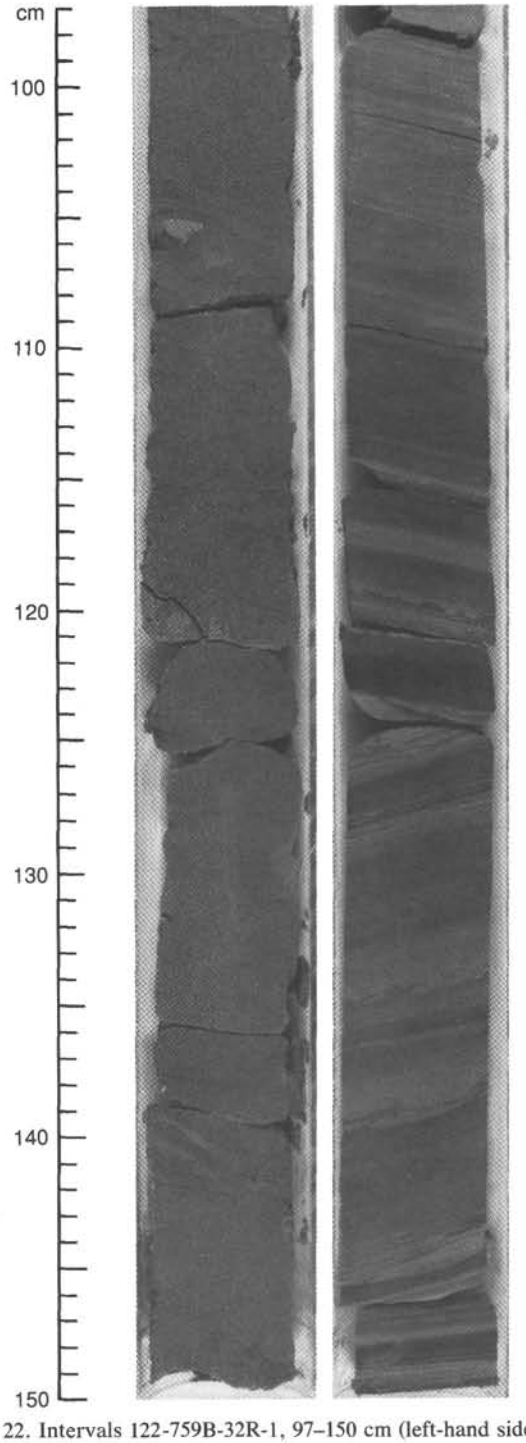

Figure 22. Intervals 122-759B-32R-1, 97–150 cm (left-hand side), and -32R-2, 97–150 cm (right-hand side). Gray, cross-laminated, silty sandstone (right-hand side), deposited in an environment dominated by thin-bedded to laminated silty claystone, typical of Unit V. The sandstone is quartzose and contains pyrite, coal fragments, and a sideritic nodule; it is probably a tempestite formed as the result of a storm. The claystone contains sideritic laminae and load casts.

through -5R-CC is within Zone N7 (early Miocene). The nannofossil age of this material is within Zones NN4 or NN5, which are of late early Miocene or early middle Miocene age. Foraminiferal Zone N7 correlates with nannofossil Zone NN4 in most time scales (e.g., Berggren et al., 1985; Haq et al., 1987), but not with nannofossil Zone NN5 (the age preferred by the nannofossil paleontologists on the basis of the range of *Discoaster formosus*). This problem, which may result from

Table 3. Biostratigraphic summary of ODP Hole 759B.

Cores	Lithologic unit	Foraminifer zone	Nannofossil zone	Radiolarian zone	Palynological zone	Age
122-759B-						
3R to 4R-4, 25 cm	IA Nannofossil-foraminifer ooze	N22	NN19 to NN22	Rare Quaternary taxa	Barren	Quarternary
4R-4, 25 cm to 4R-CC	IB Nannofossil-foraminifer ooze	N7	NN4 to NN5	Barren	Barren	early Miocene
5R	II Quartz-foraminifer sand	N22 and N7	NN19-22 and NN4/5	Rare Quaternary taxa	Barren	early Miocene
6R to 16R-1, 40 cm	III Carbonates, mudstones	Rare Triassic taxa	Barren	Barren	*Minutosaccus crenulatus* Zone	late Triassic (Norian)
16R-1, 40 cm to 23R-3	IV Transitonal	Rare Triassic taxa	Barren	Barren	*Minutosaccus crenulatus–Samaropollenites speciosus* Zone	late Triassic (Carnian-Norian)
23R-3 to 39R-CC	V Mudstones, minor carbonates	Rare Triassic taxa	Common Triassic taxa	middle or late Triassic taxa	*Samaropollenites speciosus* Zone	late Triassic (Carnian)

the diachroneity of one of the microfossil zones, warrants further investigation.

The most definitive ages for the Triassic are provided by palynology, and are in the Carnian to Norian interval. The ages from other fossil groups concur, given the low resolution currently possible in this interval. This sequence shows potential for the future development of an integrated Upper Triassic biostratigraphy on the basis of calcareous nannoplankton, foraminifers, and palynology.

From the distribution of the various microfossil groups, it can be concluded that a large part of Units III–V were deposited in nonmarine or paralic environments, with the exception of two intervals between Cores 122-759B-25R and -27R and Cores 122-759B-36R and -39R, which were deposited under more open marine conditions.

Summary

Hole 759B recovered Cenozoic sediments resting directly on a section of Triassic age. The Cenozoic section consists of a Quaternary sequence resting unconformably on sediments of early Miocene age. These sediments in turn lie unconformably on a section of late Triassic (Carnian-Norian) age.

PALEOMAGNETICS

The archive core sections from Hole 759B were measured at 10-cm intervals using the 2G-Enterprise 760R cryogenic magnetometer. All of these sections were also demagnetized at 9 mT and remeasured.

The natural remanent magnetization (NRM) intensities from the nannofossil-foraminiferal oozes of Unit I (Cores 122-759B-3R to -5R) range from 1.5 to 5 $\times$ 10^{+2} A/m. After 9-mT alternating-field demagnetization the intensity decreased to 10%–50% of NRM. The declination changes dramatically but the inclination remains mostly unchanged. Inclinations from these oozes average about −40°, which is very close to the present magnetic field direction at this site (about −32°); Unit I was dominated by negative values, which indicate normal southern hemisphere polarity. However some short polarity-reversal events were measured in Unit I.

The quartz-foraminiferal sand of Unit II (Core 122-759B-5R) is somewhat less magnetized, so the NRM intensities in this Unit II range from 0.8 to 1.5 $\times$ 10^{+2} A/m. The effect of 9-mT alternating-field demagnetization is very significant and the intensities decreased to 50% of NRM, but there was no dramatic change in the direction of the magnetization. These directions indicate a normal polarity with several reversal events. The quartz-foraminiferal sand unit may correspond to the upper part of Chronozone C5C (Haq et al., 1987), which shows two short reversal events, labeled 5C-1 and 5C-2 by Harland et al. (1982).

The mudstones of Triassic Units III through V are weakly magnetized. The NRM intensities range from 0.5 to 1.5 $\times$ 10^{+3} A/m. The 9-mT alternating-field demagnetization had little effect on the NRM intensities, which decreased slightly, whereas the inclination became shallower. The directions are mostly of normal polarity, except for a few spikes in sections that show positive inclination with very strong intensity. However, after AF demagnetization most of these positive inclinations became negative and intensity dropped dramatically.

Owing to severe core disturbance and probable magnetic overprinting, the whole-core measurements of Units III through V proved of little practical use. Moreover, two major factors prevented us from interpreting these data: (1) poor paleomagnetic records in the sediments (especially Unit III), and (2) inability to completely remove overprints with the 9-mT field available on the shipboard pass-through system. The latter problem cannot be remedied, but the overprints should be removable after shore-based analysis of discrete samples with alternating field demagnetization at higher field intensities and/or thermal treatment.

For this reason, a pilot set of 10 discrete samples from Cores 122-759B-22R to -39R was measured with the cryogenic magnetometer. The pilot samples were thermally demagnetized with the Schonstedt TSD-1 demagnetizer because this technique is more effective for Mesozoic limestones (see "Paleomagnetics," "Explanatory Notes" chapter, this volume). After an initial unstable component was removed at 100°C, the intensity decreased drastically. Above this temperature the magnetization decreased slowly and there was no change in direction. This treatment could not be employed at high temperature because of a probable mineralogical alteration between 300°C and 350°C (i.e., the breakdown of clay minerals and creation of magnetite) that induced a viscous magnetic component. To isolate a stable remanent magnetization component in these mudstones it will be necessary to use alternating field demagnetization at high field intensities or a mixed treatment (200°C and subsequent AF demagnetization).

ORGANIC GEOCHEMISTRY

Samples from Hole 759B provided 52 carbonate carbon analyses, 84 Rock-Eval and organic carbon analyses, and 37 low-molecular-weight hydrocarbon analyses. The procedures

Table 4. Concentration of inorganic carbon, total organic carbon (TOC), and calcium carbonate, Site 759. Inorganic carbon percentages were measured coulometrically. TOC values are from Rock-Eval pyrolysis. Calcium carbonate percentages were calculated assuming the carbonate content to be pure calcite.

Core, section, interval (cm)	Depth (mbsf)	Inorganic carbon (%)	TOC (%)	$CaCO_3$ (%)
122-759B-				
3R-2, 96–98	15.0	10.1	0.01	84.2
3R-4, 79–81	17.8	10.3	0.01	85.8
4R-1, 96–98	23.0	10.0	0.01	83.3
4R-3, 93–95	25.9	9.9	0.09	82.5
6R-1, 92–95	41.4	<0.1	1.53	0.3
7R-1, 86–88	50.9	<0.1	2.53	0.3
7R-2, 81–82	52.3	11.1	0.02	92.5
8R-1, 52–55	60.0	10.1	0.01	84.1
11R-1, 8–10	88.1	8.5	0.25	70.8
12R-1, 99–101	98.5	11.7	0.01	97.5
13R-1, 88–90	108.4	11.6	0.03	96.6
13R-2, 119–121	110.2	0.9	1.04	7.5
14R-1, 87–89	117.4	9.2	0.18	76.6
14R-2, 17–19	118.2	0.1	1.33	1.3
16R-1, 56–59	136.1	4.0	0.09	33.3
17R-1, 14–16	145.1	3.6	0.06	30.0
18R-1, 57–60	155.1	0.1	3.46	0.8
19R-2, 18–20	165.7	0.1	1.10	1.2
19R-3, 123–124	168.2	11.6	0.24	96.6
20R-1, 98–102	174.5	0.3	1.08	2.5
20R-2, 84–85	175.8	<0.1	1.70	0.6
20R-3, 35–37	176.9	<0.1	0.30	0.5
21R-1, 102–104	184.0	0.1	0.93	0.9
21R-3, 32–34	186.3	<0.1	0.82	0.3
22R-1, 93–95	193.4	0.2	1.88	1.4
22R-3, 63–66	196.1	11.5	0.04	95.8
23R-1, 77–79	202.8	9.6	0.28	79.4
23R-2, 97–99	204.5	10.7	2.63	89.1
24R-2, 97–99	214.0	0.2	1.30	1.4
27R-1, 101–104	236.5	0.3	1.55	2.4
28R-1, 89–91	240.9	0.2	0.83	1.6
28R-2, 104–107	242.5	0.2	1.35	2.0
29R-3, 105–107	249.6	0.2	1.56	1.6
30R-1, 118–120	251.7	0.2	1.06	2.0
30R-3, 64–66	254.1	0.4	1.30	3.4
31R-1, 101–103	256.0	0.2	1.30	1.7
31R-3, 131–133	259.3	0.1	1.27	1.1
32R-1, 58–60	260.6	0.3	0.38	2.6
32R-2, 100–102	262.5	0.5	1.38	4.0
32R-3, 81–83	263.8	0.2	1.03	1.4
33R-1, 107–110	266.1	0.6	1.06	4.8
33R-3, 43–46	268.4	0.9	0.81	7.5
34R-1, 47–49	270.5	0.7	0.97	5.8
34R-3, 12–14	273.1	0.6	1.13	5.0
35R-2, 129–132	277.3	0.9	0.75	7.5
36R-1, 106–108	280.6	0.3	2.00	2.9
36R-3, 105–108	283.6	0.5	1.17	4.3
37R-1, 24–25	284.2	1.2	0.72	10.0
37R-2, 86–88	286.4	9.1	0.24	75.8
38R-4, 27–29	293.8	0.3	1.20	2.5
39R-2, 40–43	300.0	0.4	1.15	3.4

used for these determinations are outlined in the "Explanatory Notes" (this volume) and were described in detail by Emeis and Kvenvolden (1986).

Inorganic and Organic Carbon

Concentrations of inorganic and organic carbon of Hole 759B samples are given in Table 4. Percentages of calcium carbonate are calculated from the inorganic carbon values, assuming that the carbonate content is pure calcite. The presence of other carbonate minerals, such as dolomite or siderite, would modify these calculated percentages. Although the carbonate contents of these sediments and rocks are quite variable, reflecting the mixed lithologies found in this drill hole, samples from below 41 mbsf are generally lower in carbonate content than those from the upper (Neogene and Quaternary) section. In general, organic carbon concentrations are inversely related to the carbonate contents of these samples. Highest levels are found in samples from below 41 mbsf, which are from Triassic mudstones that contain little carbonate.

Rock-Eval Results

The results of Rock-Eval analyses are given in Table 5, which lists the measured S_1, S_2, S_3, and T_{max} data and the derived hydrogen index (HI), oxygen index (OI), production index (PI), and total organic carbon (TOC) parameters. Samples from Site 759B run on the Rock-Eval/TOC (total organic carbon) instrument included all the physical-properties samples, aliquots of most of the squeeze cakes from the interstitial-water samples, and many of the headspace samples. Several of the data in Table 5 are suspect. Instrument malfunctions (e.g., seal failure or mechanical mishandling) may have led to low estimates of the TOC value, creating very high hydrogen and oxygen indices (S_2/TOC and S_3/TOC, respectively). Oxygen index values in excess of about 150 to 180 mg/g rock are assumed to have arisen from a significant contribution of CO_2 from pyrolysis of carbonates. T_{max} values greater than about 575°C resulted from a flame ionization detector signal that increased from about 550°C to 600°C. This spurious signal may have been caused by pore-water salt on the crucibles or, more likely, in the samples.

Values in Table 5 are widely scattered. This is believed to be valid, and it is assumed to be the effect of variable (but generally large) amounts of recycled and/or oxidized organic debris in the sediments. This assumption is consistent with a nearshore depositional environment and the presence of large proportions of land-plant organic matter in these samples.

Total Organic Carbon Concentrations

The TOC value ranged from 0% in carbonate-rich samples to 3.5% in dark-colored mudstones, except for the coaly material from Section 122-759A-20R-4, which yielded TOC values between 10% and 30%, depending on the coaliness of the individual samples. In general, the samples with <0.5% TOC were those that contained >4% inorganic carbon (equivalent to about 34% calcite).

Thermal Maturity

The level of thermal maturity is interpreted to be equivalent to a vitrinite reflectance of about 0.4% R_o. This is based on the T_{max} values of about 420°C for the organic-carbon-rich layer (Section 122-759A-20R-4) and on the very low PI values ($S_1/[S_1 + S_2]$), which were usually below 0.06. Although other thermal maturation parameters are needed to validate this interpretation, these Triassic rocks appear to be thermally immature.

Organic Matter Type

The van Krevelen-type plot of HI versus OI (Fig. 23) suggests that all samples analyzed from this site are dominated by type III organic matter. A few samples have HI values of about 400 mg/g TOC or greater, but these invariably have low TOC values, and hence their indices are more prone to error. Those above 500 are inferred to be artifacts resulting from TOC analytical error, while those in the 400 to 500 range may be the result of the incorporation of small amounts of liptinite macerals (spore, pollen, cuticle, or phytoplankton debris) into the sediment under unusual depositional conditions. The presence of liptinite-rich coaly materials was previously re-

Table 5. Rock-Eval data from Hole 759B samples (see text for discussion of terms).

Core, section, interval (cm)	Depth (mbsf)	Wt. (mg)	T_{max} (°C)	S_1	S_2	S_3	PI	S_2/S_3	PC	TOC (%)	HI	OI
122-759B-												
6R-1, 40–42	40.92	100.1	445	0.15	3.96	0.39	0.04	10.15	0.34	1.86	212	20
7R-2, 0–5	51.50	99.6	461	0.00	0.26	1.12	0.00	0.23	0.02	0.99	26	113
7R-2, 80–82	51.31	100.7	463	0.00	0.10	0.21	0.00	0.47	0.00	0.02	500	1050
8R-1, 52–55	60.02	100.6	460	0.00	0.07	1.00	0.00	0.07	0.00	0.01	0	0
8R-1, 73–78	60.23	131.9	417	0.01	0.58	0.62	0.02	0.93	0.04	0.47	123	131
9R-1, 16–21	69.16	104.0	602	0.10	2.80	1.00	0.03	2.80	0.24	1.50	186	66
10R-CC, 13–18	87.50	132.9	361	0.00	0.01	0.94	0.00	0.01	0.00	0.02	50	4700
11R-1, 8–10	88.08	100.2	352	0.00	0.00	0.97	0.00	0.09	0.00	0.25	36	388
11R-1, 138–148	89.38	102.4	606	0.17	1.47	0.70	0.10	2.10	0.13	2.12	69	33
11R-1, 146–150	89.46	102.0	426	0.17	3.67	0.39	0.04	9.41	0.32	1.53	239	25
12R-1, 99–101	98.49	99.5	407	0.01	0.20	0.16	0.05	1.25	0.01	0.01	2000	1600
13R-1, 88–90	108.38	121.4	496	0.00	0.20	0.87	0.00	0.22	0.01	0.03	666	2900
13R-2, 119–121	110.19	100.0	358	0.00	0.05	2.26	0.00	0.02	0.00	1.04	4	217
13R-2, 148–150	110.48	101.8	531	0.00	0.40	1.74	0.00	0.22	0.03	0.87	45	200
14R-1, 87–89	117.37	100.2	406	0.04	0.70	0.41	0.05	1.70	0.06	0.18	388	227
14R-1, 140–150	117.90	102.9	462	0.00	1.37	0.90	0.00	1.52	0.11	0.11	1245	818
14R-2, 0–2	118.00	101.9	605	0.01	0.68	1.07	0.01	0.63	0.05	1.07	63	100
14R-2, 17–19	118.17	100.7	594	0.06	2.92	0.80	0.02	3.65	0.24	1.33	219	60
16R-1, 10–12	135.60	99.9	589	0.00	0.26	1.61	0.00	0.16	0.02	0.06	433	2683
16R-1, 10–12	135.60	102.5	405	0.00	0.08	1.04	0.00	0.07	0.00	0.04	200	2600
16R-1, 56–59	136.06	97.5	340	0.06	0.45	1.69	0.12	0.26	0.04	0.09	500	1877
17R-1, 14–16	145.14	106.5	434	0.00	0.29	0.08	0.00	3.62	0.02	0.06	483	133
17R-1, 148–150	146.98	103.4	466	0.00	3.26	1.16	0.00	2.81	0.27	1.60	203	72
18R-1, 57–60	155.07	101.7	471	0.00	0.28	1.59	0.00	0.17	0.02	3.46	8	45
18R-1, 148–150	155.98	102.5	477	0.00	2.42	3.88	0.00	0.62	0.20	1.42	170	273
19R-2, 18–20	165.68	101.6	450	0.15	2.80	1.07	0.05	2.61	0.24	1.10	254	97
19R-2, 140–150	166.90	101.6	584	0.40	2.92	1.91	0.12	1.52	0.27	2.29	127	83
19R-3, 0–2	167.00	99.6	454	0.02	2.90	1.21	0.01	2.39	0.24	2.73	106	44
19R-3, 123–124	168.23	98.6	318	0.13	0.26	2.41	0.34	0.10	0.03	0.24	108	1004
20R-1, 98–102	173.48	102.6	546	0.01	0.85	1.21	0.01	0.70	0.07	1.08	78	112
20R-2, 84–86	175.84	103.4	401	0.03	2.31	1.70	0.01	1.35	0.19	1.70	135	100
20R-3, 35–37	176.85	103.9	470	0.00	2.06	1.58	0.00	1.30	0.17	0.30	686	526
20R-4, 0–2	179.50	97.4	421	0.19	22.43	2.52	0.01	8.90	1.88	10.61	211	23
20R-4, 0–2	179.50	100.3	419	0.39	49.91	4.43	0.01	11.26	4.19	16.97	294	26
20R-4, 0–2	179.50	100.8	412	0.50	29.32	2.77	0.02	10.58	2.48	11.62	252	23
20R-4, 12–13	179.62	21.1	429	0.23	33.08	5.21	0.01	6.34	2.77	29.36	112	17
21R-1, 102–104	184.02	101.9	497	0.00	1.85	1.52	0.00	1.21	0.15	0.93	198	163
21R-3, 0–2	186.00	102.9	449	0.04	2.63	1.68	0.02	1.56	0.22	0.82	320	204
21R-3, 32–34	186.32	99.9	443	0.01	1.96	1.49	0.01	1.31	0.16	0.82	239	181
22R-1, 93–95	192.43	100.9	447	0.00	2.02	0.04	0.00	50.50	0.16	1.88	107	2
22R-1, 0–2	192.50	101.4	432	0.03	1.85	2.09	0.02	0.88	0.15	2.08	88	100
22R-3, 63–66	196.13	103.5	533	0.00	0.08	0.51	0.00	0.15	0.00	0.04	200	1275
23R-1, 77–79	202.77	103.5	420	0.00	0.27	0.79	0.00	0.34	0.02	0.28	96	282
23R-2, 97–99	204.47	104.0	428	0.11	2.33	1.50	0.05	1.55	0.20	2.63	88	57
23R-3, 22–23	205.22	100.6	433	0.05	3.46	2.34	0.01	1.47	0.29	2.40	144	97
24R-2, 97–99	213.97	103.4	598	0.10	1.78	1.43	0.05	1.24	0.15	1.30	136	110
24R-2, 140–150	214.40	108.8	457	0.02	2.30	1.59	0.01	1.44	0.19	0.35	657	454
24R-3, 0–2	214.50	99.9	536	0.07	3.03	1.58	0.02	1.91	0.25	0.42	721	376
25R-2, 123–125	223.73	99.5	446	0.00	3.17	1.38	0.00	2.29	0.26	1.37	231	100
26R-1, 148–150	231.98	100.7	510	0.03	2.09	2.58	0.01	0.81	0.17	1.33	157	193
27R-1, 101–104	236.51	99.1	520	0.00	1.03	3.71	0.00	0.27	0.08	1.55	66	239
27R-1, 138–140	236.88	103.6	496	0.05	1.44	2.87	0.03	0.50	0.12	1.12	128	256
27R-1, 148–150	236.90	100.2	546	0.01	2.26	3.63	0.00	0.62	0.18	1.58	143	229
28R-1, 89–91	241.39	100.7	497	0.00	2.25	2.17	0.00	1.03	0.18	0.83	271	261
28R-2, 104–106	243.04	101.5	525	0.01	2.41	3.21	0.00	0.75	0.20	1.35	178	237
28R-2, 104–106	243.04	101.5	525	0.01	2.41	3.21	0.00	0.75	0.20	1.35	178	237
28R-2, 123–125	243.23	99.9	600	0.00	0.92	3.88	0.00	0.23	0.07	1.10	83	352
29R-3, 105–107	249.55	102.1	541	0.01	2.64	2.84	0.00	0.92	0.22	1.56	169	182
30R-1, 118–120	251.68	99.9	601	0.01	1.16	2.13	0.01	0.54	0.09	1.06	109	200
30R-1, 148–150	251.98	98.2	602	0.00	1.28	1.92	0.00	0.66	0.10	1.07	119	179
30R-3, 64–66	254.14	99.7	587	0.01	1.73	3.39	0.01	0.51	0.14	1.30	133	260
31R-1, 101–103	256.01	105.2	593	0.00	1.29	2.12	0.00	0.60	0.10	1.30	99	163
31R-2, 148–150	257.98	100.7	447	0.00	2.53	1.97	0.00	1.28	0.21	1.42	178	138
31R-3, 131–133	259.31	101.5	476	0.00	2.58	1.26	0.00	2.04	0.21	1.27	203	99
32R-1, 58–60	260.58	106.1	600	0.00	1.48	1.23	0.00	1.20	0.12	0.38	389	323
32R-2, 100–102	262.50	100.7	611	0.00	1.26	3.57	0.00	0.35	0.10	1.38	91	258
32R-2, 148–150	262.98	97.7	605	0.00	1.44	1.64	0.00	0.87	0.12	0.82	175	200
32R-3, 81–83	263.81	100.6	542	0.00	0.53	1.76	0.00	0.30	0.04	1.03	51	170
33R-1, 107–110	266.07	100.8	472	0.02	0.50	2.21	0.04	0.22	0.04	1.06	47	208
33R-1, 148–150	266.48	100.2	585	0.00	2.90	2.95	0.00	0.98	0.24	1.37	211	215
33R-3, 43–46	268.43	100.7	465	0.00	0.30	4.38	0.00	0.06	0.02	0.81	37	540
34R-1, 47–49	270.47	99.4	454	0.02	0.42	3.07	0.05	0.13	0.03	0.97	43	316
34R-2, 138–140	272.88	100.6	509	0.03	1.26	1.59	0.02	0.79	0.10	1.37	91	116
34R-2, 140–150	272.90	102.0	495	0.04	1.46	3.74	0.03	0.39	0.12	1.07	136	349
34R-3, 12–14	273.12	102.2	603	0.01	0.90	2.28	0.01	0.39	0.07	1.13	79	201

Table 5 (continued).

Core, section, interval (cm)	Depth (mbsf)	Wt. (mg)	T_{max} (°C)	S_1	S_2	S_3	PI	S_2/S_3	PC	TOC (%)	HI	OI
35R-2, 129–132	277.29	102.0	519	0.02	0.68	3.56	0.03	0.19	0.05	0.75	90	474
35R-2, 148–150	277.48	100.0	455	0.00	0.33	2.07	0.00	0.15	0.02	0.71	46	291
36R-1, 106–108	280.56	100.3	449	0.01	3.46	1.47	0.00	2.35	0.28	2.00	173	73
36R-2, 148–150	282.48	100.2	585	0.00	1.34	2.34	0.00	0.57	0.11	1.17	114	200
36R-3, 105–108	283.55	99.9	583	0.02	2.06	3.30	0.01	0.62	0.17	1.17	176	282
37R-1, 24–25	284.24	100.8	566	0.00	0.56	4.38	0.00	0.12	0.04	0.72	77	608
37R-2, 86–88	286.36	101.5	477	0.00	0.33	11.82	0.00	0.02	0.02	0.24	137	4925
37R-2, 148–150	286.98	99.8	472	0.00	3.02	1.38	0.00	2.18	0.25	1.36	222	101
38R-3, 148–150	293.48	99.2	458	0.01	0.49	1.18	0.02	0.41	0.04	1.03	47	114
38R-4, 27–29	293.77	99.8	445	0.01	2.63	0.91	0.00	2.89	0.22	1.20	219	75
39R-2, 90–93	300.90	99.1	579	0.01	1.59	3.30	0.01	0.48	0.13	1.15	138	286
39R-5, 86–89	305.36	99.2	610	0.00	1.39	7.78	0.00	0.17	0.11	1.37	101	567
39R-3, 148–150	305.98	96.9	549	0.00	1.65	1.57	0.00	1.05	0.13	1.33	124	118

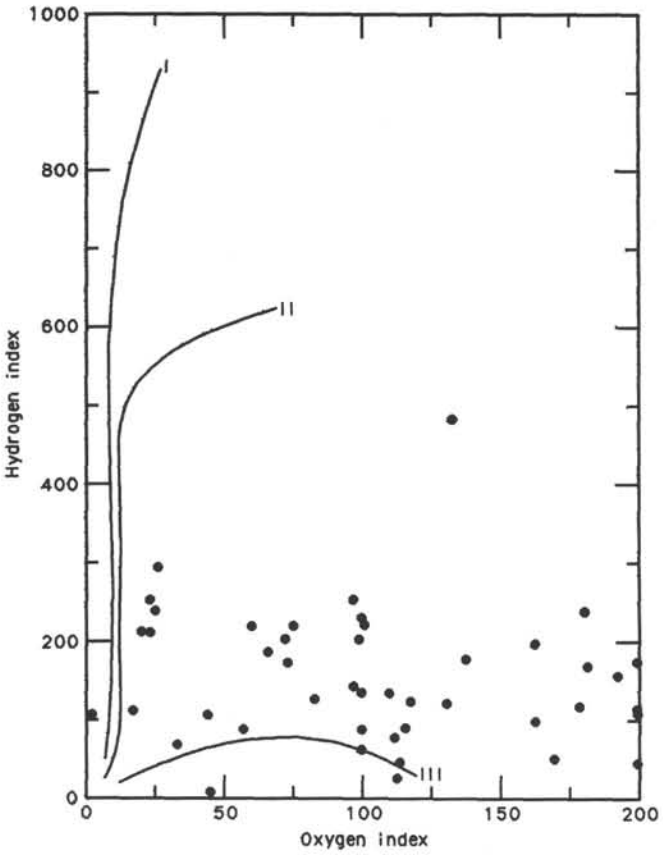

Figure 23. Van Krevelen-type plot of Rock-Eval hydrogen and oxygen indexes of samples from Hole 759B. Units for HI are mg total hydrocarbons/g total organic carbon; for OI, mg CO_2/g total organic carbon.

ported by Cook et al. (1985) in Triassic samples (equivalent to those encountered at Site 759) from Exmouth Plateau exploration boreholes.

Low-Molecular-Weight Hydrocarbons

Concentrations of gaseous hydrocarbons obtained from Hole 759B cores by headspace analysis and by vacutainer sampling are shown in Table 6.

Concentrations are low throughout the various lithologies encountered in this hole. The highest value, 17 ppm of methane, was found in Sample 122-759B-20R-4, 0–2 cm, which was a coaly stringer present in a late Triassic mudstone. Virtually no hydrocarbons having molecular weights higher than methane were present in any of these samples. Only in Section 122-759B-39R-3 were measurable amounts of ethane found. Because concentrations were so low, no attempt was made to use the Hewlett-Packard 5890 Natural Gas Analyzer, which was suffering from the failure of the ship's regulated electrical power supply.

Table 6. Low-molecular-weight hydrocarbon concentrations from Hole 759B samples. Analyses were done by Carle gas chromatograph. Data, except where noted, are from headspace samples. Concentrations are given in parts per million of headspace or vacutainer volume.

Core, section, interval (cm)	Depth (mbsf)	C_1	C_2	C_1/C_2
3R-3, 140–145	16.9	2	nd	—
4R-3, 145–150	26.5	2	nd	—
7R-2, 0–5	51.5	3	nd	—
8R-1, 73–78	60.3	2	nd	—
9R-1, 16–21	69.2	2	nd	—
10R-CC, 13–18	88.0	3	nd	—
11R-1, 146–148	89.5	3	nd	—
12R-2, 0–5	99.0	2	nd	—
13R-2, 148–150	110.5	3	nd	—
14R-2, 0–5	118.0	4	nd	—
16R-1, 10–12	135.6	2	nd	—
17R-1, 148–150	146.5	3	nd	—
18R-3, 0–2	157.5	7	tr	—
19R-3, 0–2	167.0	5	tr	—
20R-4, 0–2	178.0	17	tr	—
21R-3, 0–2	186.0	6	nd	—
22R-1, 0–2	192.5	4	tr	—
24R-3, 0–2	214.5	5	nd	—
25R-2, 123–125	223.7	3	nd	—
26R-1, 148–150	232.0	5	nd	—
27R-1, 138–140	236.9	4	nd	—
28R-2, 123–125	243.5	5	nd	—
29R-2, 148–150	248.5	5	nd	—
30R-1, 148–150	252.0	5	nd	—
31R-2, 148–150	258.0	5	nd	—
32R-2, 148–150	263.0	4	nd	—
33R-2, 148–150	268.0	8	nd	—
34R-2, 138–140	272.9	5	nd	—
35R-2, 148–150	277.5	3	nd	—
36R-2, 148–150	282.5	2	nd	—
37R-2, 148–150	287.0	5	nd	—
38R-3, 148–150	293.5	5	nd	—
39R-3, 0–1 vac	301.5	2	nd	—
39R-3, 5–7	301.6	6	<1	8
39R-3, 148–150	303.0	10	1	10
39R-4, 0–1 vac	303.0	2	nd	—
39R-5, 105–107	307.6	5	nd	—

Note: nd = not detected; tr = trace; vac = vacutainer sample.

An important parameter used to distinguish biogenic hydrocarbon gases from thermogenic gases is the C_1/C_2 ratio (e.g., Claypool and Kvenvolden, 1983). In Section 122-759B-39R-3, this ratio was about 10 (Table 6), which is characteristic of thermogenic hydrocarbons. Given the overall low amounts of gases in the stratigraphic unit from which this section originated and the Type III organic matter present (Table 5), it is probable that the low-molecular-weight hydrocarbons in this core section were created *in situ*. As such, they did not represent a safety hazard. This conclusion, however, might not be valid in other situations.

INORGANIC GEOCHEMISTRY

Introduction

The major objectives of the inorganic geochemistry program on Leg 122 were: (1) to study vertical gradients in the chemical composition of the pore waters within each site and compare the variations between sites; (2) to study the chemistry of Triassic sediment pore waters, which to our knowledge have not been previously sampled, and (3) to correlate changes in sediment pore water chemistry and in lithology to paleoceanographic cycles. The sampling program at Site 759 encompassed primarily the first part of objective 1 and objective 2. Shipboard X-ray-diffraction (XRD) analyses of the solid phases corresponding to the pore waters were conducted on selected samples from the Wombat Plateau sites. The results from Sites 759, 760, and 761 are given in Table 7 (no XRD analyses were done on samples from Site 764).

Interstitial Waters

The methods employed for shipboard interstitial-water analyses are described in the "Explanatory Notes" (this volume). A total of eight samples were obtained from Hole 759B, and results of analyses appear in Table 8 and Figure 24. The data reveal several significant changes in the concentration of major constituents as a function of depth below seafloor. The first sample was derived from a 5-cm whole round core, whereas the latter seven were squeezed from 10-cm intervals. Samples were collected from the first core, and subsequently from every third core if sufficient sediment was recovered. When ≤ 10 cm^3 of fluids were obtained, we omitted the determination of alkalinity and pH in order to allow measurement of the major dissolved constituents. This situation arose with Samples 122-759B-19R, 140–150 cm, -27R, 140–150 cm, and -34R, 140–150 cm.

Magnesium (Mg^{2+}) and Calcium (Ca^{2+})

Mg^{2+} is the constituent that exhibits the largest downhole concentration gradient (Fig. 24). Its concentration of 52.6 mM at 17.0 mbsf is slightly depleted relative to surface seawater (54.0 mM), decreases linearly downhole to 26.7 mM at 236.9 mbsf, and appears to be essentially unchanged at 272.9 mbsf (27.1 mM). The decrease in Mg^{2+} concentration is accompanied by a less pronounced and steady increase in the Ca^{2+} concentration from 11.1 mM at 17.0 mbsf, a value slightly enriched relative to seawater (10.5 mM), to 13.6 mM at 89.4 mbsf. Downhole changes in the Ca^{2+} concentration do not exhibit definitive trends below 89.4 mbsf, and pore-water Ca^{2+} levels reach 14.3 mM at 272.9 mbsf (Fig. 24). Changes in the Mg^{2+}/Ca^{2+} ratio occur with depth in the sediment (Fig. 24).

The major change in the Mg^{2+}/Ca^{2+} ratio from 4.75 to 3.11 observed in the upper portion of the hole (17.0–89.4 mbsf) results from both the decrease in Mg concentration and the increase in Ca^{2+} concentration, whereas the nearly linear change between 89.4 and 236.9 mbsf is primarily controlled by changes in the Mg concentration. The Mg^{2+}/Ca^{2+} ratio appears to stabilize near 1.9 in the last two pore-water samples recovered between 236.9 and 272.9 mbsf. The downhole concentration gradients observed for Mg^{2+} and Ca^{2+} do not appear to be related directly to the percent carbonate (Fig. 25) (see "Organic Geochemistry," this chapter), although there is a strong correlation between Mg^{2+} and SO_4^{2-} (Fig. 26). Interstitial water from 214.4 mbsf (Sample 122-759B-24R-2, 140–150 cm) displays a slight deviation from the trends observed in other samples; this may result in part from contamination of the sample with drill water.

Overall changes in the interstitial-water concentrations of Mg^{2+} and Ca^{2+} may be attributed to several processes. These include diagenetic reactions, the replacement of calcite by dolomite, and ion-exchange reactions between Ca^{2+} and other cations (e.g., Na^+ and K^+) in clay minerals. The Mg^{2+} and Ca^{2+} behavior exhibited by pore waters from Hole 759B has also been observed in many other Ocean Drilling Program (ODP) and Deep Sea Drilling Project (DSDP) sites.

Sulfate (SO_4^{2-})

Sulfate concentrations in the pore waters from Hole 759B display a steady decrease downhole from 29.5 mM at 17.0 mbsf (slightly enriched over the seawater concentration, 28.9 mM) to 15.8 mM at 272.9 mbsf (Fig. 24). An unexpected increase in SO_4^{2-} observed at 214.4 mbsf is likely to result from contamination by drill water. The less-indurated sediment from which this sample was obtained would allow drill water to diffuse through the core section prior to the extraction of interstitial waters. The common presence of pyrite in the sediments recovered in Hole 759B (see "Lithostratigraphy," this chapter) is not entirely consistent with the measured SO_4^{2-} concentrations but suggests that dissolved Fe released from clays or oxides has reacted with S^{2-} originally produced during the oxidation of organic matter present within the sediments.

Silica (SiO_2)

Apart from a large initial decrease from 872 mM to 312 mM between 17.0 and 51.4 mbsf (Fig. 24), downhole changes in SiO_2 concentration are not very pronounced, although they are more than one order of magnitude greater than the uncertainty of the analytical method (3%–5% relative). A rise in the dissolved SiO_2 is observed between 51.4 mbsf and 117.9 mbsf. This is followed by a gradual decrease to 214.4 mbsf (although the latter datum may be suspect, as discussed above) and a subsequent increase to 272.9 mbsf. These changes may result from SiO_2 diagenesis in clays and changes in the proportions of amorphous to crystalline SiO_2 in the sediments of Hole 759B. The incomplete alkalinity data from Site 759, however, do not provide evidence in support of diagenetic processes, which should also be accompanied by increases both in alkalinity and Ca^{2+} concentration (note that the latter was observed; see Fig. 24).

Salinity and Chlorinity

The salinity of the pore waters of the uppermost 118 m of Hole 759B lie in a narrow range from 35.2 to 34.7 g/kg, which is close to the salinity of average seawater (35.2 g/kg); it appears that interstitial water salinity in this part of the hole is related to the salinity of bottom water. Between 117.9 and 272.9 mbsf (Fig. 24) an overall significant decrease in the downhole salinity to near 33 g/kg is observed, except at 214.4 mbsf (contaminated sample). Although the decreased salinities observed in the lower half of Hole 759B are consistent with the proposed fluviodeltaic origin (i.e., lower-salinity water) of the sediments and coal sequence found near 200 mbsf (see "Lithostratigraphy," this chapter) the data between

Table 7. Mineralogy of of selected samples from Sites 759, 760, and 761, determined by X-ray-diffraction analysis.

Core, section, interval (cm)	Treatment[a]	Mineral phases present[b] Major	Minor[c]
122-759B-			
22R-2, 40	UBN	Quartz[d]	Feldspar, illite, chlorite, (smectite)
25R-2, 80	UBN	Quartz[d]	Feldspar, illite, chlorite, (siderite)
33R-2, 102	UBN	Siderite	Quartz, (calcite)
34R-2, 107	UBN	Siderite	Quartz, (calcite)
54R-2, 98	UBN	Pyrite	Quartz
122-760A-			
1H-4, 145	UBN	Calcite	Quartz
2H-4, 145	UBN	Calcite	Quartz
5H-4, 145	UBN	Calcite	Quartz, (smectite)
4H-5, 145	UBN	Calcite	Quartz, (smectite, illite)
5H-5, 145	UBN	Calcite	Quartz, (chlorite, illite, smectite, siderite)
6H-5, 140	UBN	Calcite	Quartz, (smectite)
7H-5, 140	UBN	Calcite	Quartz, chlorite, (smectite)
8H-4, 145	UBN	Calcite	Quartz
9H-5, 10	UBN	Quartz, calcite	Opal-CT
9H-5, 20	UBN	Calcite, quartz	Opal-CT, smectite, illite?
9H-5, 21	UBN	Calcite	δ-MnO_2, quartz
9H-5, 145	UBN	Quartz, plagioclase, smectite	Illite, chlorite
10H-2, 140	UBN	Quartz, feldspar	Smectite, chlorite, illite
16X-4, 55	UBN	Quartz	Illite, chlorite, feldspar
16X-4, 140	UBN	Quartz	Illite, chlorite, feldspar
19X-2, 140	UBN	Quartz, illite, chlorite	Feldspar, smectite
25X-4, 49	UBN	Quartz	Illite, chlorite[d]
25X-4, 140	UCN	Chlorite, illite	Quartz
25X-4, 140	USN	Quartz	Feldspar, chlorite, illite
30X-5, 140	UCN	chlorite, illite	Quartz, feldspar, (smectite)
30X-5, 140	USN	Quartz	Feldspar, chlorite, illite, (smectite)
35X-3, 140	UCN	Chlorite, illite	Smectite, quartz[d], (feldspar)
35X-3, 140	USN	Quartz	Feldspar, chlorite, illite[d]
37X-CC, 0	UBN	Aragonite	Quartz, shell fragments
122-760B-			
6R-1, 52	UBN	Calcite, Mg-kutnahorite	Quartz (light color)
6R-1, 72	UBN	Mg-kutnahorite	Calcite, quartz (dark color)
10R-1, 140	UCN	Smectite, illite, chlorite	Quartz
10R-1, 140	USN	Quartz	Feldspar, chlorite, illite, smectite
11R-3, 86	UBN	Quartz, feldspar	Illite, smectite
122-761B-			
29X-CC, 26	UBN	Smectite	(Mg-kutnahorite, calcite)
30X-1, 142	UBN	Quartz, feldspar	Smectite
30X-2, 16	UBN	Quartz, calcite	Feldspar, clinoptilolite, smectite
30X-2, 20	UBN	Quartz, calcite	Feldspar, clinoptilolite, illite, smectite
122-761C-			
7R-1, 55	UBN	Smectite	
8R-1, 109	OCN	Smectite	Calcite, corundum?
8R-1, 109	USN	Smectite	Calcite, quartz, feldspar
8R-1, 122	UBN	Smectite	
8R-1, 139	UBN	Calcite, quartz	Smectite
8R-2, 23	OCN	Smectite	(Quartz)
8R-2, 23	USN	Smectite	Biotite, calcite, feldspar
9R-2, 8	UBN	Smectite, calcite	
9R-2, 10	OCN	Smectite[d]	
9R-2, 10	UBN	Smectite	Calcite
9R-CC, 2	OCN	Smectite	(Quartz)
9R-CC, 4	UBN	Smectite	Quartz
10R-1 19	UCN	Smectite	(Calcite, quartz)
10R-1, 38	OCN	Smectite	Feldspar
10R-1, 41	UCN	Smectite	(Calcite, quartz)
10R-1, 41	USN	Calcite, quartz	Smectite, clinoptilolite, illite
10R-2, 43	UCN	Smectite	Quartz, calcite, feldspar, clinoptilolite
10R-2, 45	USN	Quartz, feldspar	Illite, smectite
23R-4, 22	UBN	Calcite	Quartz, smectite
33R-CC, 0	UBC	Chlorite or kaolinite, illite	Quartz, feldspar
33R-CC, 0	UBS	Quartz, feldspar	Chlorite or kaolinite, illite

[a] Key to treatment type: U = unoriented, O = oriented, B = bulk, C = clay fraction, S = silt fraction, N = no treatment.
[b] Components are listed in approximate order of abundance estimated from peak intensities.
[c] Minerals in parentheses are present at trace levels or their identification was made on the basis of fewer than three reflections. The identification of chlorite versus kaolinite remains uncertain without heat treatments, pending additional shore-based analyses.
[d] Indicates presence of halite, resulting from our not rinsing samples free of sea-salt prior to analysis.

Table 8. Summary of interstitial-water analyses, Site 759.

Core, section, interval (cm)	Depth (mbsf)	Volume (cm^3)	pH	Alkalinity (mM)	Salinity (g/kg)	Mg^{2+} (mM)	Ca^{2+} (mM)	Mg^{2+}/Ca^{2+}	Cl^- (mM)	SO_4^{2-} (mM)	Silica (mM)
122-759B-											
3R-3, 145–150	16.95	48	7.65	3.411	35.2	52.6	11.1	4.75	556	29.5	0.873
7R-1, 140–150	51.4	30	7.78	4.345	35.2	47.4	12.4	3.81	557	28.0	0.312
11R-1, 138–148	89.4	24	7.67	2.985	34.8	42.3	13.6	3.11	537	27.1	0.377
14R-1, 140–150	117.9	13	7.84	3.235	34.7	40.1	13.8	2.91	542	22.3	0.412
19R-2, 140–150	166.9	4			33.0	33.5	13.3	2.51	542	18.3	0.345
24R-2, 140–150	214.4	45	7.42	2.377	34.7	29.9	13.7	2.17	560	19.9	0.233
27R-1, 140–150	236.9	10			33.6	26.7	13.6	1.96	558	15.9	0.295
34R-2, 140–150	272.9	8			33.0	27.1	14.3	1.90	558	15.8	0.424

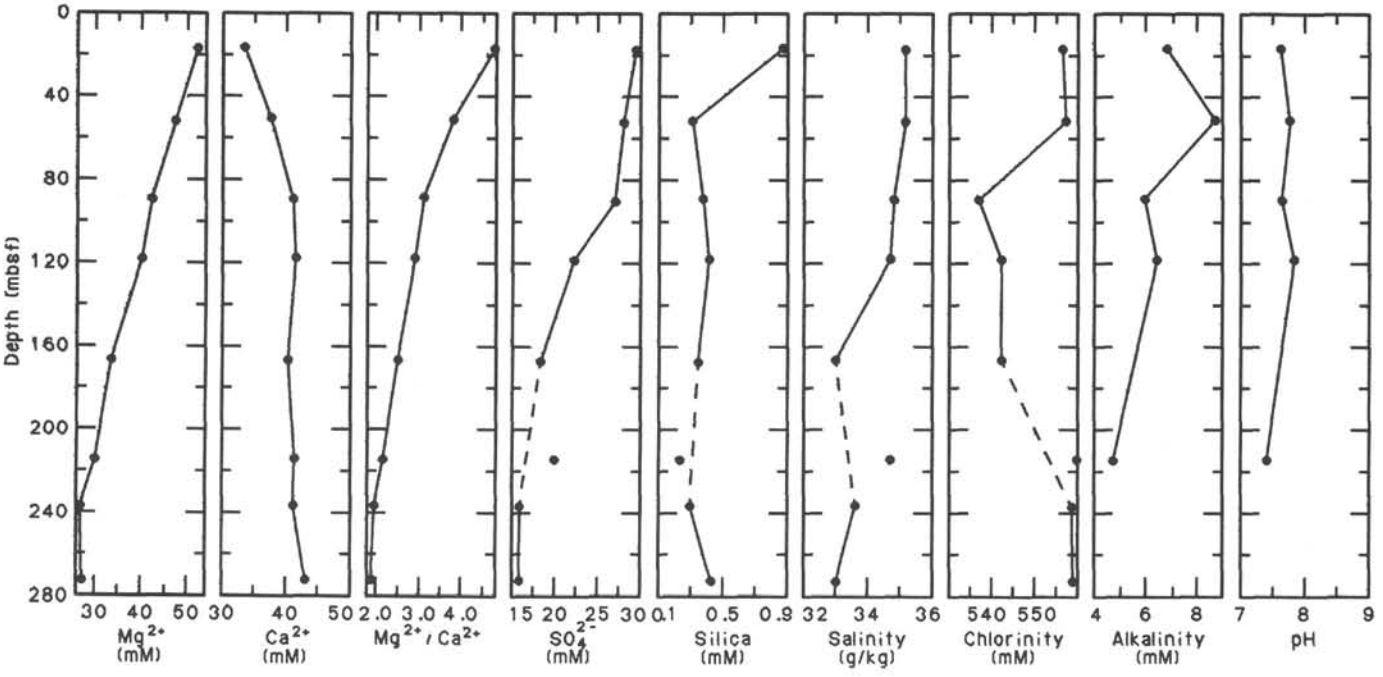

Figure 24. Summary of interstitial-water analyses, Site 759, as a function of depth.

236.9 and 272.9 mbsf are not entirely consistent with the chlorinity data shown in Figure 24.

Examination of Table 8 reveals that apart from the contaminated sample from 214.4 mbsf, the chlorinity of pore waters from Hole 759B remains in a narrow range between 535 and 559 mM (seawater = 559 mM). The lower values found between 89.4 to 166.9 mbsf may reflect the conservative behavior of Cl^- and represent dilution of nearshore surface seawater by continental runoff in a shallow fluviodeltaic environment. The return to high chlorinity between 236.9 and 272.9 mbsf suggests reestablishment of a marine environment, which is consistent with the limestone and turbidite lithologies recovered in this interval (see "Lithostratigraphy," this chapter). Mass-balance calculations reveal that the downhole decrease of salinity can be attributed primarily to the decrease in the concentrations of Mg^{2+} and SO_4^{2-}.

Alkalinity and pH

The pH of pore waters from Hole 759B (Fig. 24) shows little variation and ranges from 7.42 to 7.84. The inadequate sample size recovered in the lower portion of the hole (except for the suspect sample at 214.4 mbsf) precludes the identification of any significant trend downhole. Alkalinity measurements also suffer from the same paucity of recovered fluids, although a significant increase in alkalinity was observed at 51.4 mbsf (Fig. 24). One possible source of increased alkalinity include the oxidation of organic matter. Another is the dissolution of limestone, which we found to begin at this depth (see "Lithostratigraphy," this volume), although Ca^{2+} and Mg^{2+} data do not support the dissolution interpretation. In general, the alkalinity of interstitial waters appears to decrease downhole as expected (Gieskes, 1981).

PHYSICAL PROPERTIES

Introduction

Routine physical properties measured on sediments from Hole 759B include compressional-wave velocity, velocity anisotropy, thermal conductivity, and the index properties (bulk density, grain density, porosity, and water content; see "Explanatory Notes," this volume). As Hole 759B was drilled with the rotary core barrel (RCB), the GRAPE and *P*-wave logger were not used because cores were disturbed by drilling. Owing to malfunction and resistant lithologies encountered in the hole, neither vane shear nor resistivity data were collected at Hole 759B. An additional data problem at Hole 759B was the poor core recovery in the upper part of the hole. Some cores recovered less than 30 cm of fractured sediment, which is unsuitable for physical-property measurements. Repeated poor recovery led to some

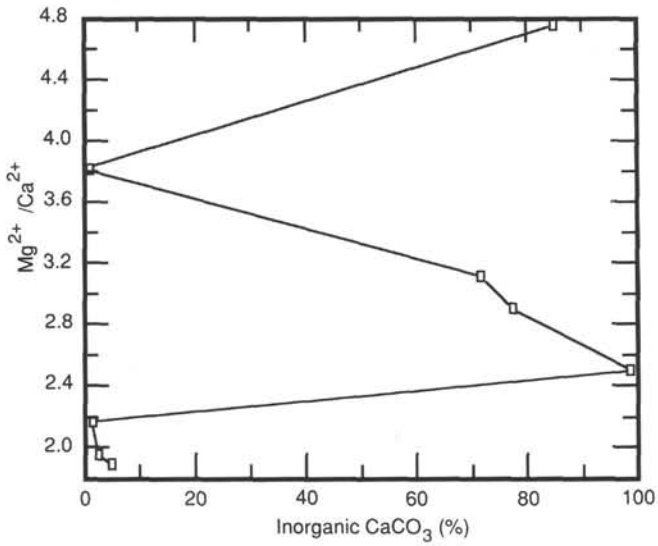

Figure 25. Mg^{2+}/Ca^{2+} ratio versus percent $CaCO_3$, Hole 759B.

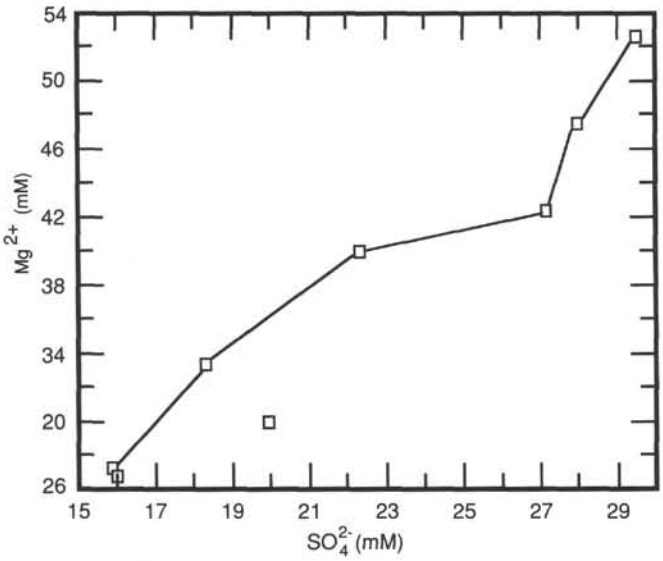

Figure 26. Mg^{2+} versus SO_4^{2-}, Hole 759B.

large gaps in the downhole physical-properties data (e.g., 60–100 mbsf). The values of the various physical properties are listed in Table 9 and their trends with depth are illustrated in Figure 27.

Velocity

The velocity data from Hole 759B, determined with the Hamilton Frame (Fig. 27), show a range from 1.51 to 6.95 km/s. This unusually extreme range reflects the range in lithology from the carbonate ooze of Unit I to the recrystallized limestones and dolomites of Units III, IV, and V. In general, the fine-grained clastic sediments show a gradual downhole increase in velocity from 1.51 km/s at the top of the hole (14.94 mbsf) to 2.25 km/s at the bottom (305.36 mbsf). Departures from this trend are attributed to limestone, dolomite, sandstone, and siderite lithologies. These lithologies are interbedded with the softer mudstones and claystones, and therefore alternating high (usually >4 km/s) and low (about 2 km/s) velocities occur. Although the limestone/dolomite velocities are unusually high, they are in accordance with typical velocities from these lithologies (Rider, 1986). Anisotropy in the velocity measurements (Fig. 27) ranges between 0% and 15% and shows no consistent trend for most of the hole. Samples from the bottom of the hole show mostly positive anisotropy, as drilling disturbance was minimal and bedding angles do not exceed about 10°.

Thermal Conductivity

Thermal conductivity (Fig. 27) ranges from 1.052 to 2.183 W/m·K between 24 and 224 mbsf. Values from measurements on samples above 50 mbsf are lower, whereas values from measurements on samples deeper in the section are generally higher but more variable. Lithified samples display higher thermal conductivity. Between 170 and 190 mbsf the less lithified samples seem to have anomalously high conductivity.

Index Properties

Grain densities (Fig. 27) are in the range of 2.6–2.8 g/cm^3, reflecting the dominant quartz and calcite/dolomite composition of the sediments. Bulk density measurements (Fig. 27) of the clastic rocks (Units III–IV) show a downhole increase from 1.9 to 2.25 g/cm^3. Lithified carbonate lithologies depart from this trend, occurring in a range between 2.5 and 2.75 g/cm^3. The shallow carbonate oozes between 0 and 30 mbsf show a consistently low bulk density of around 1.6 g/cm^3. Measurements on a siderite sample from 286 mbsf show high values of bulk density (3.53 g/cm^3) and grain density (3.56 g/cm^3).

Porosity and water content values (Fig. 27) show good correlation throughout the borehole and an inverse correlation with bulk density and velocity. Quaternary carbonate oozes near the top of the hole contain high porosities of 60%–75% and water contents of around 45%. Clastic sediments display a gradual downhole decrease from water contents of 25%–30% and porosities of 45%–50% at 41 mbsf to water contents of 10%–15% and porosities of 25%–35% at 305 mbsf. In contrast, the lithified carbonate sediments between 50 and 205 mbsf display consistently low porosities and water contents of 0%–15%. Siderite lithologies in the lower 80 m of the hole contained virtually no porosity or pore water.

Relationship of Physical Properties to Lithology and Wireline Logs

All physical properties at Hole 759B show consistent values and trends that allow for a division into three distinct intervals and provide a correlation to lithology and wireline logs (see "Downhole Measurements," this chapter). Interval 1 (0 to 50.9 mbsf) contains constant velocities, porosities >50%, and bulk densities <2.0 g/cm^3. Interval 2 (50.9 to 204.5 mbsf) contains physical properties that vary according to the dominant lithology. Lithified carbonate sediments in Interval 2 are characterized by high velocities and bulk densities. Interval 3 (204.5 to 308.0 mbsf) consists of predominantly clastic sediments whose properties either gradually increase or decrease as a result of compaction.

Physical properties show a good correlation with wireline logs. The Hamilton frame velocity measurements correspond closely to the interval transit times, although the level of resolution is lower because of the discrete (rather than continuous) manner in which the samples are measured. The limestone velocities range from 3.1 to 7.6 km/s on the wireline logs, with an average velocity of about 4.4 km/s. These velocities correspond relatively well with the Hamilton Frame velocities, which range from 3.5 to 6.9 km/s, with an average velocity of 4.5 km/s.

Table 9. Physical-property data, Site 759.

Core, section, interval (cm)	Depth (mbsf)	V_{ph} (km/s)	V_{pv} (km/s)	Anisotropy (%)	Grain density (g/cm^3)	Bulk density (g/cm^3)	Porosity (%)	Water content (%)	Thermal conductivity (W/m·k)
122-759B-									
3R-2, 94	14.94	1.5110				1.57	72.30	45.4	
3R-4, 85	17.85	1.5250			2.38	1.57	66.50	45.7	
4R-1, 98	22.98				2.74	1.59	69.00	45.1	
4R-2, 75	24.25								1.309
4R-3, 75	25.75								1.257
4R-3, 95	25.95				2.71	1.57	69.50	46.0	
4R-4, 28	26.78								1.052
6R-1, 92	41.42	1.6580	1.698	−2.38	2.64	1.96	48.40	26.5	
7R-1, 93	50.93	1.6740	1.660	0.84	2.63	1.92	49.50	27.4	
7R-2, 80	52.30	4.3760			2.74	2.74	7.90	3.1	
8R-1, 37	59.87								2.023
8R-1, 52	60.02	4.6710			2.73	2.67	3.60	1.4	
11R-1, 8	88.08	3.6570	3.567	2.49	2.79	2.51	16.40	6.7	
12R-1, 99	98.49	6.7690	6.686	1.23	2.70	2.69	0.60	0.2	
13R-1, 48	107.48								1.826
13R-1, 87	107.87	5.7880	5.233	10.07	2.66	2.65	4.10	1.6	
13R-2, 89	109.39								1.655
13R-2, 121	109.71	1.8120	1.749	3.54	2.65	2.04	42.60	22.2	
13R-3, 13	110.13								1.562
14R-1, 86	117.36	4.0720	4.401	−7.77	2.69	2.63	6.50	2.6	
14R-2, 16	118.16	1.9800	1.914	3.39	2.62	2.14	38.10	19.3	
16R-1, 56	136.06	4.6820	4.110	13.01	2.64	2.65	3.50	1.4	
17R-1, 12	145.12	5.1830	5.355	−3.26	2.66	2.68	0.90	0.3	
18R-1, 58	155.08	1.9500	1.939	0.57	2.61	2.15	35.10	17.4	
18R-2, 42	156.42								1.660
19R-2, 19	165.69	2.0180	2.044	−1.28	2.60	2.09	38.80	19.8	
19R-3, 123	168.23	4.9470			2.74	2.81	12.50	5.0	
20R-1, 98	174.48	1.9130	1.888	1.32	2.64	2.09	35.10	17.3	
20R-1, 110	174.60								1.255
20R-2, 84	175.84	1.8000	1.800	0.00	2.67	2.07	37.90	18.9	
20R-2, 129	176.29								1.441
20R-3, 45	176.95	1.9150	2.073	−7.92	2.68	2.12	35.50	17.2	
20R-3, 122	177.72								
21R-1, 34	183.34								1.769
21R-1, 102	184.02	1.9020	1.945	−2.24	2.63	2.15	35.10	17.3	
21R-2, 77	185.27								2.183
21R-3, 32	186.32	2.1190	2.102	0.81	2.64	2.15	33.50	16.2	
21R-3, 56	186.56								2.090
22R-1, 93	193.43	2.0230	1.960	3.16	2.63	2.12	34.90	17.1	
22R-3, 63	196.13	6.3210	6.687	−5.63	2.82	2.82	0.05	0.2	
23R-1, 76	202.76	4.7800			2.78	2.75	5.00	1.9	
23R-2, 97	204.77	4.9560	5.127	−3.39	2.70	2.66	4.70	1.8	
24R-2, 77	213.77	1.8750	1.823	2.81	2.61	2.06	37.80	19.1	
25R-3, 24	224.24								1.813
27R-1, 101	236.51	2.0650	2.128	−3.01	2.62	2.19	32.90	16.0	
28R-1, 89	241.39	2.1140	2.110	0.19	2.59	2.13	35.60	17.8	
28R-2, 102	243.02	2.1640	2.086	3.67	2.66	2.22	34.10	16.5	
28R-3, 105	244.55	2.1330	2.147	−0.65	2.67	2.22	34.80	16.9	
30R-1, 117	251.67	2.1860	2.168	0.83	2.65	2.19	36.00	17.7	
30R-3, 62	254.12	2.1590	2.180	−0.97	2.63	2.19	34.90	17.2	
31R-1, 99	255.99	2.1700	2.120	2.33	2.61	2.16	33.40	15.9	
31R-3, 130	259.31	2.1700	2.170	0.00	2.61	2.17	32.90	15.5	
32R-1, 97	260.97	2.1210	2.062	2.82	2.70	2.14	41.00	19.6	
32R-3, 80	263.80	2.2010	2.103	4.55	2.58	2.19	29.20	13.7	
33R-1, 107	266.07	2.2430	2.103	6.44	2.62	2.20	30.30	14.1	
33R-3, 43	268.43	2.2360	2.059	8.24	2.63	2.20	30.50	14.2	
34R-1, 48	270.48	2.1215			2.71	2.27	37.50	16.9	
34R-3, 12	273.12	2.0570	1.942	5.75	2.61	2.18	29.90	14.1	
35R-2, 129	277.29	2.1440	2.127	0.80	2.68	2.28	30.70	13.8	
36R-1, 106	280.56	2.2520	2.055	9.15	2.59	2.22	29.40	13.6	
36R-3, 106	283.56	2.1910	2.048	6.75	2.59	2.22	26.90	12.4	
37R-1, 21	284.21	2.1690	2.040	6.13	2.65	2.26	27.50	12.5	
37R-2, 87	286.37	5.5420	5.317	4.14	3.56	3.53	1.30	0.4	
38R-2, 100	291.50	2.1510	2.073	3.69	2.60	2.22	27.60	12.8	
38R-4, 27	293.77	2.1770	2.076	4.75	2.62	2.22	29.60	13.7	
39R-2, 90	300.90	2.1400	2.203	−2.90	2.69	2.23	30.70	14.1	
39R-5, 86	305.36	2.2100	2.120	4.16	2.61	2.23	25.80	11.8	

Note: V_{ph} = compressional-wave velocity, horizontal; V_{pv} = compressional-wave velocity, vertical.

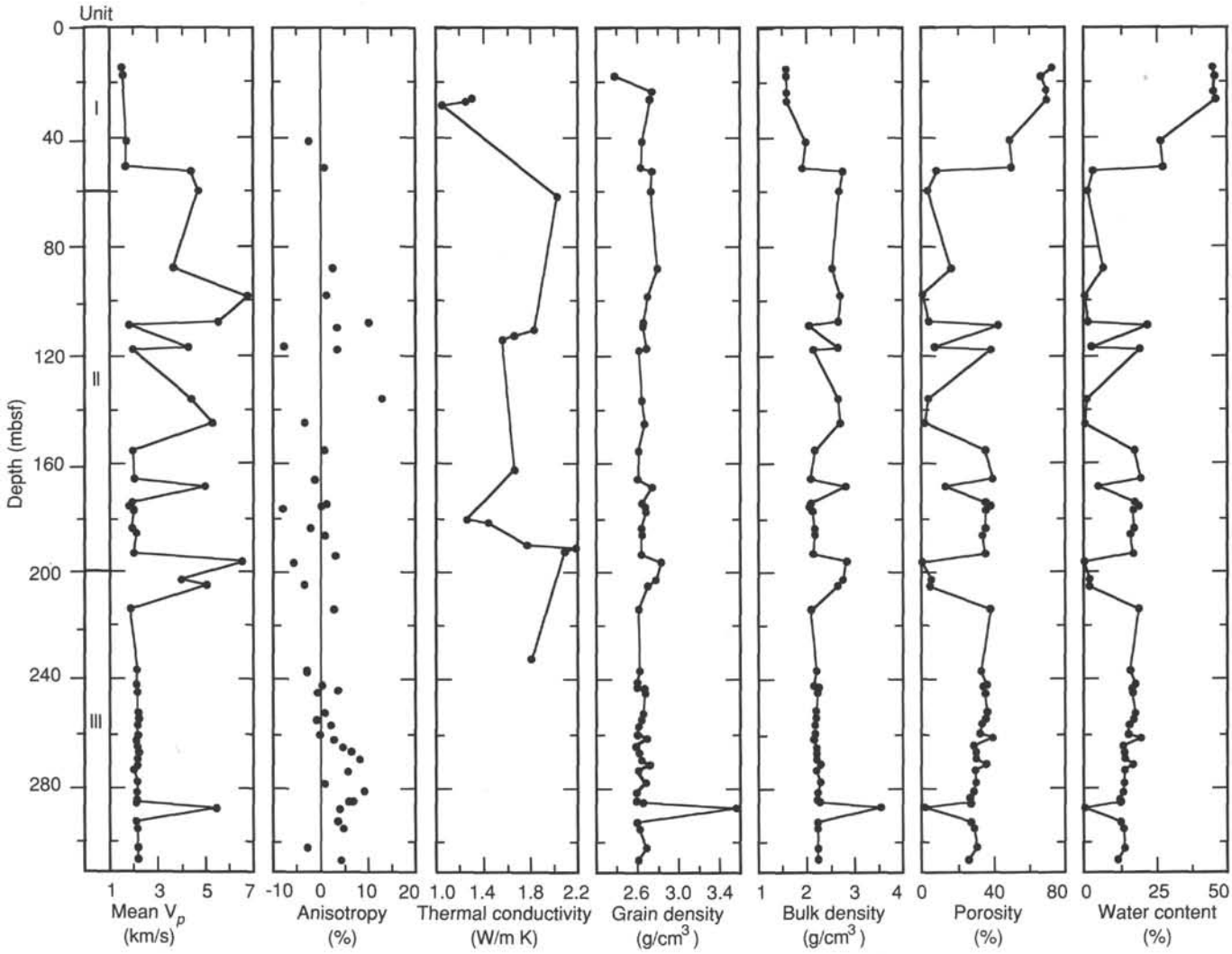

Figure 27. Downhole changes in physical properties and index properties, Hole 759B.

SEISMIC STRATIGRAPHY

See "Seismic Stratigraphy," Site 764 chapter, for a combined report of Sites 759, 760, 761, and 764.

DOWNHOLE MEASUREMENTS

Operations

Logging operations at Hole 759B began at 1900 hr (all times given in local time) on 10 July 1988 with hole conditioning and bit release. The Schlumberger seismic stratigraphic tool combination and wireline heave compensator were rigged up between 0215 hr and 0425 hr on 11 July. At this site the tool string consisted of the auxiliary measurement sonde (AMS), the three-axis magnetometer-inclinometer accelerometer tool (GPIT), the spectral gamma ray (NGT), phasor induction (DIT-E), and digital array sonic (SDT) tools. At 0520 hr the tool string was at the bottom (306 mbsf) of the hole with all tools functioning. As uphole logging was being attempted, the logging computer crashed. Subsequent attempts to read the data were unsuccessful and indications were that there was a telemetry overload. At 0745 hr, the tool string was run up to the rig floor and the AMS and GPIT were removed from the tool string. The modified tool combination was tested in the pipe by logging up from 100 to 50 mbrf (meters below rig floor); data were successfully collected and recorded. The tool combination was lowered out of the pipe into the open hole to calibrate the spectral gamma ray tool, and then run to the bottom of the hole.

At 0945 hr the tool string reached the bottom and logging commenced at the rate of 215 to 250 meters per hour. Power problems at 177 mbsf affected the induction and sonic tools but not the spectral gamma ray. The problem was corrected at 144 mbsf and all tools functioned normally through the end of the logging run at the base of pipe (69 mbsf). A repeat section was attempted to obtain resistivity and sonic data, but the tools were only run from 150 to 96 mbsf, missing the critical interval. Logging terminated at 1210 hr and the tool string was brought to the rig floor. Rig-down was completed by 0130 hr. Lack of time precluded running the other two tool strings at this site.

Log Quality

The seismic stratigraphic logging tools recorded high-quality data from near the bottom of the hole (300 mbsf) to the end of the drill pipe (66 mbsf) with the exception of an interval between 144 mbsf and 173 mbsf in which electrical-power problems in the tool string produced invalid readings of electrical resistivity and interval transit time (velocity). Total and spectral gamma ray as well as caliper data were of

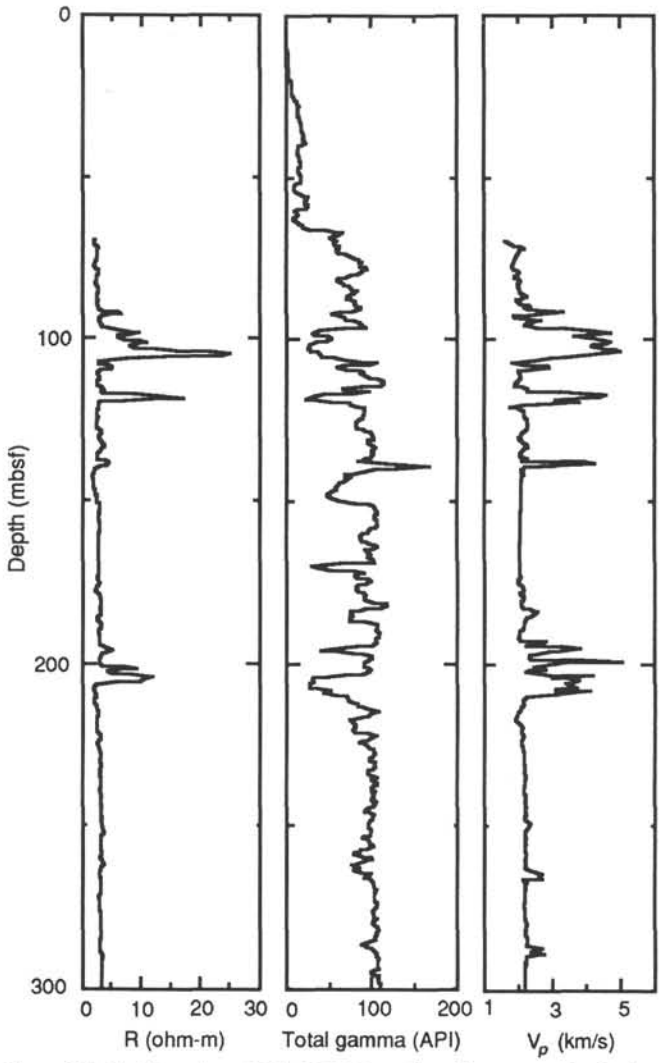

Figure 28. Well logs from Hole 759B. Logs have been smoothed using a 1-m running average computed at 0.5-m-intervals. R = resistivity; total gamma = total gamma-ray counts; V_p = compressional-wave velocity.

excellent quality throughout the entire logging run in the open hole (Fig. 28). In addition, the tools were run inside the drill pipe from 66 mbsf to the mud line. Total gamma radiation measured through the pipe (discussed below) exhibited variations that aid in elucidating the distribution of lithologies in the upper 66 m of the sedimentary section.

As the coring operations in the upper 250 m of Hole 759B were typified by recovery of 0%–40%, the geophysical well logs represent the only opportunity to characterize accurately the vertical distribution and abundance of the lithofacies at Site 759. All of the various logs show extreme variability on scales of meters to tens of meters over the poorly cored section of Hole 759B; this suggests cyclic lithofacies variations poorly described by examination of the limited core recovered. The problem of understanding lithofacies distribution in poorly cored sediments is heightened by the probability of selective recovery of core; that is, lithologies that core well are likely to be proportionately over-represented in the recovered portions of the cored intervals.

The following discussion addresses the problem of lithofacies distribution rather than the particular behavior of the individual geophysical parameters measured by the seismic stratigraphic logging tool string. Comparisons of absolute compressional-wave velocities from the logs to measurements made on samples taken from the core (see "Physical Properties," this chapter) are noted where necessary to better understand the log behavior, but are not examined in a comprehensive manner. Core descriptions and physical-property data are used to relate the recovered sediments to the overall log profiles.

Table 10. Well log identification of lithologies from Hole 759B.

Lithology	Gamma ray	Resistivity	Velocity
Limestone	Low	High	High
Sand/sandstone	Low-medium	Low	Low-medium
Clay/claystone	High	Low	Low

Lithologies

The well log response at Hole 759B can generally be interpreted in light of the behavior of three end-member lithologies sampled in the core: (1) limestone, (2) sands or sandstone, and (3) clays or claystone. The relative well log behaviors of these lithologies are presented in Table 10. An expanded section of the logs illustrating the three responses is presented in Figure 29. Each lithology has a characteristic signature in the well logs, but note that in many intervals the logging data reflect different mixtures of these components. This can result from either the nature of the sediments (e.g., sandy claystone or clayey sandstone) or the manner in which the logging tools average properties on the order of one half to one meter owing to the spacings of sources and receivers on the various tools.

Limestone

Samples of limestone recovered in the core were characterized by extremely low porosities on the order of a few per cent or less. Carbonate content analyses (see "Organic Geochemistry," this chapter) verified bulk- and grain-density measurements, which suggests that these strata approach pure calcium carbonate in composition. Sample compressional wave velocities measured with the Hamilton Frame exceed 6.0 km/s and are the fastest measured in the core.

Limestone intervals in the borehole are characterized by low gamma ray counts. The extremely low natural radiation production of calcium carbonate and the purity of the limestone samples are the reason for the lack of gamma ray response.

The low gamma ray count values are complemented in the limestones by relatively high resistivities and compressional-wave velocities. Both of these properties are a result of the low porosity and high degree of cementation of the limestones, as seen in the cores. The primary path of electrical conduction in sediments and sedimentary rocks is the pore spaces. Given a relatively uniform conductivity of the pore fluids (as appears to be the case at Hole 759B), resistivity varies inversely with porosity. Layers of nearly impermeable limestone act as resistors in the sediment and yield greater resistivities than the surrounding porous materials.

In much the same manner, it is the low porosity of the limestones that is responsible for the high velocities measured by the well logs. Porosity is the first order control of velocity in well-cemented sedimentary rocks. The fact that the well-log velocities are lower than the measured limestone sample velocities reflects the observation in the recovered core that the limestones are not massive and continuous sequences, but rather are interlayered with other lithologies. The limestone

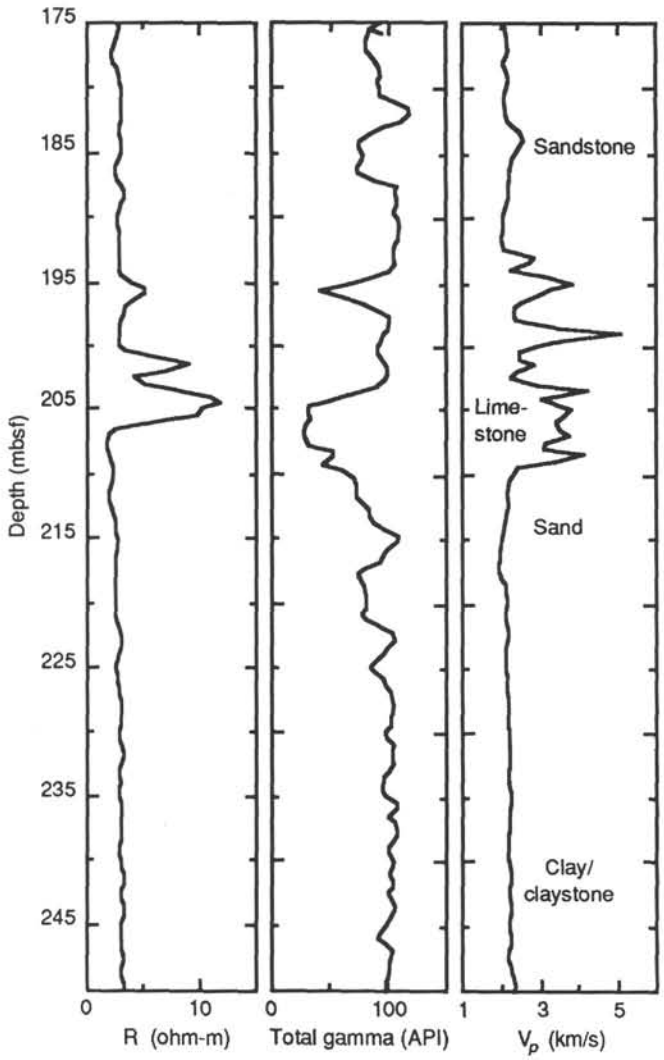

Figure 29. Expanded section of well logs from Hole 759B. Lithologies were recognized by log response and correlation with physical properties of the core. R = resistivity; total gamma = total gamma-ray counts; V_p = compressional-wave velocity.

intervals in the logs are interpreted as zones where limestone is the dominant (rather than the only) rock type.

Sands and Sandstones

Sands and sandstones in Hole 759B are represented by a wider range of property variations than are the limestones, attesting to their more inhomogeneous nature. A clean, well-cemented sandstone exhibits low gamma-ray counts, low resistivity, and moderate-to-high compressional wave velocities. In the ideal case the gamma-ray counts would be as low as limestone, but at Hole 759B the sands and sandstones are far from ideal and can be considered "dirty" (clayey) at best. The measured porosities of sandstone samples from Hole 759B range from 20% to 40% (see "Physical Properties," this chapter). The sandstones contain varying amounts of clay and other fine-grained materials that produce gamma radiation. The variability of the nature and amount of the accessory minerals in the sandstones is reflected in the low-to-moderate gamma-ray counts that sandstones exhibit on the well logs.

The electrical resistivity of both sands and sandstones is also low because of the volume and interconnection of the pore spaces, and because the clays in the pores exhibit surface conductance characteristics that offset their effects in reducing porosity.

Compressional-wave velocities are moderately fast in cemented sandstones, governed by the total porosity of the rock. A factor influencing the compressional wave velocities of sands is the amount of cementation of the grains in the strata. Loose sands may exhibit fairly low porosities, but also have low velocities because the grains are not connected by cements and the overall structure is weak. As cementation in the sands increases, so does the velocity, even though the porosity may decrease by only a small amount.

Clays and Claystone

The highest gamma-ray counts on the well logs correlate with clay and organic-matter-rich intervals in the core. Samples from these intervals have low compressional wave velocities and high porosities. Both organics and clays tend to be rich in uranium, thorium, and potassium (the elements that account for most of the natural radioactivity in sediments and rocks). In addition, there are several minerals that are high in uranium and thorium content (e.g., apatite and monazite) and are resistant to dissolution. These fine-grained products of terrestrial weathering accumulate in the same low-energy environments favored by clays and/or material rich in organic matter.

A lack of cementation abets the high porosity of the clays in lowering the compressional-wave velocities. There may be zones where the clays have been cemented by silica or siderite and have somewhat elevated velocities, particularly in the lower levels of the hole. However, these velocities are still considerably lower than either the cemented sandstones or the limestones.

SUMMARY AND CONCLUSIONS

Introduction

Site 759 (latitude 16°57.24'S, longitude 115°33.63'E, water depth 2092 m) is located near the top of the southeast flank of Wombat Plateau. Hole 759B was continuously cored by rotary drilling to a depth of 308 mbsf and successfully logged in less than five days. Thirty-nine rotary cores were taken with a total recovery of 129.6 m (= 42%), above average for early Mesozoic highly indurated sediments alternating with soft mudstones. Recovery ranged from 0%–100%, being very poor in loose sands and alternating sequences of hard limestone, soft sand, and mudstone in the upper third of hole. The recovery rate increased substantially in the lower third of the hole, where half-cores (4.5–5.0 m) were cut.

The major objectives of Site 759, in conjunction with the three other Wombat Plateau Sites (Sites 760, 761, and 764), were the reconstruction of the Mesozoic paleoenvironment, the early rift, early drift, uplift, and subsidence history of this continental margin, as well as the test of eustatic sea level fluctuations in relation to tectonics and sediment supply (see "Background and Objectives," this chapter). Sites 759, 760, 761, and 764 form a transect of sites with successively younger Mesozoic sections being truncated by a major unconformity (Fig. 2), which will provide a fairly complete record of the evolution of this margin from Upper Triassic to Recent times.

The section at Site 759 predicted from seismic profiles was expected to consist of a few tens of meters of soft Neogene to Quaternary, and a thick underlying Jurassic sequence, underlain by Triassic. However, Triassic (Carnian to Norian) rocks were penetrated directly, underlying a major unconformity at 26.7 mbsf. The section drilled at this site resulted in a number of unexpected discoveries and

extended the record of the oldest marine sediments drilled during DSDP and ODP to late Triassic (Carnian-Norian, 231–215 Ma). Of all the commercial wells drilled on the Exmouth Plateau, only Jupiter-1 contained a pre-Norian (Anisian to Ladinian) section of fluviodeltaic clastics.

Sediment Facies and Paleoenvironment

A summary of the sediment facies and a preliminary paleoenvironmental interpretation of the Late Triassic to Quaternary section at Site 759 (subdivided into five lithological units; see "Lithostratigraphy," this chapter) appears in Figure 2A, "Summary and Highlights," this volume (in back pocket). The lithofacies are very diversified, with widely varying texture and sedimentary structures and minimal core disturbance.

Carnian: The Oldest Marine Rocks Drilled by DSDP/ODP—An Upward-Shallowing Prodeltaic Sequence (Unit V, 308.0–205.0 mbsf)

The oldest sediments recovered in Hole 759B (and in all DSDP/ODP holes) are a 103-m-thick sequence of silty claystone alternating with clayey siltstone and sand. These sediments were dated as late Carnian (early Late Triassic) on the basis of palynomorphs (see "Biostratigraphy," this chapter). The silty claystones are very dark gray to black, mostly laminated, and contain pyrite concretions (which increase in abundance upward) and thin siderite layers, lenses, and nodules (decreasing upward in abundance) and rare sandstone (turbidites?). An algal limestone layer noted in Section 122-759B-32R-2 was interpreted as a reworked deposit. An interesting nannoflora noted between Cores 122-759B-25R and -27R and 122-579B-36R and -39R proves the section to be marine. However, the lack of a normal-marine mollusk fauna, the black color (possibly a result of high organic carbon content), the abundance of pyrite and siderite, and the excellent preservation of laminations (i.e., lack of bioturbation) indicate that the sediments were deposited under restricted-marine, low-energy conditions. This suggests a distal prodelta setting in a water depth between a few tens of meters to about 100 m (i.e., below wave depth).

Unit V consists of a major upward-shallowing (regressive) sequence that grades upward from a marine, low-energy, nannofossil-bearing, distal prodelta facies at the base of Hole 759B to a deltaic marginal-marine to nonmarine, somewhat higher-energy muddy sandstone facies at the top of this unit. This indicates a seaward migration of the strandline during the deposition of Unit V that could have been produced by a drop in sea level, a delta prograding northward from the Australian continent towards the neo-Tethys, or the lateral shift of a delta.

Abundant thin siderite layers, lenses, nodules, and burrow fills were observed in these mudstones. Siderite is precipitated during early diagenesis under conditions of slightly negative Eh and intermediate pH, and abundant Fe^{+2}, high pCO_2 and low S^{+2} concentrations in the pore water (i.e., below the zone of bacterial sulfate reduction, where pyrite is precipitated). Siderite is a good facies indicator because the CO_2 comes from the microbiological degradation of organic matter during burial, a result of CO_2 reduction during methanogenesis. Sideritization was commonly observed in hemipelagic continental rise mudstones (e.g., Site 603, offshore of the northeastern United States; see von Rad and Botz, 1987) and in organic-matter-rich prodelta mudstone environments (e.g., Site 397, offshore of northwestern Africa; see Einsele and von Rad, 1979).

We infer a restricted distal prodelta setting for Site 759, which either faced the open ocean (e.g., the present Niger Delta) or had adjacent carbonate banks that formed a partial barrier against the open-marine Tethys Sea (e.g., the present setting of the Mississippi delta and the Florida and Yucatan carbonate platforms).

Carnian Nearshore Fluviodeltaic to Carbonate Environment (Units IV and III, 205.0–40.5 mbsf)

This sequence consists of an alternation of neritic carbonates and dark-gray, paralic, silty claystone, with a general increase of the proportion of carbonates from Unit IV to III. Medium-grained quartz sandstone is common only in some intervals (see Fig. 2A, "Summary and Highlights," this volume, in back pocket).

The observed alternation best approximates a coal-measure cycle. An ideal coal-measure cycle would be a regressive, generally upward-coarsening cycle starting with limestone or mudstone (representing bay or prodelta environments) at the base and grading upwards into claystone with sandstone lenses (distal bar?), siltstone to cross-bedded sandstone (distributary mouth bar), and finally into organic-rich silty claystone with rootlets and (locally) thin coal seams (interdistributary-plain swamps). However, the cyclicity observed in Hole 759B (e.g., Core 122-759B-20R) is often obscure. Most sequences contain only an organic-matter-rich mudstone with shell and coal debris (lagoonal?), overlain by massive and bioturbated mudstone, laminated shale, and capped by sandstone.

The progradational fluviodeltaic sandstone sequences, carbonate intervals, and mudstones are more easily identified in the gamma-ray and velocity logs (see "Downhole Measurements," this chapter) than in the cores. Logs proved to be especially important at this site because of the poor recovery. Several upward-fining transgressive sequences (sandstone or mudstone overlain by restricted-marine to open-marine carbonates) were identified between 200 and 130 mbsf (Fig. 2A, "Summary and Highlights," this volume, in back pocket). The best example is at the boundary between Units IV and III, where a thick sandy unit is overlain by a transgressive calcareous quartz sandstone to mudstone containing oyster shells and wood fragments (Fig. 2A, "Summary and Highlights," this volume, in back pocket).

The carbonate rocks in this sequence contain (in decreasing order) calcareous mudstone to wackestone, grainstone, oolitic grainstone, and dolomite. A detailed shore-based microfacies analysis will be necessary, but preliminary results indicate a marginal-marine, predominantly low-energy intertidal setting (indicated by wackestones and dolomites) with tempestites (i.e., storm deposits, indicated by grainstones) and higher-energy deposits (e.g., rudstones and oolites) on local carbonate shoals, bars, or in tidal channels. In general, however, the carbonate facies is mud-dominated, suggesting a low-energy, shallow subtidal environment.

The typical facies change from a fluviodeltaic to littoral to lagoonal/intertidal to open-marine/intertidal or shallow subtidal environment shown in Figure 2A, "Summary and Highlights," this volume (in back pocket) indicates *relative* sea level changes, which can be caused by (1) eustatic sea level fluctuations and consequent migrations of coastline, (2) temporal and spatial variations of the volume and transport direction of fluviodeltaic sedimentation (e.g., multiple delta-lobe migration over a seaward, marginal-marine interdistributary bay; cf. the Holocene Mississippi River delta), (3) differential tectonic or load-induced subsidence or uplift, or (4) a combination of these factors. In general, the influence of fluviodeltaic progradation appears to decrease upwards between Units IV and III. There is some indication of a few upward-shallowing cycles between 200 and 46 mbsf, with the

coal seams and sandstones around 190, 90, and 50 mbsf representing the end point of the regressive cycles.

The 200-m.y. Hiatus

The Norian (Upper Triassic) rocks at Site 759 are unconformably overlain by yellow quartz sand mixed with Early Miocene foraminifers. This suggests a hiatus of as much as 200 m.y. at this site, caused by the strong continuous denudation of the uplifted southern flank of the northward tilted Wombat Plateau horst. The timing of the Wombat Plateau rifting event and the duration of the erosion is better constrained by Sites 760 and 761, which have a more complete record underlying and overlying this unconformity. However, the strong truncation of the southern edge of the Wombat Plateau provides us with a "window" to sample the oldest record of pre- and syn-rift margin history ever recovered by DSDP/ODP.

Hemipelagic Lag Deposit of Cretaceous(?) to Paleogene(?) Age (Unit II, 40.5–31.0 mbsf)

The 200-m.y. unconformity described above (seismic reflector E shown in Fig. 4 of the "Introduction," this volume) is overlain by a 9.5-m-thick sequence of yellow-brown coarse quartz sand that is mixed with pelagic foraminifers and nannofossils of Quaternary to Early Miocene age. We think that the foraminifers and nannofossils were mixed into a barren terrigenous sand by downhole contamination resulting from the high pump pressure used for drilling through the unconformity. From our knowledge of Unit III of Site 761 and of dredged rocks of the northern Exmouth Plateau (von Stackelberg et al., 1980), we estimate an early Cretaceous age for this hemipelagic lag, deposited during a long period of winnowing, nondeposition, and erosion.

Early Miocene to Quaternary Eupelagic Sedimentation (Unit I, 31.0–0.0 mbsf)

The youngest sediments cored at Site 759 are 4.2 m of Early Miocene, light-blue gray to greenish-gray nannofossil ooze (Subunit IB), unconformably overlain by Quaternary light red-brown to pink foraminifer nannofossil ooze. This sediment sequence is much less completely developed than at Site 760 or 761 because the upper slope of the uplifted southern edge of the Wombat Plateau horst was dominated by slumping, erosion, and winnowing during most of the Neogene to Quaternary period.

Biostratigraphy

Hole 759B recovered a pelagic sequence of Quaternary sediments that lie unconformably over a hemipelagic sequence of early Miocene ooze. The Cenozoic rests unconformably over a nearshore paralic section of Late Triassic (Carnian-Norian) age.

The Carnian-Norian sediments at Site 759 represent the oldest marine sediments cored during the history of DSDP and ODP. Triassic nannofossils were encountered in moderate abundance at two levels in the lowermost unit (Unit V, Cores 122-759B-25R through -27R and 122-759B-36R through -39R), and only in rare abundance and sporadically in Unit III. These primitive nannoliths may prove to be the earliest known occurrence of nannofossils in the world and may help in the subdivision of the younger Triassic. Dinoflagellates, radiolarians, and foraminifers were not encountered in any significant numbers in the Triassic part of the section. Spores and pollen proved to be the best source of age information for Triassic nonmarine to paralic depositional paleoenvironments.

Organic Geochemistry

The Triassic sediments were carefully monitored for hydrocarbons. Recycled and/or oxidized organic debris (from land plants) derived from the nearby continent is abundant. Total organic matter ranged from 0% to 3.5%. The land-derived organic matter proved to be thermally immature (vitrinite reflectivity, R_o, about 0.4%), with T_{max} values of 420°C for an organic-rich layer in Section 122-759B-20R-4. The highest gas value was 17 ppm methane in a coal stringer (Sample 122-759B-20R-4, 0–2 cm). Only in the lowermost core (122-759B-39R) did we encounter measurable ethane contents (the methane:ethane ratio was about 10:1), but at a very low gas concentration. Since type III organic matter was present (see Fig. 23), the gas encountered at this site was probably formed *in situ* and thus did not present a safety hazard.

Physical Properties, Logging and Seismic Stratigraphy

Owing to the poor recovery and disturbed rotary cores from Hole 759B, the representativeness of the bulk density, grain density, porosity, and water content measurements is difficult to assess. Velocities ranged from 1.51 km/s in carbonate oozes to 6.95 km/s in recrystallized limestones, with a gradual downhole increase of the average sonic velocities from 1.5 km/s at the top to 2.25 km/s at the base of Hole 759B. The thermal conductivity was 1.0–2.2 W/m·K.

In Units III and IV, sonic velocity, porosity, and bulk density vary according to the dominant lithology (mudstone, sandstone, or limestone); the velocity and density values correlate very well with the limestone content. In Unit V the predominantly clastic rocks show a gradual downhole increase of bulk density and good correlation with the gamma and resistivity logs.

The single logging run in Hole 759B yielded logs of spectral gamma ray, electrical resistivity, and sonic velocity. In addition, the borehole caliper log indicated excellent hole conditions for high-quality downhole measurements. The logs proved important in understanding the lithofacies sequence in intervals with poor core recovery (generally the sandier intervals), and in tracing upward-shoaling or -deepening events within the sequences. The log response in the hole indicates that mudstones are the dominant lithology in the Triassic part of the section, followed by limestones and sandstones. Facies analysis from log data confirms the interpretation of a prograded delta environment in the lowermost unit (308 to 210 mbsf). Within the carbonate unit, a gamma-ray peak (with high Th/K ratio) is interpreted as resulting from heavy mineral concentration in a sandstone placer deposit; the high matrix density apparently produced a concomitant increase in sonic velocity. The high gamma ray level may represent a transgressive surface, separating highstand systems tracts below and above.

The interpretation of seismic-stratigraphy data at Site 759 and the other Wombat Plateau sites (Sites 760, 761, and 764) is discussed on a regional basis in the Site 764 chapter.

REFERENCES

Berggren, W. A., Kent, D. V., and Van Couvering, J. A., 1985. Neogene chronology and chronostratigraphy. *In* Snelling, N. J. (Ed.), *The Chronology of the Geologic Record:* Geol. Soc. Mem. (London), 10, 211–260.

Blow, W. H., 1969. Late middle Eocene to Recent planktonic foraminiferal biostratigraphy. *In* Brönnimann, P., and Renz, H. H. (Eds.), *Proc. 1st Intl. Conf. Planktonic Microfossils,* 1: 199–421.

Claypool, G. E., and Kvenvolden, K. A., 1983. Methane and other hydrocarbon gases in marine sediment. *Ann. Rev. Earth Planet. Sci.,* 11:299–327.

Cook, A. C., Smyth, M., and Vos, R. G., 1985. Source potential of Upper Triassic fluvio-deltaic systems of the Exmouth Plateau. *APEA J.,* 25:204–215.

Dolby, J., and Balme, B. E., 1976. Triassic palynology of the Carnarvon Basin, Western Australia. *Rev. Palaeobot. Palynol.,* 22:105–168.

Einsele, G., and von Rad, U., 1979. Facies and paleoenvironment of Lower Cretaceous Sediments at Site 397 and in the Aaiun Basin (Northwest Africa). *In* von Rad, U., Ryan, W.B.F. et al., *Init. Rept. DSDP,* 47: Washington (U.S. Govt. Printing Office), 559–598.

Emeis, K.-C., and Kvenvolden, K. A., 1986. Shipboard Organic Geochemistry on *JOIDES Resolution. ODP Tech. Note,* 7.

Exon, N. F., von Rad, U., and von Stackelberg, U., 1982. The geological development of the passive margins of the Exmouth Plateau off northwest Australia. *Mar. Geol.,* 47:131–152.

Exon, N. F., and Willcox, J. B., 1978. Geology and petroleum potential of the Exmouth Plateau area off Western Australia. *AAPG Bull.,* 62:40–72.

Exon, N. F., and Williamson, P. E., 1988. Sedimentary basin framework of the northern and western Exmouth Plateau. *Rig Seismic* Research Cruises 7 and 8. Post-Cruise Rept., *BMR Record 1988,* 30.

Gieskes, J. M., 1981. Deep-sea drilling interstitial waters: implications for chemical alteration of the oceanic crust, Layer I and II. *Soc. Econ. Paleontol. Mineral. Spec. Publ.,* 31:149–167.

Haq, B. U., Hardenbol, J., and Vail, P. R., 1987. Chronology of fluctuating sea levels since the Triassic. *Science,* 235:1156–1167.

Harland, W. B., Cox A. V., Llewellyn, P. G., Pickton, C.A.G., Smith, D. G., and Walters, R., 1982. *A Geologic Time Scale:* Cambridge (Cambridge Univ. Press).

Helby, R., Morgan, R., and Partridge, A. D., 1987. A palynological zonation of the Australian Mesozoic. *Mem. Assoc. Australas. Palaeontol.,* 4:1–94.

Jafar, A. S., 1983. Significance of Late Triassic calcareous nannoplankton from Austria and Southern Germany. *Neues Jahrb. Geol. Palaeontol. Abh.,* 166:218–259.

Martini, E., 1971. Standard Tertiary and Quaternary nannoplankton zonation. *In* Farinacci, A. (Ed.), *Proc. 2nd Planktonic Conf.:* Rome (Ed. Tecnoscienza), 739–785.

Rider, M. H., 1986. *The Geologic Interpretation of Well Logs:* Glasgow and London (Blackie/Halsted Press).

Vincent, E., 1977. Indian Ocean Neogene planktonic foraminiferal biostratigraphy and its paleoceanographic implications. *In* Heirztler, J. R., et al. (Eds.), *Indian Ocean Geology and Biostratigraphy,* Washington (American Geophysical Union), 469–584.

von Rad, U., and Botz, R., 1987. Authigenic Fe-Mn carbonates in Cretaceous and Tertiary sediments of the continental rise off eastern North America, Deep Sea Drilling Project Site 603. *In* Van Hinte, J. E., Wise, S. W., Jr., et al., *Init. Rept. DSDP,* 93: Washington (U.S. Govt. Printing Office), 1061–1077.

von Rad, U., and Exon, N. F., 1983. Mesozoic-Cenozoic sedimentary and volcanic evolution of the starved passive margin off northwest Australia. *AAPG Mem.,* 34:253–281.

von Rad, U., Exon, N. F., Williamson, P. E., and Boyd, R., 1986. *Revision of ODP Proposal 121/B (ODP Leg Exmouth Plateau-Argo Abyssal Plain) after the site survey by BMR's Rig Seismic Cruise 55 and 56 (March–May 1986).* Unpublished Report, JOIDES/ODP Site Survey Data Bank, Proposal 121/B (revised).

von Rad, U., Schott, M., Exon, N. F., Mutterlose, J., Quilty, P., and Thurow, J., in press. Petrography and microfacies of Mesozoic sediments and volcanic rocks, dredged from the northern Exmouth Plateau during the Rig Seismic-56 Cruise (1986). *BMR J. Aust. Geol. Geophys.*

von Stackelberg, U., Exon, N. F., von Rad, U., Quilty, P., Shafik, S., Beiersdorf, H., Seibertz, E., and Veevers, J. J., 1980. Geology of the Exmouth and Wallaby Plateaus off northwest Australia: sampling of seismic sequences. *BMR J. Aust. Geol. Geophys.,* 5: 113–140.

MS 122A-105

NOTE: All core description forms ("barrel sheets") and core photographs have been printed on coated paper and bound as Section 3, near the back of the book, beginning on page 387.